Alma Mater Studiorum-Università di Bologna

Faculty of Engineering and Architecture

INTERNATIONAL MASTER COURSE

IN CIVIL ENGINEERING

Master thesis in

ADVANCED DESIGN OF STRUCTURES

APPLICATION OF CRESCENT-SHAPED BRACES IN REINFORCED CONCRETE STRUCTURES

Candidate:

OMAR KAMMOUH

Supervisor:

Prof. STEFANO SILVESTRI

Co-supervisor:

Dr. MICHELE PALERMO

Session I

Academic year 2014/2015

Contents

INTRODUCTION 1
1. Background 1
2. Executive summary and objective 4
3. Organization of the work 5
1. THE DEVICE 8
1.1 Review of the analytical relationships of CSB 9
1.1.1 Equilibrium equations 9
1.1.2 The lateral stiffness 10
1.1.3 The yield strength 12
1.1.4 Design formulas 13
1.2 Behavior of the device 14
1.2.1 CSB constitutive law (tension and compression) 14
1.2.2 Effect of the section profile 18
1.3 Positioning of the device 21
2. THE STRUCTURE 28
2.1 Geometry of the structure 28
2.2 Material 32
2.3 Analysis of load 33
2.3.1 Permanent loads on the floors 33
2.3.2 Partition walls which are not placed over the beams 35
2.3.3 Partition walls which are placed over the beams 38
2.3.4 Variable loads 39
2.4 Modeling 40
2.5 Modal Analysis 42
2.6 Elastic Response spectra (Serviceability and Ultimate) 44
3. METHODS OF ANALYSIS 47
3.1 Nonlinear Dynamic (Time-history) analysis 47
3.1.1 Codes regulations 48
3.1.2 Constructing the Accelerograms 50
3.2 Nonlinear Static (Pushover) analysis 57

4. BEHAVIOR OF THE NAKED STRUCTURE 60
4.1 Linear analysis 60
4.2 Non-Linear analysis (The Actual Capacity Curve) 62
4.2.1 General 62
4.2.2 Nonlinear analysis of reinforced concrete sections 63
4.2.3 Nonlinear analysis results 67
5. BEHAVIOR OF THE EQUIPPED STRUCTURE 70
5.1 Design of the CSB devices 70
5.1.1 Method I (flexible structures) 70
5.1.2 Method II (Stiff structures) 78
5.2 Analysis of the linear structure equipped with the non-linear devices 86
5.3 Non-Linear analysis (The Actual Capacity Curve) 87
5.3.1 Method 1: Nonlinear Time-history analysis 88
5.3.2 Method 2: N2 method 89
5.3.3 Comparison of the 2 methods 100
6. COMPARISON 102
7. CONCLUSION AND FURTHER DEVELOPMENT 105
Acknowledgements 107
Bibliography 108

INTRODUCTION

1. Background

The design of building structures that is capable of providing prescribed seismic performance is the fundamental objective of the Performance-Based Design Approach. Nowadays, Buildings are designed (or strengthened) in order to fulfill the predefined performances (**Figure 1**). Existing buildings in particular fall in the inacceptable performance area. Therefore, our aim is to bring them under the minimum safety level.

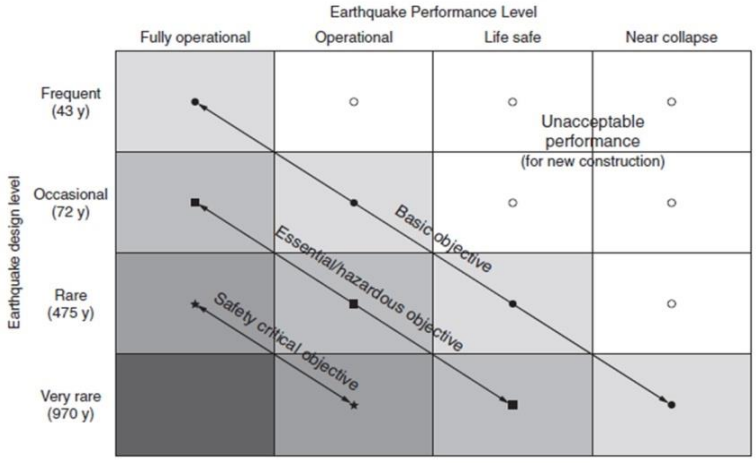

Figure 1- Performance-Based Design Objectives

Buildings in general are not characterized by a lateral force-displacement curve close to the desired seismic "Objective curve" (**Figure 2).** For this reason, specific system that is capable of independently matching the required properties in terms of stiffness, strength, and ductility should be added.

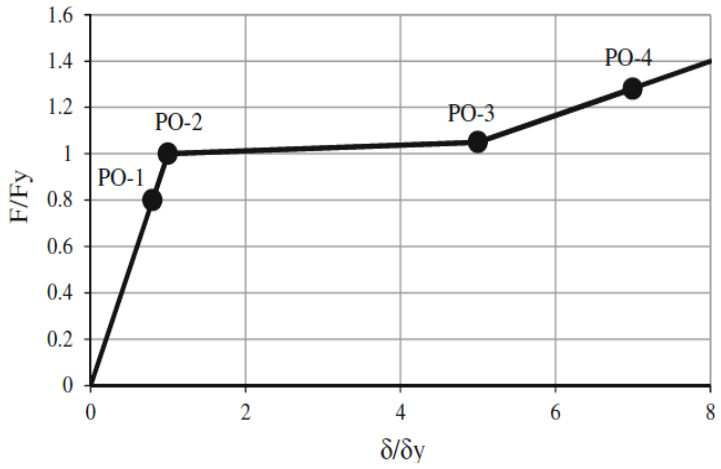

Figure 2- A qualitative objective curve

Building structures for their particular use must be capable of providing a high degree of safety, which is compatible with today's society expectations. With respect to earthquake input, the strategies commonly adopted for the seismic design of building structures may be substantially traced back to two strategies:

1) The maximization of the structural ductility capacity;

2) The minimization of energy transmitted by the earthquake to the structural system.

The first strategy (traditional approach) is based upon the hysteretic dissipation, which occurs when structural elements develop non-linear behavior. This excursion in the non-linear field leads to advantages in terms of energy dissipation, but at same time, to considerable damage in the structural system (beams and columns). The second strategy (innovative approach) is based upon innovative technologies for the seismic protection of building structures aimed at guaranteeing the capacity of the structure of facing strong earthquake ground motions without recourse to structural ductility as main resource. Examples of such seismic protection systems are added dampers and base isolators. It is thus clear that the first approach is characterized by

low cost but low efficiency, whilst, on the contrary, the second one is characterized by high cost but high efficiency.

It is gradually being recognized that effective means of protecting structures from earthquake forces are by way of using various methods of structural control. They are not only effective for mitigating earthquake forces, but also are equally useful in controlling undesirable vibrations of structures produced due to wind and other dynamic excitations. In addition, there are a number of other factors that have emerged in recent years that require the control of the structural response. These factors include increased flexibility of the structural systems, increased safety levels, stringent performance level, and economic considerations. As a result, research in the area of structural control has intensified since the 1980s and many structural control methodologies have been developed, with some now being implemented in practice.

Broadly, methods of structural control can be classified as passive and active control methods. In the passive control, the mass, the damping, stiffness, a combination of any two, or all are modified by adding some components into the structure. These components are actuated by the movements of the structure and provide control forces according to their dynamic characteristics. No external source of energy is required to activate the system. In the active control, an external source of energy is used to activate the control system by providing an analog signal to it.

The work presented in this thesis is directed towards the behavior of a new innovative lateral resisting system, namely “the crescent shaped braces”, when installed in reinforced concrete structures. CSB is classified under the passive systems as it is activated when it is exposed to displacement. An in-depth study for the local and global behavior of this lateral system will be presented.

2. Executive summary and objective

In this work, the global behavior of a new innovative passive technology for resisting the lateral actions induced by earthquakes, namely Crescent shaped bracing, will be studied in depth. The CSB, as a new system, has not been undergone much research. As far as the global behavior of structures is concerned, only the behavior of SDOF steel structures with this device being installed was studied in the past [1]

The aim of this research is to study the behavior of MDOF reinforced concrete structures equipped with CSB. In order to achieve this goal, an understanding study of the local behavior of the bracing element will be carried out using fiber-based finite element software (Seismostruct). Once the behavior (constitutive law) is determined, it will be possible to extend the research to cover the global behavior of the element (element+structure) through a real case study.

The preliminary design of structural elements has always been a main concern in the structural engineering world, and crescent shaped braces are no exception. For this reason, a performance-based design approach for both stiff and flexible structures equipped with crescent shaped braces will be introduced. In addition, a part of this research will be dedicated to examine the effect of positioning of the braces on the distribution of the internal forces in the structural elements. This will make it possible to tell which is the best position in terms of structural behavior and architectural limitations.

Different types of nonlinear analysis (static and dynamic) will be used in this study (ex, nonlinear Pushover and nonlinear time history analyses). This will increase the reliability of the results we obtain. I addition, a simplified analysis method called “The N2-method” will be implemented in this work. This method combines the pushover analysis of a multi-degree-of-freedom (MDOF) model with the response spectrum analysis of an equivalent single-degree-of-

freedom (SDOF) system. This can be an additional source of information from which we can obtain the global seismic demand for our MDOF structure.

The main objective in this work is to improve the global behavior of RC structures by adding pre-designed CSB devices. Those devices will be designed in such a way that the actual curve of the building matches the pre-defined objective curve. In order to attain this goal, the following tasks should be studied:

1. Local behavior of the bracing element;
2. A performance-based Preliminary approach for designing of the devices;
3. Positioning and distribution of the braces in the structure;
4. Global behavior of RC structure equipped with Crescent shaped braces.

3. Organization of the work

The work is presented in six Chapters. The first chapter, *The device*, provides an extensive coverage of the local behavior of the bracing device. A review of the analytical expressions of CSB will be discussed. Additionally, Numerical simulations using fiber-based software (seismostruct) will be performed in order to obtain the structural behavior (constitutive law) and the effect of the section profile on the local behavior of the bracing element. Finally, different alternatives of brace positions will be studied in terms of axial force distribution in columns and foundations.

The second chapter, *the structure*, deals with the case study structure. A full definition of the structure in terms of geometry, material, loadings, and modeling will be carried out. In addition, Modal analysis results will be discussed.

The third chapter, *static and dynamic analyses*, provides an overview of the used analysis methods of multi degree of freedom systems. Methods include non-linear pushover analysis (static) and non-linear time history analysis (dynamic).

The fourth chapter, *behavior of the naked structure*, discusses the behavior of the case study structure without the bracing elements. Linear and non-linear analysis for the structure are performed. Linear analysis will be used to determine the level of forces induced by the earthquakes, while the nonlinear analysis will be performed to determine the capacity of the un-equipped structure. The non-linear behavior of the concrete elements will be defined (moment-curvature relationship) as it is necessary for the nonlinear analysis.

The fifth chapter, *behavior of the equipped structure*, deals with the global behavior of the system with the bracing elements being installed. As a first step we will introduce a performance-based method for dimensioning the steel CSB elements. Those braces will afterwards be inserted in the structure. Nonlinear analysis will be performed through static pushover and dynamic time-history analyses using the software SAP2000. This chapter includes an overview of a method called the N2-method, which combines the pushover analysis of a multi-degree-of-freedom (MDOF) model with the response spectrum analysis of an equivalent SDOF system in order to obtain the global seismic demand.

Finally, a comparison between the 2 structures (Equipped and Naked) will be carried out in order to check the fulfillment of our objective of reducing the amount of damage the structure undergoes when exposed to high ground motion levels.

CHAPTER 1

1. THE DEVICE

This section introduces a special lateral resisting element, herein referred to as Crescent Shaped Brace (CSB) (**Figure 3**). CSBs are characterized by a geometrical configuration which is ‘‘ad hoc’’ defined in order to provide the structure with prescribed multiple seismic performances, within the performance based seismic design framework. [2]

For a specific building, the vertical resisting system is typically designed for the static loads and most likely is not characterized by a lateral force–displacement curve close to the desired seismic ‘‘objective curve’’. Thus, in order to translate the desired ‘‘objective curve’’ into the actual structural response, a specific bracing system should be added, capable of independently matching the required properties in terms of stiffness, strength and ductility [3] [4].Common bracing devices (i.e. concentric stiff diagonal elements) do not usually allow to independently designing these three properties. Although many studies have been carried out on special typologies of steel bracing elements (e.g. eccentric bracing systems, hysteretic devices, friction devices, visco-elastic dampers, buckling-restrained braces, etc… [5] [6]), only few physical solutions allow to obtain a force–displacement response which is close to the ideal ‘‘objective curve’’ [4].

Recently, CSBs have been installed in a Hospital (‘‘Ospedale Maggiore’’) located in the city of Bologna, Italy, in order to connect the steel moment-resisting frames with two external reinforced-concrete cores. Before the installation of the devices, cyclic experimental tests were carried out.

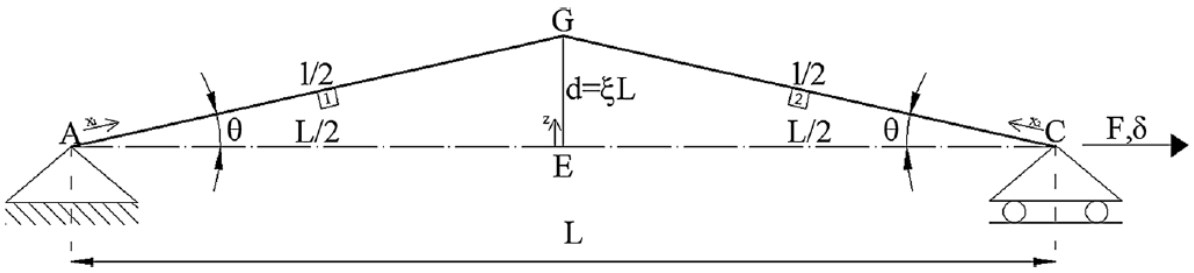

Figure 3- The geometrical configuration of the studied CSB

In the present section, the mechanical behavior of the CSB is discussed with the objective of providing the designer with the necessary tools for the seismic design of buildings equipped with such devices. First, the elastic behavior of the CSB is studied in order to provide analytical relationships for the lateral stiffness and the yield strength (elastic limit). Second, the inelastic response is studied by means of extensive numerical simulations in order to assess the post yielding behavior under monotonic loading and the hysteretic behavior under reversed cyclic loading. In addition, the influence of some geometrical and mechanical parameters of the CSB is evaluated.

1.1 Review of the analytical relationships of CSB [2]

1.1.1 Equilibrium equations

From simple equilibrium considerations, the axial force, the shear force and the bending moment acting along the two elements are equal to:

$$\begin{cases} N_1(x_1) = F.cos\theta \\ V_1(x_1) = F.sin\theta \\ M_1(x_1) = \int_0^{x1} V_1(x_1)dx_1 = \int_0^{x1} F.sin\theta\ dx_1 = F.z \end{cases} \quad (1)$$

$$\begin{cases} N_2(x_2) = F.cos\theta \\ V_2(x_2) = F.sin\theta \\ M_2(x_2) = \int_0^{x2} V_2(x_2)dx_2 = \int_0^{x2} F.sin\theta\ dx_2 = F.z \end{cases} \quad (2)$$

Where x_1 and x_2 represent the local longitudinal axes of the elements, while z represents the abscissa along segment EG (**Figure 3**). The axial and shear forces are constant along the elements (thus can be simply indicated as N_1, N_2 and V_1, V_2, respectively), while the bending moment varies linearly and achieves its maximum value at the knee point G:

$$M_G = F.d \quad (3)$$

1.1.2 The lateral stiffness

The lateral displacement d due to the horizontal force F can be evaluated by applying the principle of virtual works:

$$\delta = \delta_N + \delta_M$$

$$\delta = \int_0^{l1} \frac{N_1}{E.A} cos\theta_1 d_{x1} + \int_0^{l2} \frac{N_2}{E.A} cos\theta_2 d_{x2} + \int_0^{l1} \frac{M_1(x_1)}{E.J} z(x_1) d_{x1} + \int_0^{l1} \frac{M_2(x_2)}{E.J} z(x_2) d_{x2} \quad (4)$$

Where δ_N and δ_M are the axial and the flexural contributions to total deformation.

By introducing $\rho = L_1/L$ and $\xi = d/L$, after simple mathematical developments, the previous equation becomes:

$$\delta = F\left[\frac{L}{E.A}(\rho.cos\theta_1 + (1-\rho).cos\theta_2) + \frac{L^3.\xi^2}{3E.J}(\frac{\rho}{cos\theta_1} + \frac{1-\rho.cos\theta_1}{cos\theta_2})\right] \tag{5}$$

In order to obtain a more compact notation, the following two functions of ρ and ξ are introduced:

$$f_1(\rho,\xi) = \sqrt{\rho^2+\xi^2} + \sqrt{1-\rho^2+\xi^2} \tag{6}$$

$$f_2(\rho,\xi) = \frac{\rho^2}{\sqrt{\rho^2+\xi^2}} + \frac{1-\rho^2}{\sqrt{1-\rho^2+\xi^2}} \tag{7}$$

Which allow expressing Eq.5 as follows

$$\delta = F\left[\frac{L}{E.A}f_2(\rho,\xi) + \frac{d^2.L}{3E.J}f_1(\rho,\xi)\right] \tag{8}$$

After some mathematical manipulations, the lateral stiffness of the CSB can be expressed as follows:

$$K = \frac{F}{\delta} = \frac{E.A}{L}.\left(\frac{1}{f_2(\rho,\xi).\left(1+\frac{\delta_M}{\delta_N}\right)}\right) = K_N.\gamma \tag{9}$$

It can be recognized that the first term (K_N) represents the axial rigidity of an ideal straight member, while the second term (γ) is a reduction factor due the geometry of the system. If the diagonal reference line of the CSB configuration is inclined with an angle H with respect to the horizontal line, the inclination should be taken into account as follows:

$$K = K_N.cos^2\theta.\gamma \tag{10}$$

1.1.3 The yield strength

From the equilibrium considerations discussed in the previous section, it clearly appears that the CSB reaches the first yielding condition at the knee point G. By imposing the yielding condition ($\sigma_{max} = f_y$, i.e. the maximum stress equals the yield stress of the material), the following expression of the yield strength can be obtained:

$$F_y = f_y . \frac{W}{\xi . L} . \mu \tag{11}$$

Alternately:

$$F_y = A . f_y . \eta \tag{12}$$

Where:

$$\mu = \frac{1}{1 + \frac{h}{L} . \frac{2}{\xi} (i/h)^2} \tag{13}$$

$$\eta = \frac{1}{1 + \frac{L}{h} . \frac{\xi}{2(i/h)^2}} \tag{14}$$

The coefficients μ and η represent the reduction factors that are to be applied to the pure flexural strength ($M_y = f_y \frac{W}{d}$) and to the pure axial strength ($N_y = A . f_y$) of the member in order to obtain the effective yield strength, respectively. As illustrative example, **Figure 4** displays μ as a function of d/L for various steel profiles (i.e. for various i/h ratios), for a fixed h/L ratio equal to 0.04.

As observed before, increasing η leads to a rapid increase of the flexural contribution. Practically, for η larger than 0.10, the yield strength can be assumed equal to the pure flexural strength.

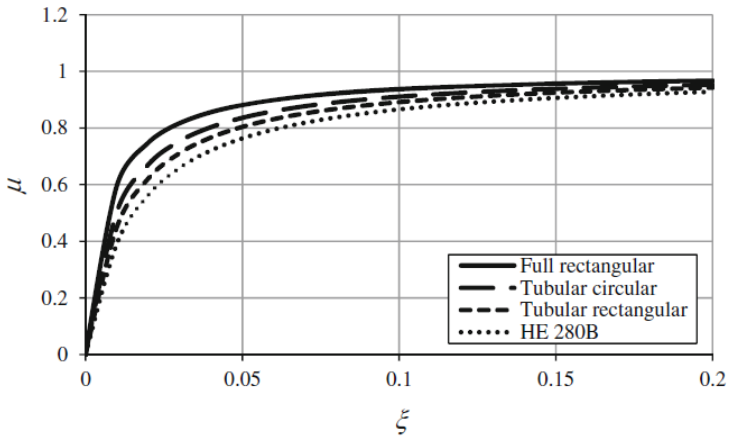

Figure 4- Coefficient μ as a function of $\xi = d/L$

1.1.4 Design formulas

From a design point of view, it is useful to provide equations, which allow sizing a specific CSB knowing the target lateral stiffness $\bar{K}$ and the target yield strength $\bar{F}_y$. If a section profile is chosen, Eqs. 9 and 11 can be rearranged in order to obtain direct design expressions for the normalized ‘‘arm’’ ξ and the modulus of inertia J:

$$\xi = 0.75\frac{(\text{E.h}.\bar{F}_y)}{\bar{K}.L^2.f_y}.\left(\sqrt{1+5.33.\left(\frac{i}{h}\right)^2.\frac{\bar{K}.L}{E}.\frac{f_y}{\bar{F}_y}}\right) \quad (15)$$

$$J = \frac{L^3.\bar{K}.\xi^2}{3E} \quad (16)$$

Equations 15 and 16 are derived assuming that the CSB axial deformability can be neglected with respect to the flexural deformability. From a design point of view, this assumption is reasonable for values of $\xi > 0.08$. The designer can use Eqs. 9 and 11, which are of a general validity, but not explicit in terms of ξ and J, so that a trial and error procedure should be used.

1.2 Behavior of the device

In this section, we will first study the post yielding behavior of the device "CSB" under monotonic loadings. After that, we will examine the effect of changing the device's section profile on the device behavior in both tension and compression. In addition, a study of the axial forces distribution in columns and foundation will be performed because in practice we do not want to over-stress some foundations while leaving others unstressed. A good distribution of the axial forces is crucial in order not to oversize the foundations underneath the building. The axial force distribution is controlled by the configuration of the device. Therefore, different configurations will be tested and the results will be compared.

All experiments have been done using the finite element software "seismostruct". Seismostuct is a fiber-based finite element package for structural analysis, capable of predicting the large displacement behavior of space frames under static or dynamic loadings, taking into account both geometric nonlinearities and material inelasticity. [Seismosoft [2014] "SeismoStruct v7.0 – A computer program for static and dynamic nonlinear analysis of framed structures," available from http://www.seismosoft.com]

1.2.1 CSB constitutive law (tension and compression)

The constitutive law of the crescent shaped brace is controlled by the configuration of the device (angle of force with respect to the line connecting the device's both ends), the device's geometry (lever arm, diagonal length, etc…), and the section characteristics (hardening ratio, yielding strength, stiffness, etc…). Without loss of generality, and for sake of conciseness, the results presented in this section are referred to the case of the symmetric bilinear configuration (**Figure 5**). The post yielding behavior of the device has been studied using extensive numerical

analysis carried out on fully non-linear finite models developed using the research software SeismoStruct v7.0.3 [7]

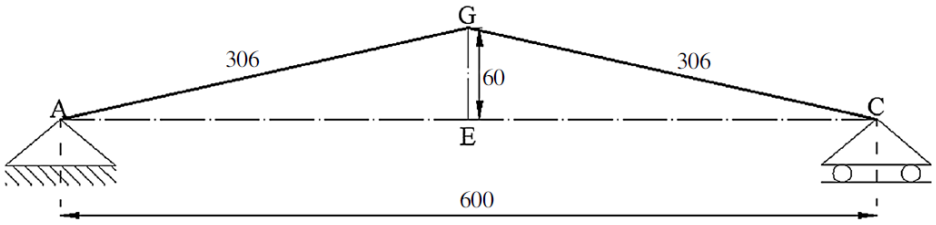

Figure 5- Geometrical parameters of the tested CSB (all dimensions are in mm)

1.2.1.1 Behavior in tension

The behavior of CSB under tension loading is firstly studied. The isotropic hardening parameter was set equal to 0.005. The section profile has been chosen to be HE200B European profile (steel S355).

The system is subjected to an increasing horizontal force F up to the complete elongation condition. **Figure 6** displays the response of force versus horizontal displacement.

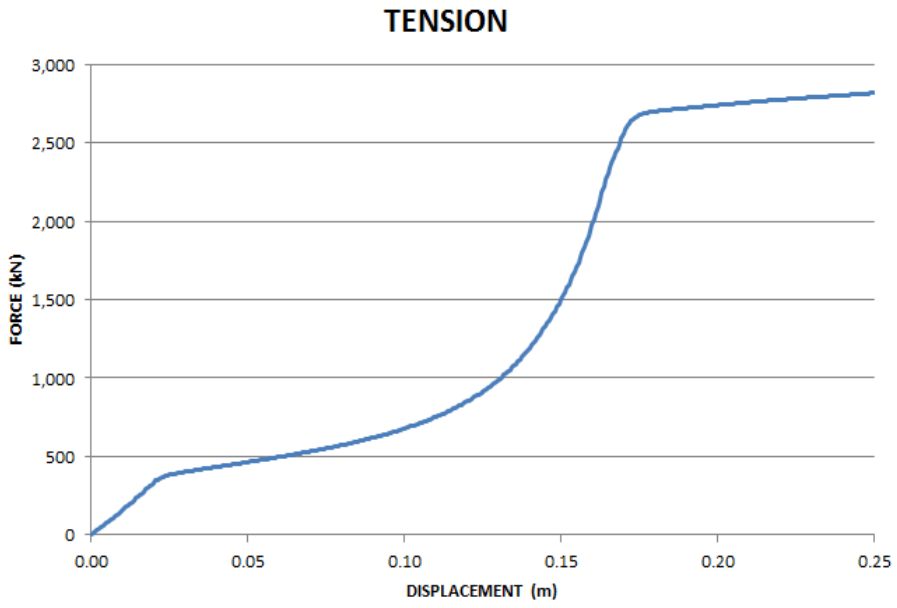

Figure 6- Behavior of the CSB under tension monotonic loading

Due to the special geometrical shape of the CSB, the device is able to resist the elongation through its axial as well as its moment capacity at the knee point G, unlike the conventional braces that resist through their axial stiffness only. **Figure 7** shows the variation of the axial and moment resistance with the horizontal displacement, while **Figure 8** displays the decrease in the normalized arm ξ versus the horizontal displacement.

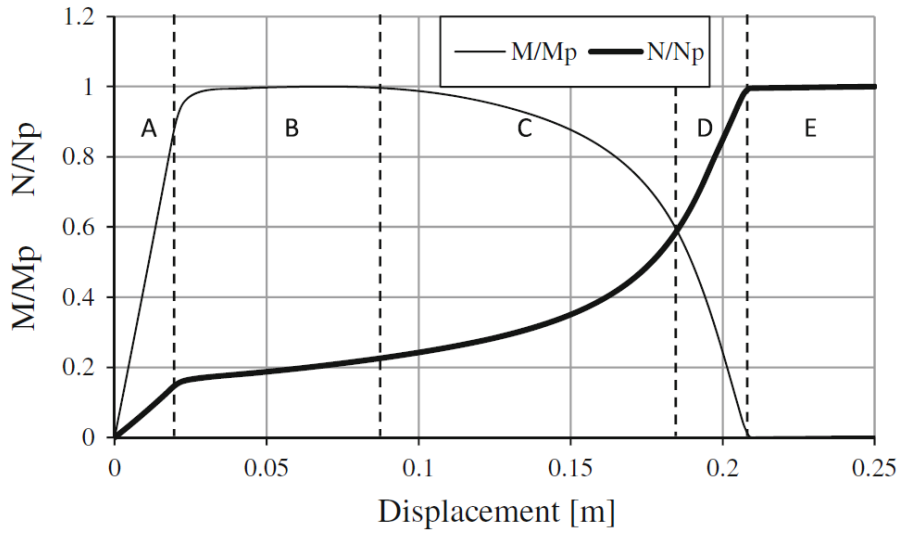

Figure 7- Normalized Bending moment and axial force versus horizontal displacement

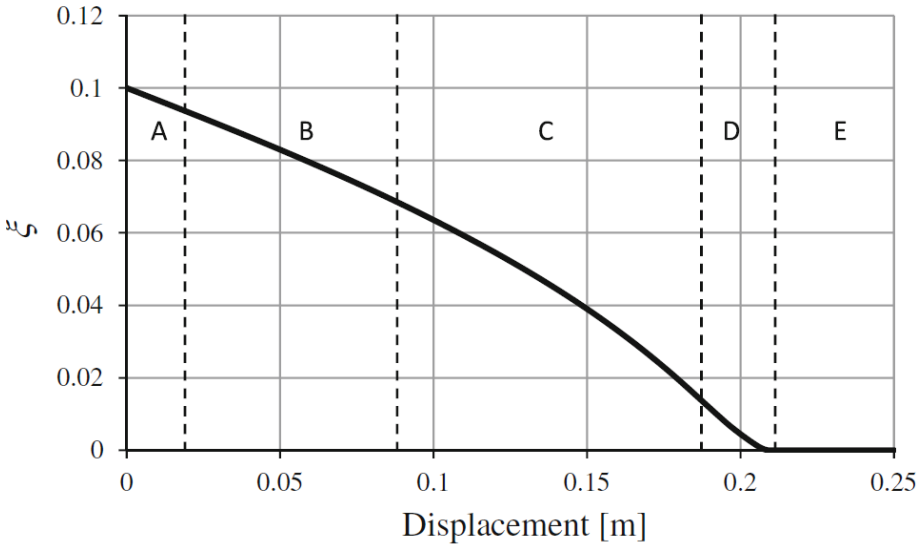

Figure 8- Decease in the normalized arm ξ versus the horizontal displacement.

Referring to **Figure 7**, it is possible to identify five different regions of behavior:

- Region A: The response of the system in the elastic field. The behavior is mostly flexural.
- Region B: The bending moment at knee section reaches the plastic moment Mp and remains constant while the axial slightly increases up to 0.2 Np.
- Region C: The bending moment at knee section decreases while the axial force significantly increases. The behavior is both flexural and axial.
- Region D: the bending moment at the knee section rapidly decreases up to vanish, while the axial force rapidly increases up to the axial capacity Np. The behavior is mainly axial.
- Region E: the axial force is constant and equal to the axial capacity Np. The system behaves as a truss in tension.

It is interesting to note the gradual drop of the moment capacity of the CSB as the arm ξ decreases. When the normalized arm reaches zero, the moment capacity will be dissipated and thus the system will continue resisting through its axial capacity only, like a conventional brace or a truss in tensile configuration.

1.2.1.2 Behavior in Compression

Similarly, the device has been tested under compressive monotonic force while keeping the same geometrical configuration and section profile. Both mechanical and geometrical nonlinearities are included in the analysis. **Figure 9** displays the response of compression force versus horizontal displacement.

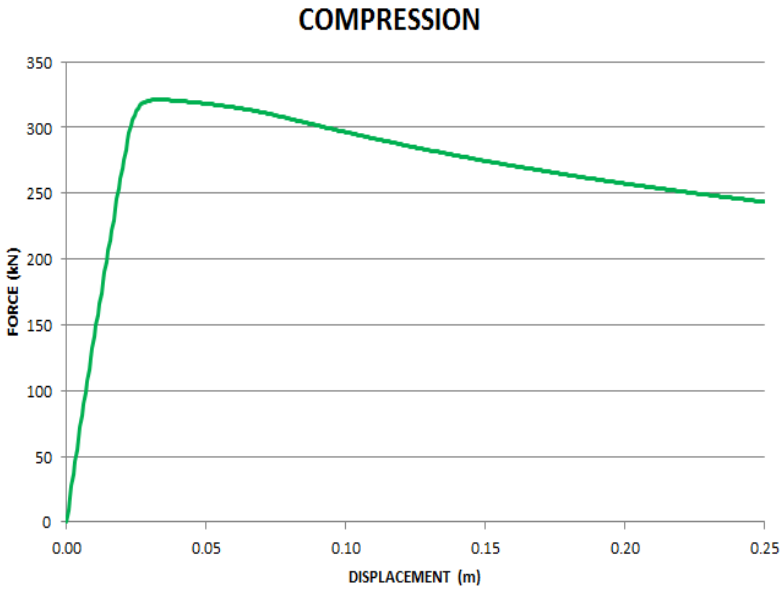

Figure 9- Behavior of the CSB under Compression monotonic loading

Inspection of the curve shows that after yielding the CSB undergoes a softening behavior after reaching the critical force level. This is due to the geometrical nonlinearity effects.

1.2.2 Effect of the section profile

Using numerical simulations, different cross-section are tested in order to identify the influence of changing the section profile on the system behavior. The profiles may be classified based on the i/h ratio.

In order to have a comparable results, all sections are set to have the same inertia J as well as the same section depth h. the lever arm ratio $\xi = d/L$ is set equal to 0.1 for all analyses. The steel yield strength has been assumed equal to 355 MPa (S355), while the hardening ratio $r = 0.005$. The mechanical parameters of the section profiles are listed in **Table 1**.

Profile	Full circular	Full rectangular	Tubular circular	Tubular rectangular	HE200B
$J(cm^4)$	5696	5696	5696	5696	5696
$H\ or\ D(cm)$	18.46	20.00	20.00	20.00	20.00
$A(cm^2)$	267.54	170.88	149.03	77.44	65.30
A/A_{HE200B}	4.10	2.62	2.28	1.19	1.00
β	1.70	1.50	1.27	1.25	1.14
β/β_{HE200B}	1.49	1.32	1.11	1.10	1.00
i/h	0.25	0.29	0.31	0.43	0.47
$Mp(kN.m)$	372.50	303.31	256.27	252.76	225.46
Mp/Mp_{HE200B}	1.65	1.35	1.14	1.12	1.00
$NP(kN)$	9497.70	6066.24	5290.54	2749.22	2318.15
$(Mp/h)/Np*100$	0.21	0.25	0.24	0.46	0.49
$Fy(kN)eq.12$	351.67	319.28	316.21	300.21	294.24

Table 1- Main properties of the different cross-section profiles considered in the study

As in the previous sections, the system will be subjected to an increasing horizontal force F up to the complete elongation condition. **Figure 10** displays the response of force versus horizontal displacement for all section profiles.

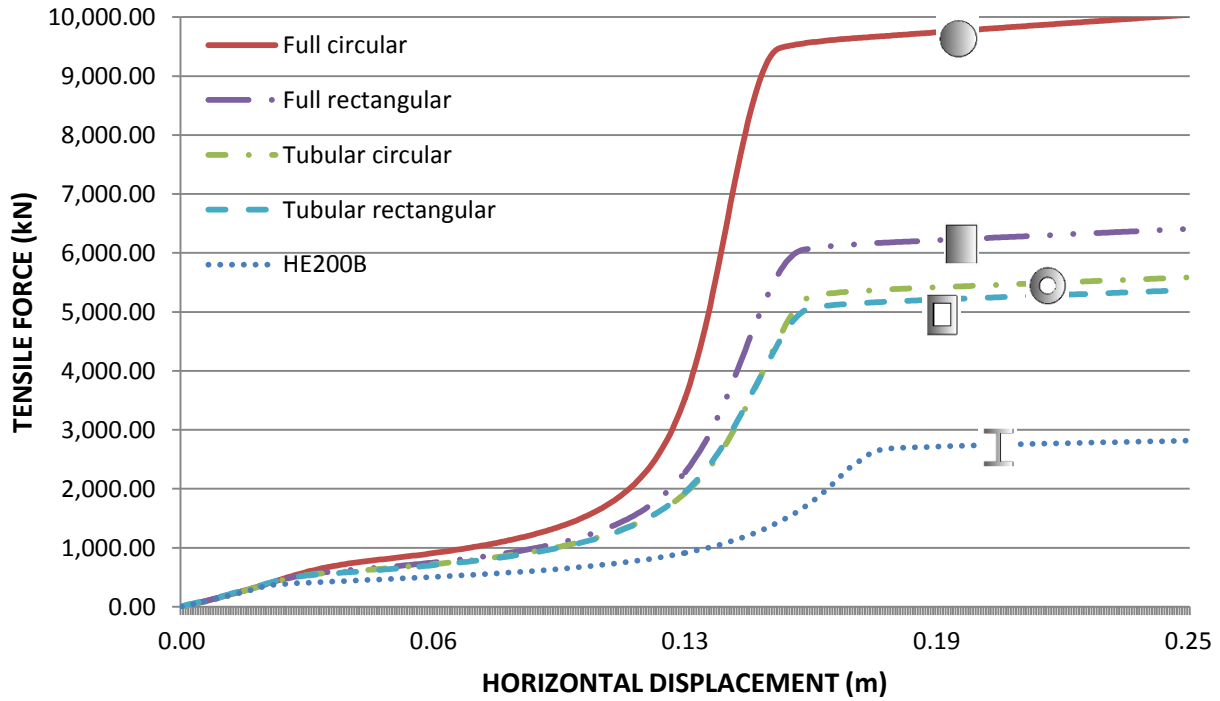

Figure 10- The response of tensile force versus horizontal displacement for all section profiles

Inspection of **Figure 10** and **Table 1** allows observing that all profiles undergo the same qualitative post-yielding response. In detail:

- Qualitatively, all profiles are characterized by almost the same ductility capacity (3/3.5).
- The strength between yielding (PO-2) and substantial hardening (PO-3) is proportional to the plastic benefit of the cross-section β.
- The HE profile exhibits a limited hardening behavior with respect to those showed by the other profiles, whilst the full circular profile exhibits the largest hardening behavior. The two tubular profiles exhibit a quite similar hardening behavior. The full rectangular profile shows a response similar to that of the tubular profiles with a slightly larger global hardening.
- In Region E, the strength is clearly proportional to the $\boldsymbol{A/A_{HE200B}}$ ratio, given that the system is reduced to a truss in tensile configuration.

The five section profiles have been put under monotonic compressive force. **Figure 11** shows the results of the static pushover analysis of all sections. As in the tension test, the full circular section resists the most, while HE200B is the first to reach yielding. The 3 other profiles, namely, full rectangular, tubular circular, and tubular rectangular show similar pre and post yielding behavior. All of the tested profiles exhibit softening behavior due to the geometrical non-linear effects.

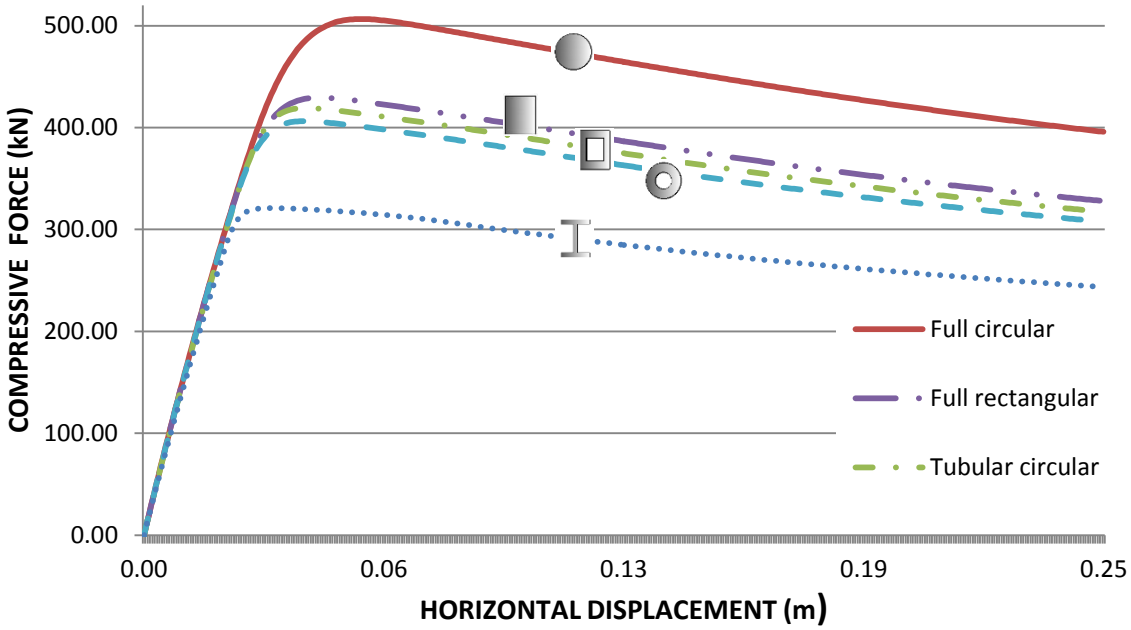

Figure 11- The response of compressive force versus horizontal displacement for all section profiles

1.3 Positioning of the device

One of the important aspects is to figure out the best configuration of the device. There are plenty of configurations but not all of them are equally effective. Bracings transform lateral forces from earthquakes and wind into axial forces in the columns, and this force is not to be neglected. What we can do about it is to find the configuration that minimizes the amount of forces transmitted.

Another issue lies in the modeling of the device. The crescent shaped brace behaves differently in tension and compression, and thus it is not said that if 2 CSBs are put together then their behavior will be the same. This is because when the first is working in tension, the other will be working in compression (**Figure 12**), so each of the two braces will produce different force under the same displacement, and thus the axial force transmitted to the columns A and B (**Figure 12)** will be different. However, given that the system is exposed to a cyclic ground

motion, the axial force envelope in the 2 columns will be the same. This also applies for the foundations.

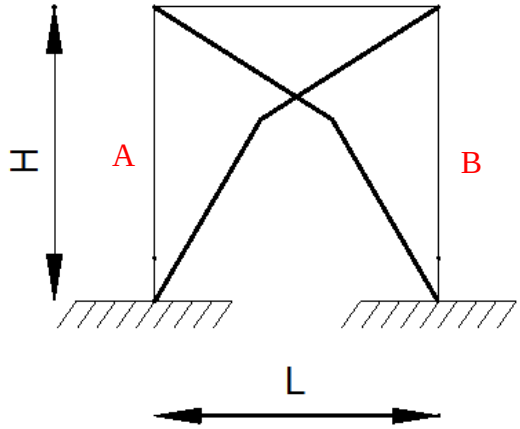

Figure 12- A configuration for a double CSB system

Given what we have said, two constitutive laws can be used in the modeling of the CSB lateral system. The first model (**Figure 13**) describes the real behavior (constitutive law) of a single CSB. It is clear that CSB develops hardening behavior when exposed to tensile forces, while it reaches much lower forces when it is put under compressive forces. This model is very accurate but in the practical point of view, it might be a little bit complicated to deal with. The second model (**Figure 14**) shows a symmetrical behavior in tension and compression. According to what we have said so far, this model does not represent the actual behavior of the system. Nevertheless, when 2 devices are inserted together (a double CSB system), when the first is exposed to a tensile force the second will be exposed to a compressive force, and thus the total resistance will be the summation of the behavior of a CSB device in tension and the behavior of another CSB in compression. Therefore, the behavior of a single CSB can be represented as the half of the sum of the constitutive laws of the device in tension and in compression. Although the

lateral resistance will be the same when using any of the two models, the axial forces transmitted to columns and foundation should be checked if they remain the same.

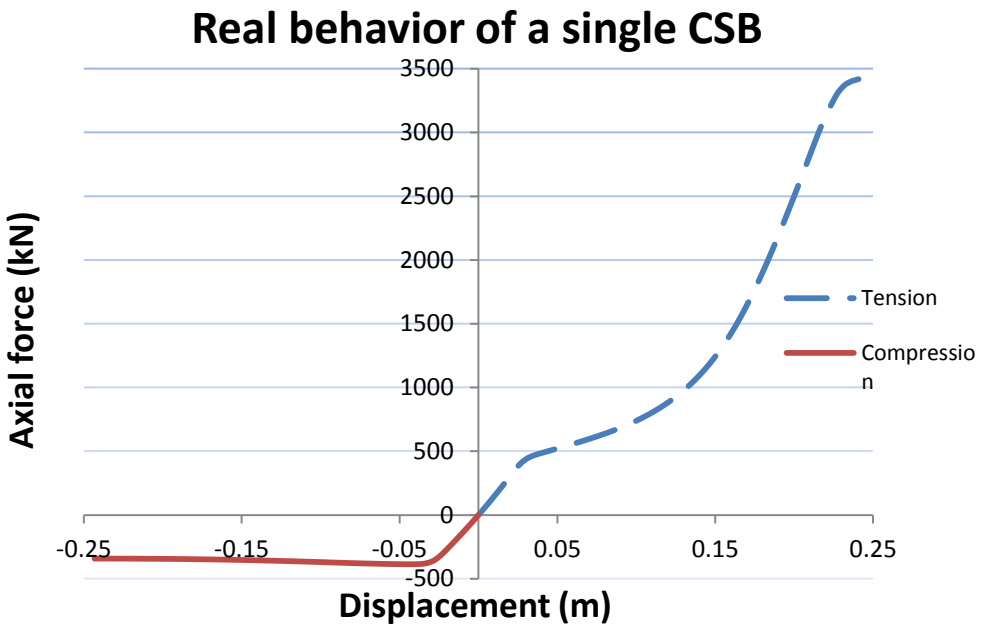

Figure 13- Real constitutive law of a single CSB

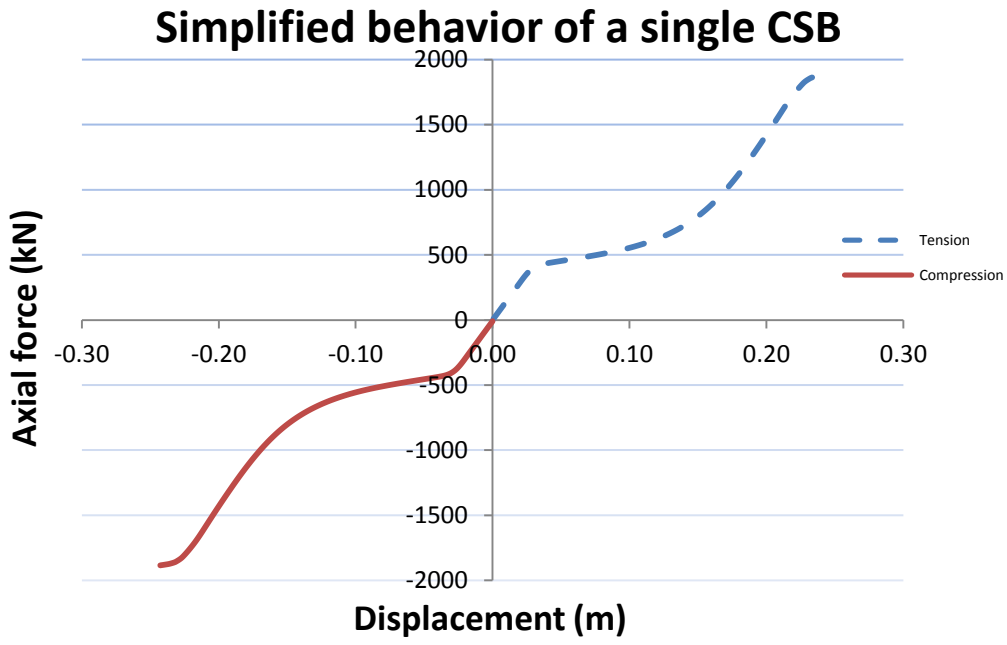

Figure 14- Simplified constitutive law of a single CSB

In order to understand the problem in a better way, we have performed a little numerical experiment that can conclude all possible configurations with their corresponding axial forces transmitted to the columns and foundations. The best configuration is the one with the lowest level of axial force transmittance into columns and foundations.

Possible configurations:

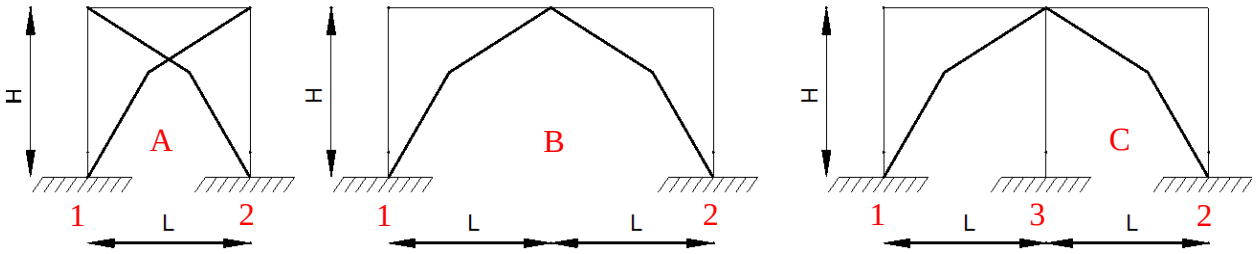

Figure 15- CSB Possible configurations

A set of 7 time history analyses (SLV EQ level) for each of the 3 configurations was performed. The average of the 7 analyses was used, as recommended by Euro code 8. The axial forces in the columns and foundations are then compared (**Table 2-Table** 3).

Configuration A shows relatively high tensile and compressive forces in columns and foundations compared to configurations B and C. Configuration C shows no axial force in columns, and the lowest amount of forces in the foundations. Configuration B shows very little axial forces in the columns when using the real model of the device, while it shows no forces when using the simplified model. As for the level of forces in the foundations, configuration B lays between the other two configurations A and C. As a result, configuration C is considered the best among all 3 when it comes to stresses in columns and foundations. However, it is not always feasible to implement due to the geometrical and architectural constraints. Configuration B can be a good solution as it produces low amount of forces in both columns and foundations. Nevertheless, the beam can be exposed to very high stresses from the bracings and this can be an

issue when the span is long. Configuration A, although it produces the highest level of forces in columns and foundations, and it is architecturally problematic, there is no interaction with the beam element. So picking the configuration depends on several factors such as the span length, the architecture's desire, and the columns capacity, especially when the braces are used as a strengthening technique, because in that case the columns are already there and have a defined capacity that we cannot exceed. Unlike in the case of design, in which we are free to define the capacity of our columns.

For configuration A, the comparison between the real model and the simplified model shows a slight difference. The simplified model is conservative in inducing tensile forces in the columns and foundations, while it underestimates the compressive forces by a maximum of 10 %. Practitioners must be aware that if they decide to use the simplified model they should take into account the underestimation of the compressive forces in the columns and the foundations. If, however, the designer decides to go with configuration B, results show that both models yield approximately the same results and thus both models are as reliable. As for configuration C, the tensile forces in some foundations are underestimated when using the simplified model, and thus the designer should be aware of that.

Configuration	Modeling	Ncol1 (kN)	Ncol2 (kN)	Ncol3 (kN)	Nfoundation1 (kN)	Nfoundation2 (kN)	Nfoundation3 (kN)
Conf. A	Real	84.03	84.81	-	192.76	189.42	-
	simplified	99.44	99.60	-	198.07	197.70	-
Conf. B	Real	3.14	3.14	-	102.64	102.02	-
	simplified	0	0	-	101.87	100.09	-
Conf. C	Real	0	0	0.18	61.76	64.30	18.67
	simplified	0	0	0	79.57	80.32	0

Table 2- tensile forces in columns and foundations induced by the braces

Configuration	Modeling	Ncol1	Ncol2	Ncol3	Nfoundation1	Nfoundation2	Nfoundation3
Conf. A	Real	-109.1	-106.9	-	-189.60	-192.21	-
	simplified	-99.60	-99.44	-	-197.70	-198.07	-
Conf. B	Real	-14.46	-14.46	-	-90.41	-92.36	-
	simplified	0	0	-	-100.09	-101.87	-
Conf. C	Real	0	0	-18.67	-82.53	-79.26	-0.18
	simplified	0	0	0	-80.32	-79.26	0

Table 3- Compressive forces in columns and foundations induced by the braces

For a better representation, the results in the table are presented using bar-chart diagrams in order to allow visual inspection of the problem.

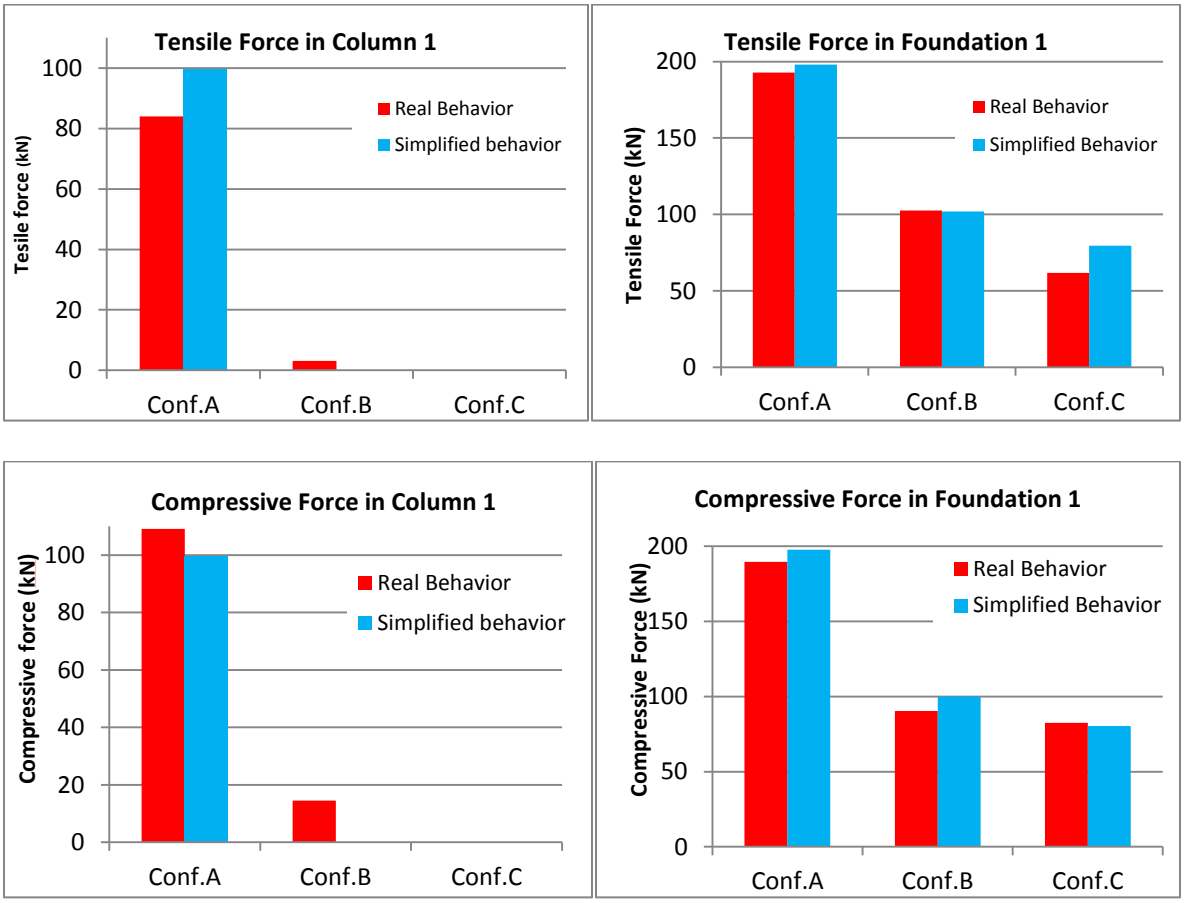

CHAPTER 2

2. THE STRUCTURE

2.1 Geometry of the structure

The building under study is the elementary school "Castle Hill" of Bisignano (CS), Italy, which was put to use in 1983 (**Figure 16**).

The building is made of three stories with a roof pavilion on the top. The geometry of the plan is rectangular. The backbone consists of four four-bay frames in the secondary direction. The frames are connected in the transverse direction by clay hollow-block floors and edge beams, while the only internal secondary beams are those that support the stairwell. The roof rests on walls and curbs, which is in turn supported by the floor of the attic (3rd level).

Figure 16- Case study structure, Bisignano (CS), Italy

The structural system is shown in **Figure 17-Figure** 20. The columns have rectangular cross sections of dimensions b = 40 cm and h = 50cm, with the long side in the direction of the

main frames. The beams that form the main frames have rectangular cross sections with b = 40 cm and h = 60 cm. The edge beams have instead b = 50 cm, h = 40 cm.

Regarding the stairwell, the side beams have square cross sections with b = h= 30 cm, unless one of those of the first layer, with dimensions of h = 60 cm, b = 25 cm. The structural thickness of the stairs landing is 15 cm.

The cover, unlike the floors of the other layers, are not straight lines from frames but instead it is made of a system of baffles perforated brick, 25 cm thick, and curbs having dimensions b = 30 cm and h = 24 cm. The baffles weigh themselves on the floor of the attic.

The slabs of the floors and the roof are clay Hollow-Block slabs with precast pre-stressed inverted RC T-beams, 12 cm wide at the base and 8 cm at the top. The joists are 12 cm wide, placed at a distance of 50 cm; the overall height of the joist, including prefabricated part and part cast in situ, is 20 cm. The thickness of the concrete slab is 4.5 cm for the floors of the first and second levels, 3 cm for those of the attic and roof. The Screed thickness is 9 cm on the floors of the first layer, 6 cm on that of the second layer, while it was absent on the attic and the roof. Finally, the thickness of the flooring is 1.5 cm on the floors of the first and second stories. The slopes are covered with roof tiles.

The geometry data were provided by the National Seismic Service of the Department of Civil Protection [SSN, and SSN in 2004, 2005 / a].

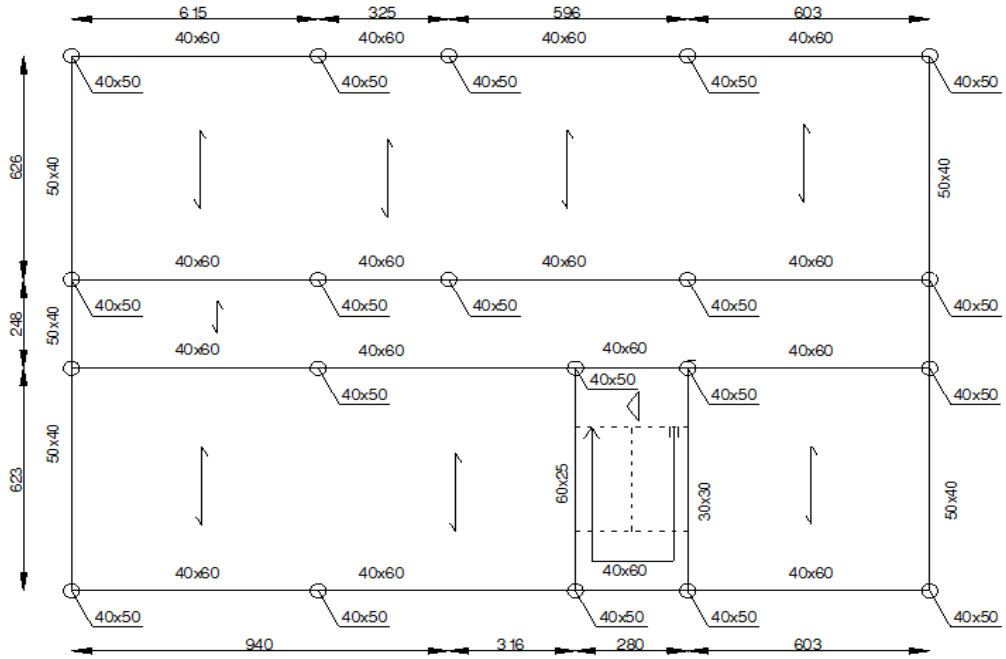

Figure 17- First level h= 3,18 m (From the upper surface of the foundation to the center of the first storey slab)

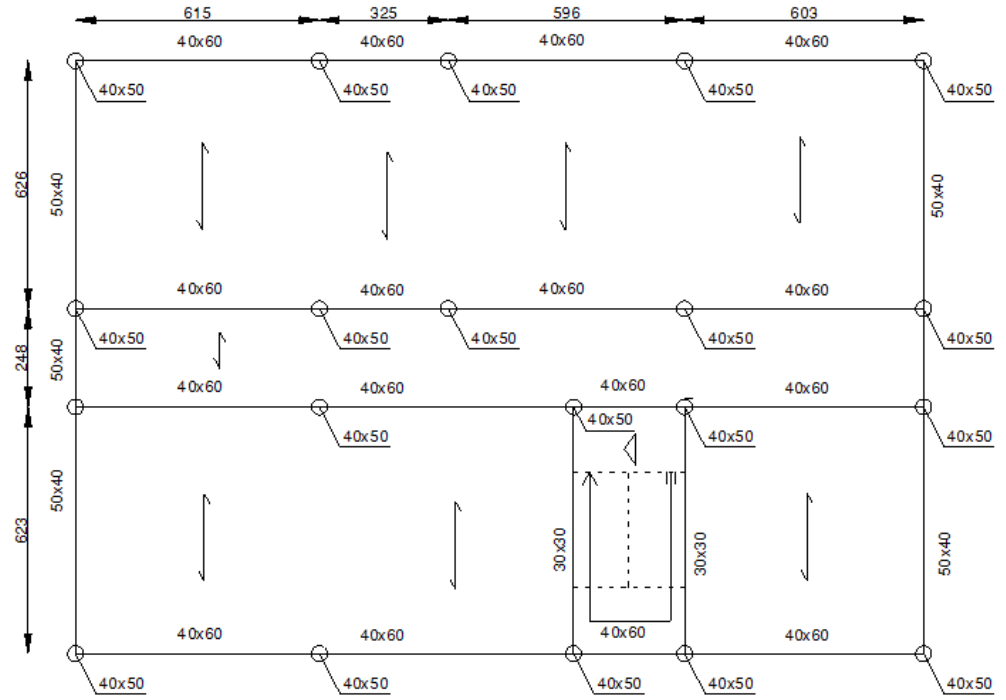

Figure 18- Second level h=6,5 m (From the upper surface of the foundation to the center of the second storey slab)

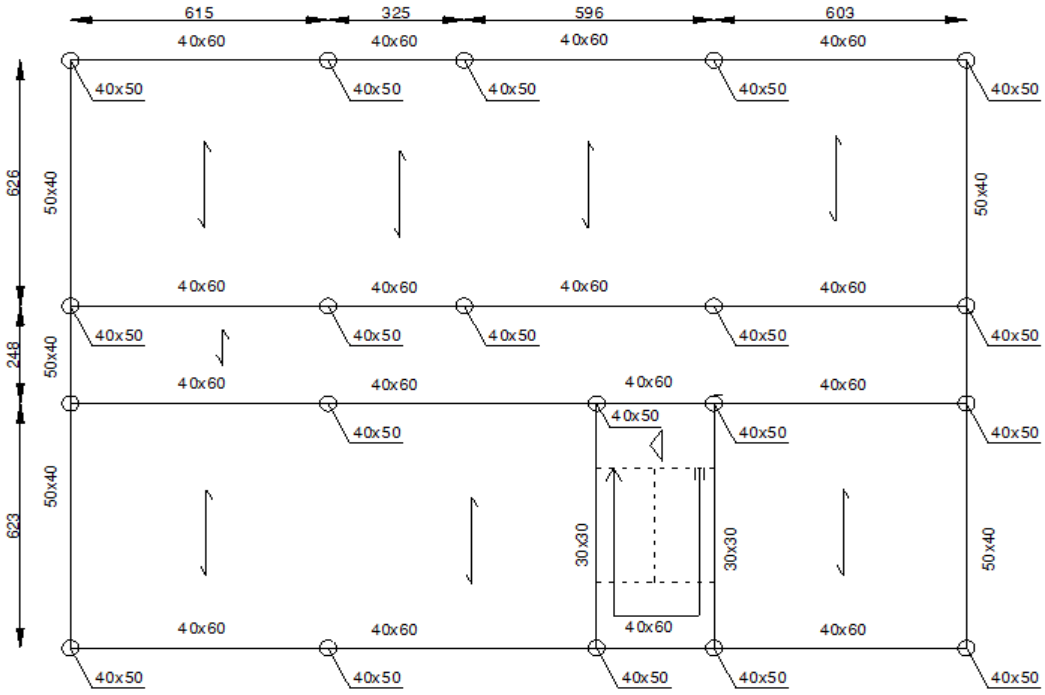

Figure 19- Third level h=9,9 m (From the upper surface of the foundation to the center of the third storey slab)

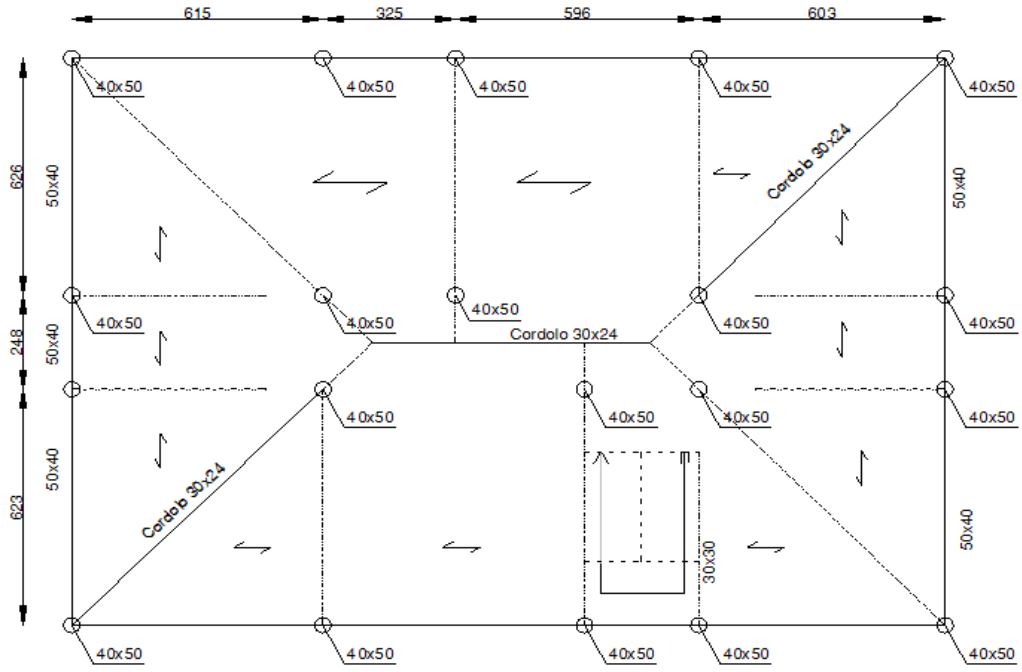

Figure 20- Roof cover h= variable, 9.9m to 11.97m (From the upper surface of the foundation)

2.2 Material

The mechanical properties of the concrete were determined by ultrasonic and rebound hammer tests, performed on 10 columns and 8 beams. The results obtained were calibrated using compression tests on core samples taken from two of the pillars and beams. The average cubic strength "R_{cm}" was found to be 35.2 MPa, The characteristic cubic strength "R_{ck}" is equal to 24.6MPa. The secant modulus of elasticity was evaluated in $E_{c,sec}$ = 25140 MPa, while the tangent modulus is estimated to be: $E_{c,tan} = 1.3.E_{c,sec} = 32682$ MPa. Finally, the bulk density of the concrete was found to be ρ_c = 2197 kg / m3; adding reinforcement, we obtain a density of about $\rho_c{}' = \rho_c + 100\ \mathrm{kg/m^3} = 2300\ \mathrm{kg/m^3}$.

As for reinforcing bars, in the absence of a specific determination of the yield stress, it is assumed that they are of steel FeB38K, with $f_{yk} = 375$ MPa.

No experimental campaigns were conducted to determine the properties of the walls forming the facades and the partitions; then, for the subsequent analysis, reference was made to the conventional values. The bulk density of the wall board, including blocks, mortar and plaster, was estimated to be $\rho_m = 1100\ \mathrm{kg/m^3}$.

The density of the mortar was assumed equal to $\rho_{sf} = 2000\ \mathrm{Kg/m^3}$, in the absence of a specific measurement. In addition, the density of plaster and tiles were assumed on the basis of usual values: $\rho_{int} = 2000\ \mathrm{Kg/m^3}$ and $\rho_{pav} = 2000\ \mathrm{Kg/m^3}$. For coating coverage (tiles, roof tiles and blankets of insulation and waterproofing), a total weight per unit area is chosen to be 1.0 kN/m^2. The clay blocks of the slab have a size b = 38 cm, h = 20 cm, L = 25 cm; the weight of one block is 0,08 kN.

The material properties have been edited by the Service Sisimico National Department of Civil Protection.

2.3 Analysis of load

2.3.1 Permanent loads on the floors

The weight is calculated for a square area having a side of 1m ($1m^2$). In this area, two joists, being the inter-axial distance = 50 cm, and eight hollow-blocks are included. On all levels the weights of the joists, the slab, and the blocks are considered. For the slabs of the first two levels, the screed, the flooring and the plaster are taken into consideration, while for the floor of the third level only the weight of the plaster is added. Finally, regarding the covering, the overloads due to the coating, which consists of mantle insulation/waterproofing and tiles are taken into account. **Figure 21-Figure** 24 illustrate the sections of the floors at the various levels.

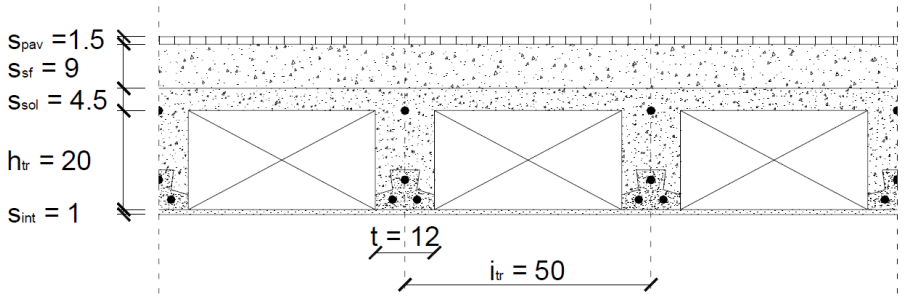

Figure 21- First floor

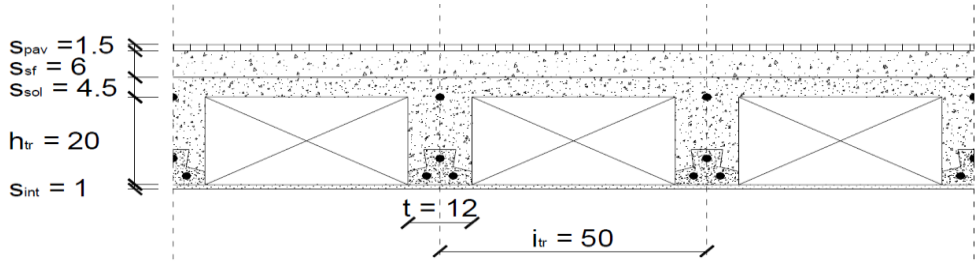

Figure 22- Second floor

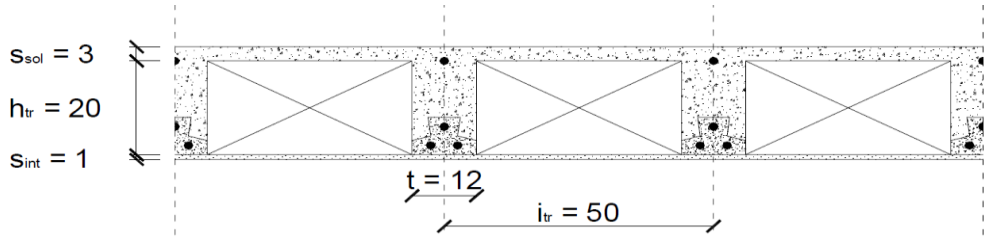

Figure 23- Third floor

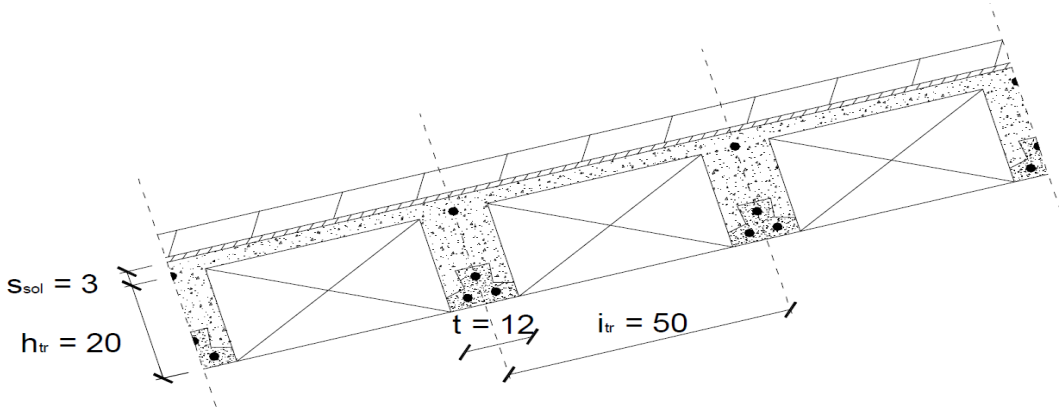

Figure 24- Roof

Level	Tiles [kN/m^2]	Screed (structural topping) [kN/m^2]	Concrete topping [kN/m^2]	Joists [kN/m^2]	Hollow Blocks [kN/m^2]	Plaster [kN/m^2]	Roof coating [kN/m^2]	Total [kN/m^2]
1	0.3	1.8	1.035	1.104	0.64	0.2	0	5.079
2	0.3	1.2	1.035	1.104	0.64	0.2	0	4.479
3	0	0	0.69	1.104	0.64	0.2	0	2.634
Roof	0	0	0.69*	1.104*	0.64*	0	1.0*	3.434*

Table 4- Permanent Loads for each floor

Table 4 shows the values of the different loads on each storey level. The asterisk (*) next to the values related to the roofing indicates that they are referred to an inclined surface at an average angle of = 15.65 °; the total load acting on a horizontal surface is obtained as:

$$p_{t,roof} = \frac{p_{t,roof}*}{\cos(i_f)} = \frac{3.434\ kN/m^2}{\cos(15.65)} = 3.566\ kN/m^2$$

Where $p_{t,roof} *$ and $p_{t,roof}$ indicate the loads respectively on a horizontal and an inclined surfaces.

2.3.2 Partition walls which are not placed over the beams

The distribution of partitions and curtain walls is shown in **Figure 25-Figure** 28. In this section, we consider only partitions that are not placed directly on the beams, which hereinafter will be also called "scattered".

The calculation is performed by multiplying the volume of the partitions of each plan by the density of the wall assumed to be 11 kN / m3, and then dividing by the area of the plan:

$$A_{floor} = 21.39m \; x \; 14.97m = 320.21 \; m^2$$

The results are summarized in **Table 5**, where for each floor the volume of the scattered partitions, its weight, and the load per unit area are reported.

Level	**Volume [m^3]**	**Weight [kN]**	**Load [kN/m^2]**
Ground	37.785	415.6383	1.298
1	17.013	187.1443	0.584
2	14.467	159.1418	0.497
3	12.285	135.1369	0.422

Table 5- Calculation of loads due to the scattered partitions

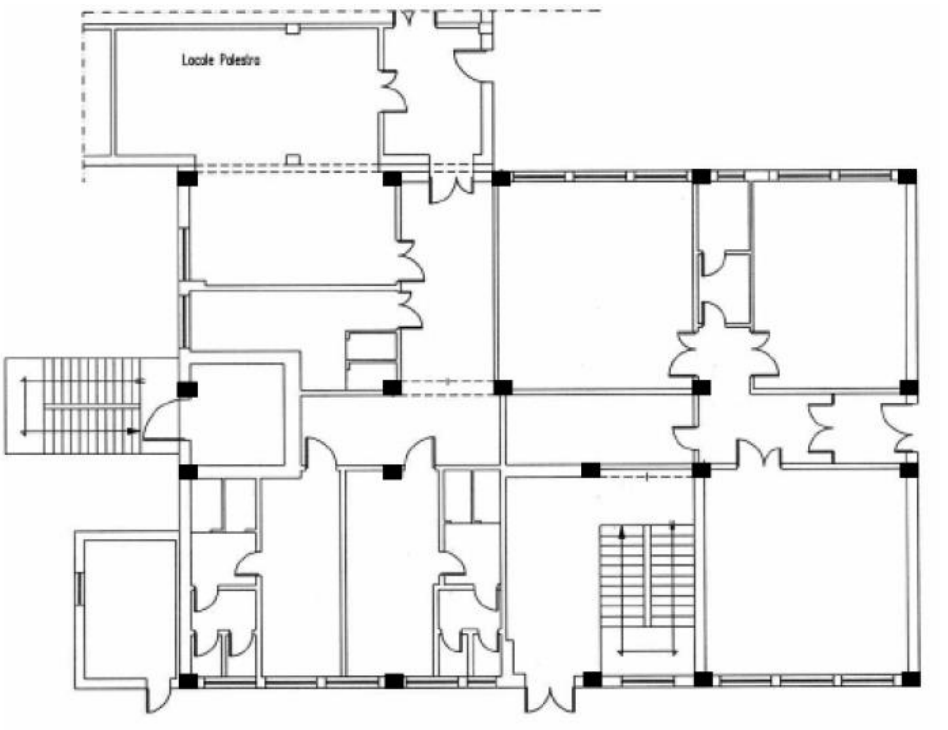

Figure 25- Ground floor

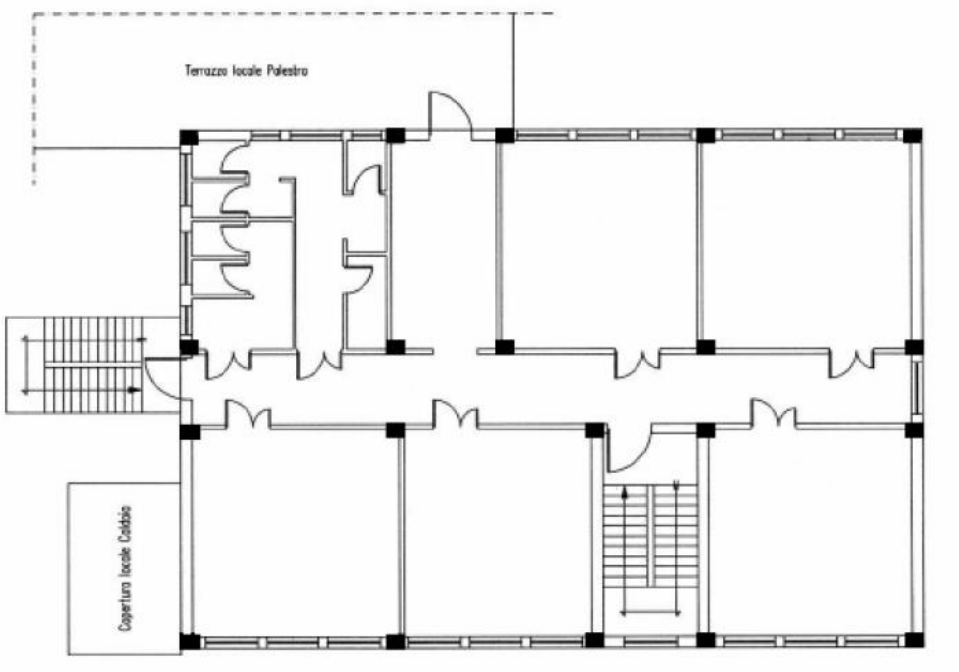

Figure 26- First floor

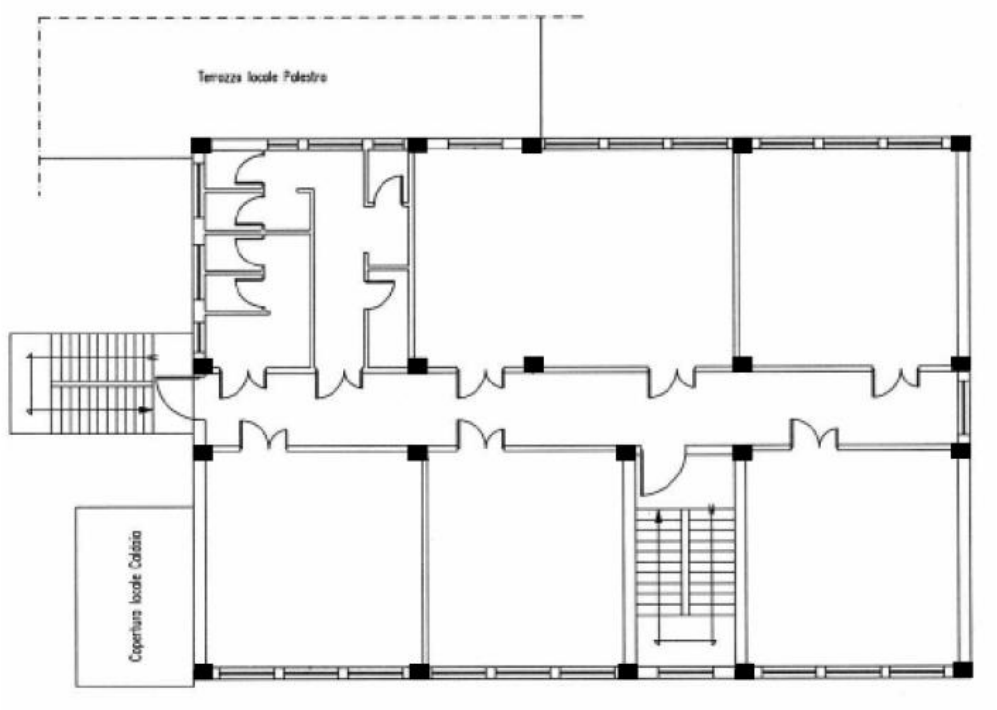

Figure 27- Second floor

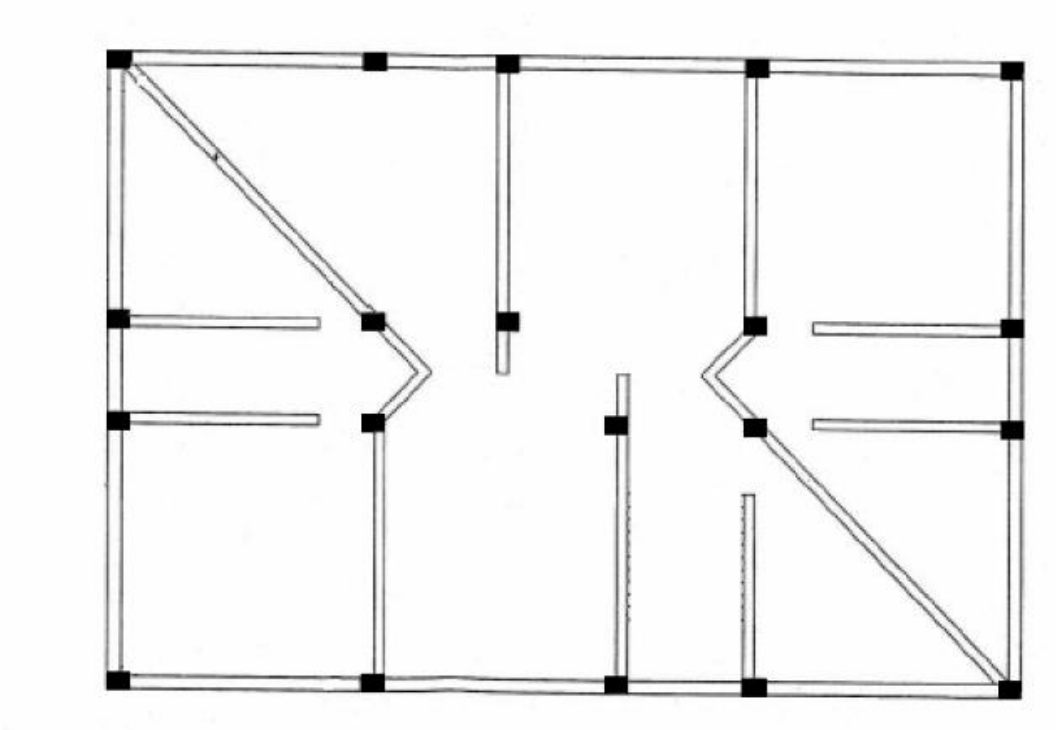

Figure 28- Attic

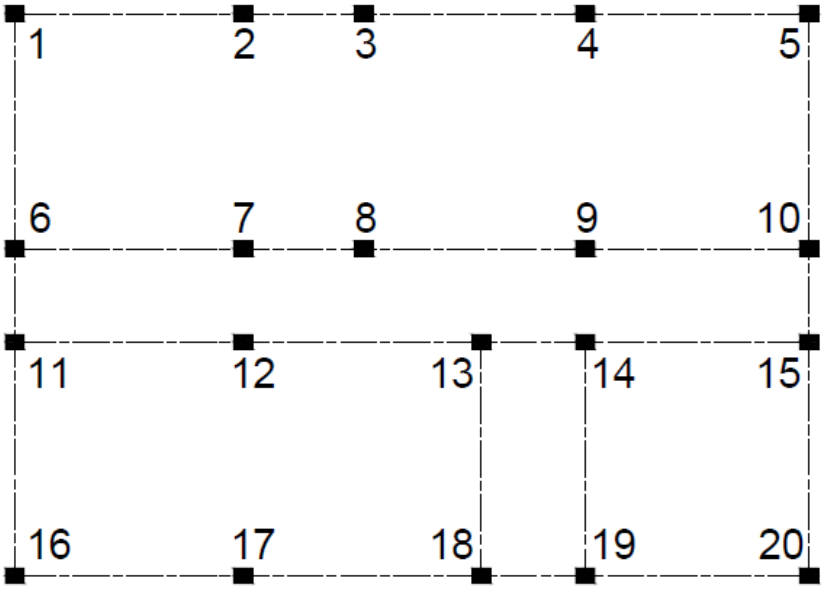

Figure 29- Numeration of the columns

2.3.3 Partition walls which are placed over the beams

Considering the plans shown in **Figure 25-Figure** 28, and by referring to the numbering of beams indicated in **Figure 29**, we calculate the linear loads of the beams due to the partition walls that are placed on them.

The loads are considered uniform and constant over the entire girder. The calculation starts with an evaluation of the volume of the walls that lay on the beams. The volume is multiplied by the unit weight of the partition walls ($11\ kN/m^3$). The result is then divided over the lengths of the beams in order to obtain the load per unit length. The results are summarized in the following tables (**Table 6-Table** 7):

Beam or Girder	Ground floor [kN/m]	First floor [kN/m]	Second floor [kN/m]
1-5	4.31	6.19	6.24
6-10	2.95	3.44	3.47
11-15	6.28	4.19	4.23
16-20	5.76	5.79	5.84
1-16	8.57	8.33	8.39
5-20	9.77	10.08	10.15
13-18	0	10.33	10.40
14-19	10.19	10.33	10.40

Table 6- Calculation of loads due to partition walls that are placed on the beams of the ground, first, and second floors.

Beams	Attic [kN/m]
6-7	1.43
9-10	1.41
11-12	1.43
14-15	1.41
13-18	2.38
14-19	1.28

Table 7-Calculation of loads due to partition walls that are placed on the beams for Attic

2.3.4 Variable loads

Variable loads are chosen according to [NTC, 2008].

First and Second Floors:

$$P_{v,L1} = P_{v,L2} = 3.0\ kN/m^2$$

The third Floor: does not present any overload, because the attic is not accessible. As for the cover, it is also not accessible.

$$P_{v,L3} = 0.5\ kN/m^2$$

2.4 Modeling

The building under investigation was modeled using the software SAP 2000 V16 (**Figure 30**). Elements of type "beam" have been used to represent beams and columns. All axes are considered coincident, though, from the available documents, it seems that the beams of the stairway are slightly eccentric, the error is 5 cm for the beam 60x25 and 10 cm for the beam 30x40.

The Young's modulus, E, is the reduced tangent bulk modulus that we have previously estimated using the secant modulus of elasticity that we obtained experimentally. . $E_c = 0.5\ x\ 32682MPa\ = 16341\ MPa$

All distributed loads have been assigned on a one-way weightless shell element, which transfers the loads in the transverse direction. Load coming from partitions that are placed directly on the top of the beams is assigned as a linear meter load on the beams. No "rigid diaphragm constraint" was assigned, but instead the correct stiffness of the slab was introduced. It was seen later that all nodes moved exactly the same amount when exposed to lateral force, so rigid diaphragm could be a good assumption for our case study.

For the sake of simplicity, the roof has not been modeled, but instead its effects have been taken as distributed loads on the 3rd level (Attic). This assumption can be correct to a high extend because the highest point of the roof is only 2 m above the attic. In the addition, the set of walls that connect the attic with the roof are relatively very stiff compared with the frame structural system. Thus, both levels can be assumed to have same seismic behavior.

The inertial effects of the seismic action shall be evaluated by taking into account the presence of the masses associated with all gravity loads appearing in the following combination of actions:

$$\sum G_{k,j}" + " \sum \psi_{E,i} \cdot Q_{k,i}$$

Where:

- $\psi_{E,i}$ is the combination coefficient for variable action i.
- $G_{k,j} = g_1 + g_2 = g_1 + dead\ load$
- $Q_{k,i} = live\ load$

The combination coefficients $\psi_{E,i}$ shall be computed from the following expression:

$\psi_{E,i} = \varphi \cdot \psi_{2,i}$

The combination coefficients $\psi_{E,i}$ take into account the likelihood of the loads $Q_{k,i}$ not being present over the entire structure during the earthquake. These coefficients may also account for a reduced participation of masses in the motion of the structure due to the non-rigid connection between them. According to Euro code 2:

$\varphi = 1$ for Roof and 0.8 for storeys with correlated occupancies

$\psi_{2,i} = 0.3\ for\ domestic\ areas\ \ and\ 0\ for\ snow\ with\ altidute < 1000m$

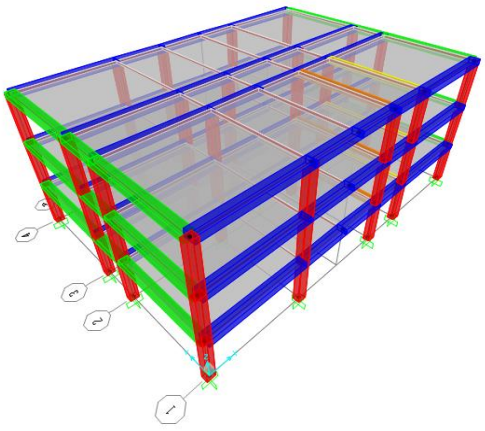

Figure 30- Modeling of the building under investigation using SAP2000 v17

2.5 Modal Analysis

According to Euro code 2 [8]:

1) This type of analysis shall be applied to buildings, which do not satisfy the conditions given in 4.3.3.2.1 (2) for applying the lateral force method of analysis.
2) The response of all modes of vibration contributing significantly to the global response shall be taken into account.
3) The requirements specified in paragraph (2) may be deemed to be satisfied if either of the following can be demonstrated:

   - The sum of the effective modal masses for the mo [8]des taken into account amounts to at least 90% of the total mass of the structure.

   - All modes with effective modal masses greater than 5% of the total mass are taken into account.

MODE	Frequency (Hz)	Period (sec)	Modal Participating Mass Ratios		
			Ux	Uy	Rz
1	1.2656	0.790165	1.02E-09	0.7969	0.00044
2	1.8383	0.543966	0.00043	0.00046	0.83382
3	1.9918	0.502047	0.82938	2.25E-07	0.00043
4	4.2996	0.23258	6.25E-11	0.15325	0.00011
5	5.7004	0.175427	6.12E-05	9.56E-05	0.12789
6	6.2713	0.159456	0.13314	3.26E-08	0.00005658
		$\sum =$	0.963011	0.950706	0.96274658

Table 8- Frequencies, periods, and participating mass rations for the forst 6 modes

Following the Euro Code, it is enough to consider the first 6 modes because the sums of the effective modal masses for those 6 modes amount 96%, 95%, and 96% in Ux, Uy, and Rz direction respectively (**Table 8**).

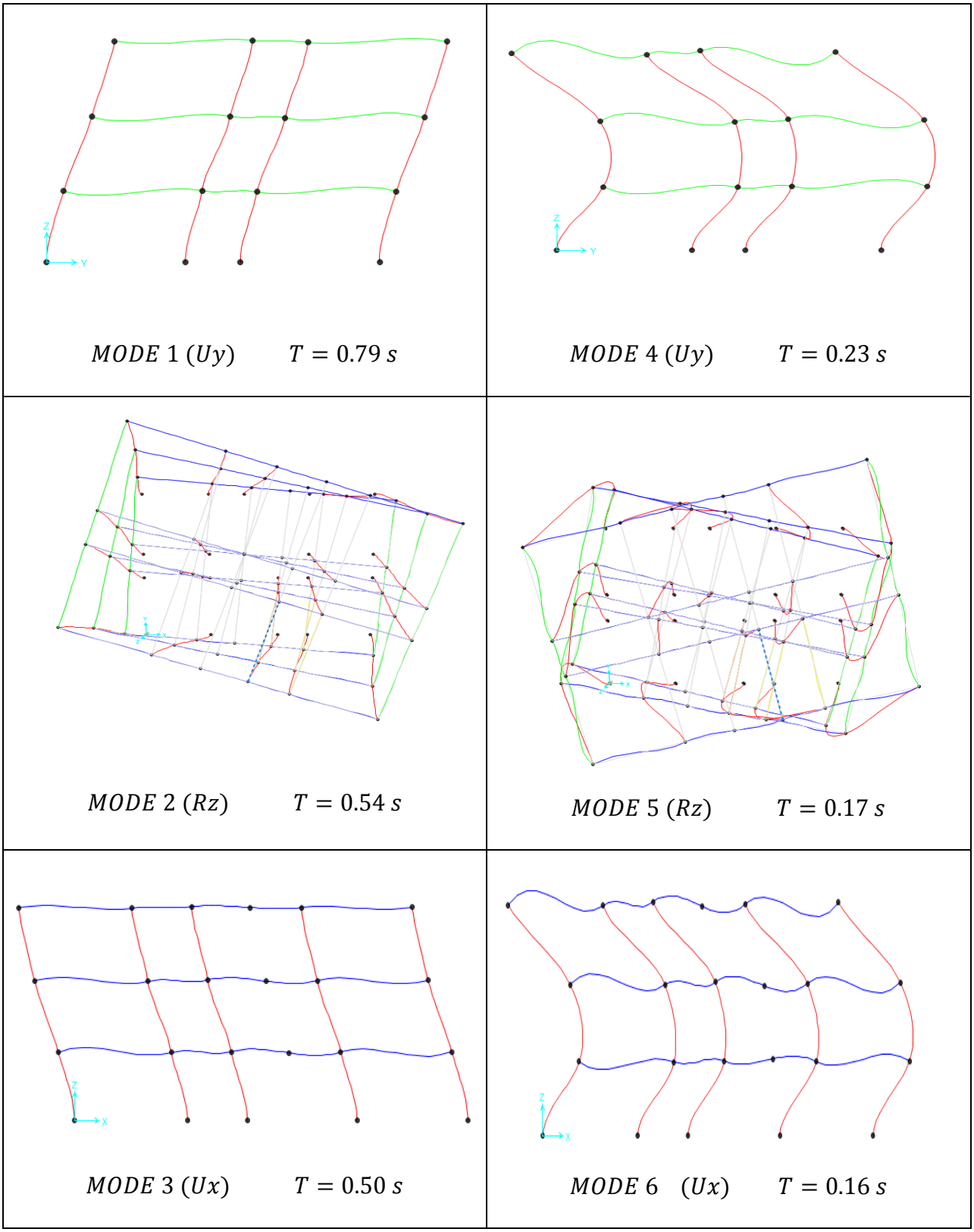

Figure 31- Modal shapes and periods for the first 6 modes.

2.6 Elastic Response spectra (Serviceability and Ultimate)

For the horizontal components of the seismic action, the elastic response spectrum Se(T) is defined by the following expressions:

$$0 \le T \le T_B \ \rightarrow \ S_e(T) = a_g \cdot S \cdot \eta \cdot F_0 \cdot \left[\frac{T}{T_B} + \frac{1}{\eta \cdot F_0} \cdot (1 - \frac{T}{T_B})\right]$$

$$T_B \le T \le T_C \ \rightarrow \ S_e(T) = a_g \cdot S \cdot \eta \cdot F_0$$

$$T_C \le T \le T_D \ \rightarrow \ S_e(T) = a_g \cdot S \cdot \eta \cdot F_0 \cdot \left[\frac{T_C}{T}\right]$$

$$T_D \le T \le 4\ s \rightarrow \ S_e(T) = a_g \cdot S \cdot \eta \cdot F_0 \cdot \left[\frac{T_C \cdot T_D}{T^2}\right]$$

Where:

- $S_e(T) = elastic\ response\ spectrum;$
- $T = vibration\ period;$
- $a_g = design\ ground\ acceleration;$
- $T_B, T_C = limits\ of\ the\ constant\ spectral\ acceleration\ branch;$
- $T_D = value\ defining\ the\ beginning\ of\ the\ constant\ displacement\ response\ range\ of\ the\ spectrum$
- $S = soil\ factor;$
- $\eta = damping\ correction\ factor\ with\ reference\ value = \sqrt{\frac{10}{(5+\xi)}};\ if\ \xi = 5\%, then\ \eta = 1$
- $F_0 = maximum\ value\ of\ the\ amplification\ factor\ of\ the\ spectrum\ in\ the\ horizontal\ acceleration, takes\ into\ account\ the\ structural\ amplification\ (F_0 \ge 2{,}2)$

- **Normal life [years]:**

  $V_N \ge 50$ For normal building, bridges, normal infrastructures, normal dams, etc.

- **Occupancy factor:** $C_U = 1.5$ for Class III: Buildings with large crowds (school)
- **Reference life [years]:** $V_R = V_N \cdot C_U = 50\ x\ 1.5 = 75\ years$
- **Coordinates of the site:** latitude 39,512 ° N Longitude 16,286 ° E.
- **Soil category:** B **Topographical category**: T1

The building under study is the elementary school "Castle Hill" of Bisignano (CS), Italy. According to the website: http://www.acca.it, **Table 9** Gives the seismic hazard parameters for the four limit states in the city of Bisignano for structures with a reference life equal to 75 years.

Parameters of Seismic Hazard				
Limit State	**Return Period** $Tr\ [years]$	a_g/g [-]	F_0 [-]	T_c^* [s]
Fully Operational	45	0.089	2.29	0.296
Damage	75	0.116	2.286	0.321
Life safety	712	0.323	2.43	0.385
Near collapse	1462	0.426	2.48	0.419

Table 9- Seismic parameters for the location "Bisignano, Italy"

In this work, we are interested in studying the Damage LS (serviceability) and Life safety LS (Ultimate). **Figure 32** shows the elastic response spectra that correspond to the 2 limit sates.

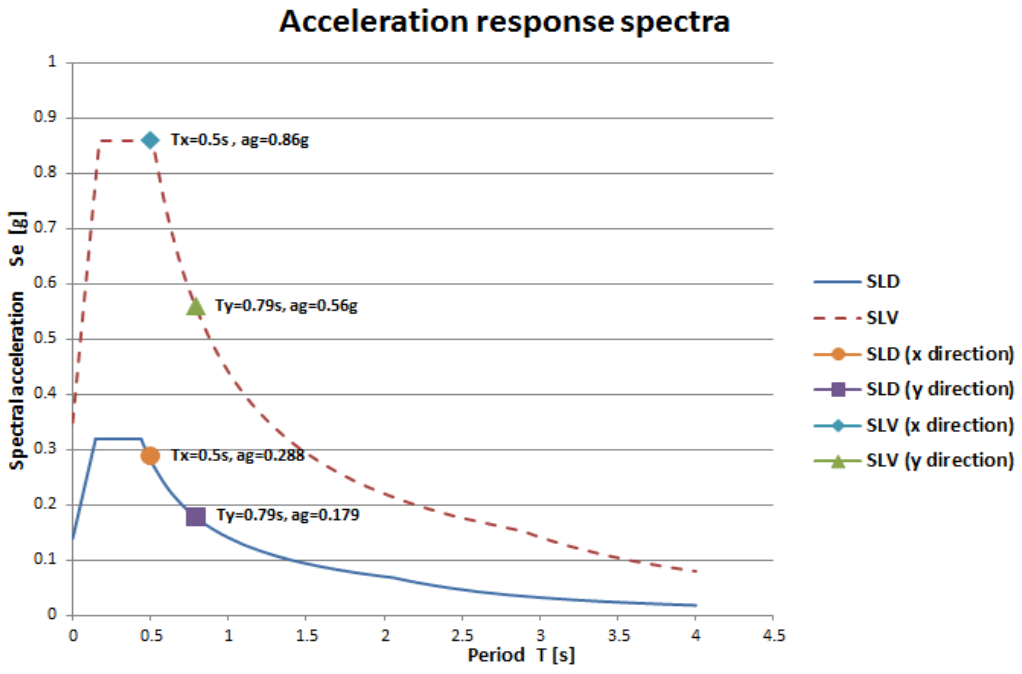

Figure 32- Response spectra for Damage (serviceability) and Life safety (Ultimate) Limit states

CHAPTER 3

3. METHODS OF ANALYSIS

Two types of analysis are performed in this work. The dynamic time-history and The static pushover analyses. **Figure 33** shows a typical reinforced concrete structure behavior (cracking, yielding, and failure).

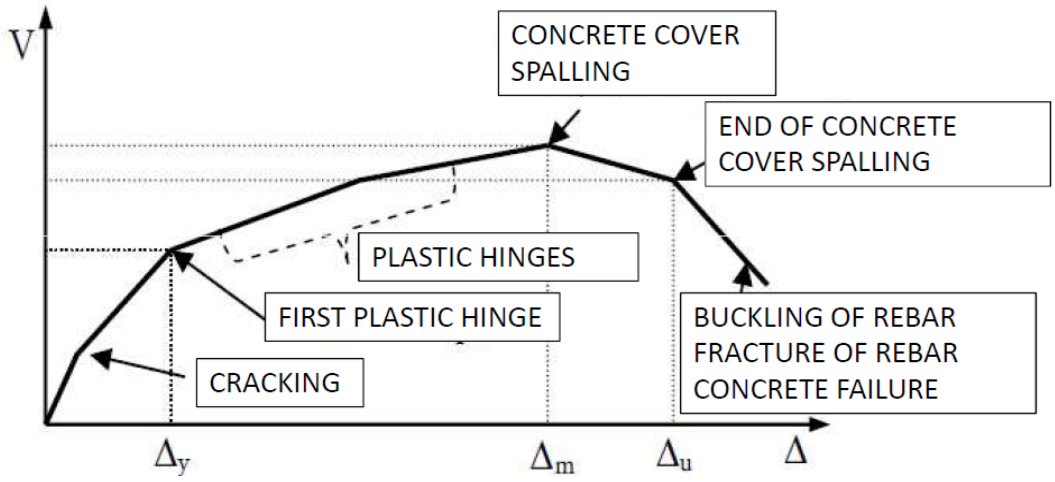

Figure 33- A schematic representation of the non-linear behavior of RC frame structures.

3.1 Nonlinear Dynamic (Time-history) analysis

Nonlinear dynamic analysis utilizes the combination of ground motion records with a detailed structural model, therefore it is capable of producing results with relatively low uncertainty. In nonlinear dynamic analyses, the detailed structural model subjected to a ground-motion record produces estimations of component deformations for each degree of freedom in the model, and the modal responses are combined using schemes such as the square-root-sum-of-squares.

In non-linear dynamic analysis, the non-linear properties of the structure are considered as part of a time domain analysis. This approach is the most rigorous, and is required by some

building codes for buildings of unusual configuration or of special importance. However, the calculated response can be very sensitive to the characteristics of the individual ground motion used as seismic input; therefore, several analyses are required using different ground motion records to achieve a reliable estimation of the Probabilistic distribution of structural response. Since the properties of the seismic response depend on the intensity, or severity, of the seismic shaking, a comprehensive assessment calls for numerous nonlinear dynamic analyses at various levels of intensity to represent different possible earthquake scenarios [9]

3.1.1 Codes regulations

According to Paragraph 4.3.3.4.3 in Euro code 8 [10], If the response is obtained from at least 7 nonlinear time-history analyses with ground motions in accordance with 3.2.3.1, the average of the response quantities from all of these analyses should be used as the design value of the action effect Ed. Otherwise, the most unfavorable value of the response quantity among the analyses should be used as Ed. The choice of the accelerograms should be representative of the actual seismicity of the site, taking into account the characteristics of the seismic source, the conditions of the site, the magnitude, the distance from the source, and the expected maximum ground (PGA).

Seismic motion may be made by using artificial accelerograms and recorded or simulated accelerograms. As we lack real data (recorded accelerograms), we will obtain the ground motion through a set of artificial accelerograms.

- Rules to consider when defining artificial accelerograms:

1) Artificial accelerograms shall be generated so as to match the elastic response spectra given in 3.2.2.2 and 3.2.2.3 for 5% viscous damping (ξ = 5%).
2) The duration of the accelerograms shall be consistent with the magnitude and the other relevant features of the seismic event underlying the establishment of a_g.
3) When site-specific data are not available, the minimum duration Ts of the stationary part of the accelerograms should be equal to 10 s.
4) The suite of artificial accelerograms should observe the following rules:
    a) A minimum of 3 accelerograms should be used (average value is not allowed);
    b) The mean of the zero period spectral response acceleration values (calculated from the individual time histories) should not be smaller than the value of ag for the site in question.
    c) in the range of periods between 0,2 T1 and 2 T1, where T1 is the fundamental period of the structure in the direction where the accelerogram will be applied; no value of the mean 5% damping elastic spectrum, calculated from all time histories, should be less than 90% of the corresponding value of the 5% damping elastic response spectrum. (EC8)

For our case study, we will run two groups of accelerograms, one for the serviceability limit state (Damage) and the other for the Ultimate limit state (Life safety). Each group is made up of 7 accelerograms; in this case, we will be able to refer to the average of the maximum values obtained from each individual analysis. If we, however, run less than seven analyses, it will be necessary to take the effect of the worst condition. Nevertheless, we steel need to use a minimum of three accelerograms for each group.

3.1.2 Constructing the Accelerograms

The design spectrum to be used for dynamic analysis of the school "Collina Castello" was built by the SIMQKE_GR software v2.7, made available by Prof. Piero Gelfi, University of Brescia, Italy. SIMQKE_GR generates statistically independent accelerograms, performs a baseline correlation on the generated motions to ensure zero final ground velocity, and calculates response spectra. One of the options in the program generates ground motions whose response spectra "match", or are compatible with, a set of specified smooth response spectra. The basis for the spectrum compatible motion generation is the relationship between the response spectrum values for arbitrary damping and the "expected" Fourier amplitudes of the ground motion (Vanmarcke, 1976). The earthquakes are synthesized by superimposing sinusoidal components with pseudo-random phase angles, and by multiplying the resulting stationary trace by a user specified function representing the variation of ground motion intensity with time. The program SIMQKE also has the capability to adjust, by iteration, the ordinates of the spectral density function to improve the agreement between computed and specified response spectra. Even without the last step, the average response spectrum (of a set of simulated motions) will match the smooth target spectrum very closely [11].

Using the software SIMQKE_GR we were able to obtain 2 groups of response spectra, each corresponding to one of the 2 limit states (SLD and SLV). Each group contains 7 non-smooth spectra matching the corresponding smooth response spectrum that we already obtained in section (2.6). In addition, and by using the same software, we were able to obtain 2 groups of time-history, with 7 accelerograms each. Those accelerograms will be used for performing non-linear time-history analysis.

3.1.2.1 Response spectra and Accelerograms for SLD

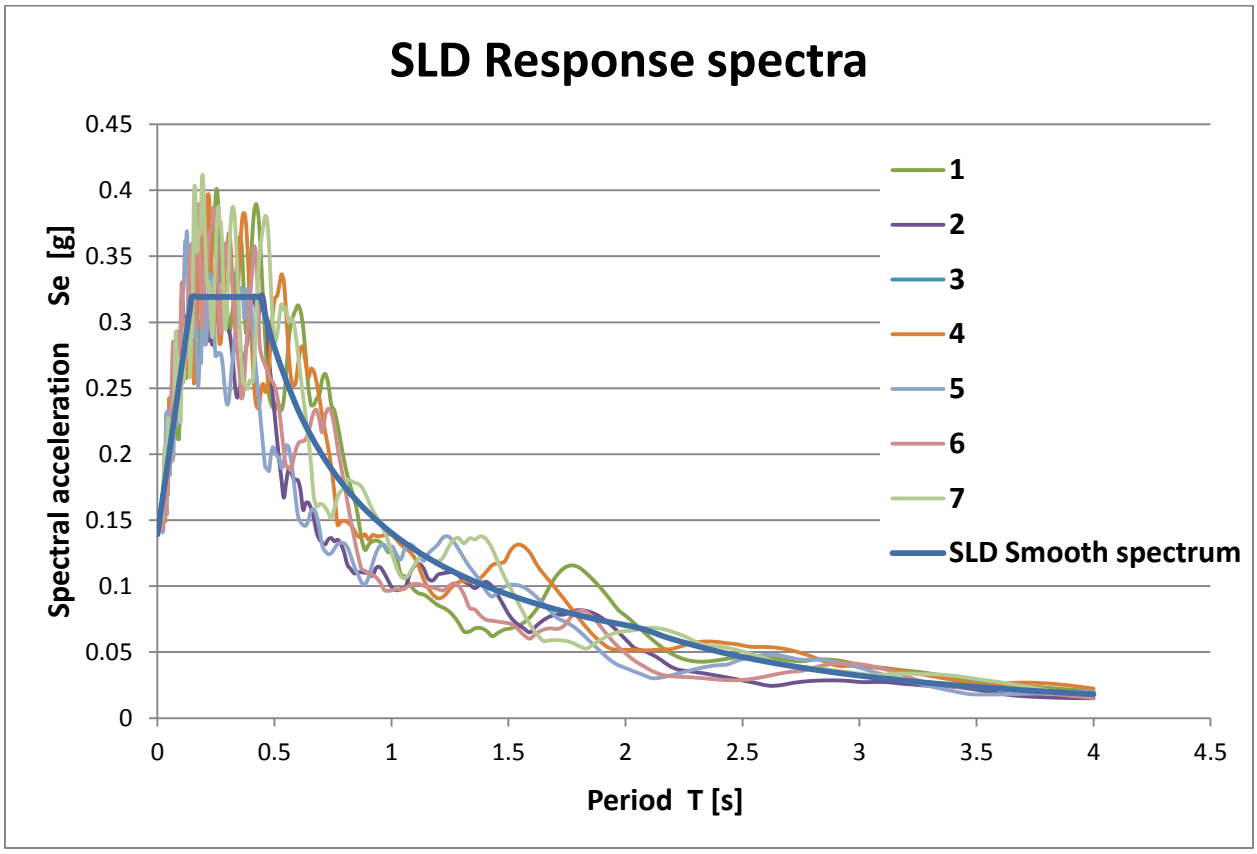

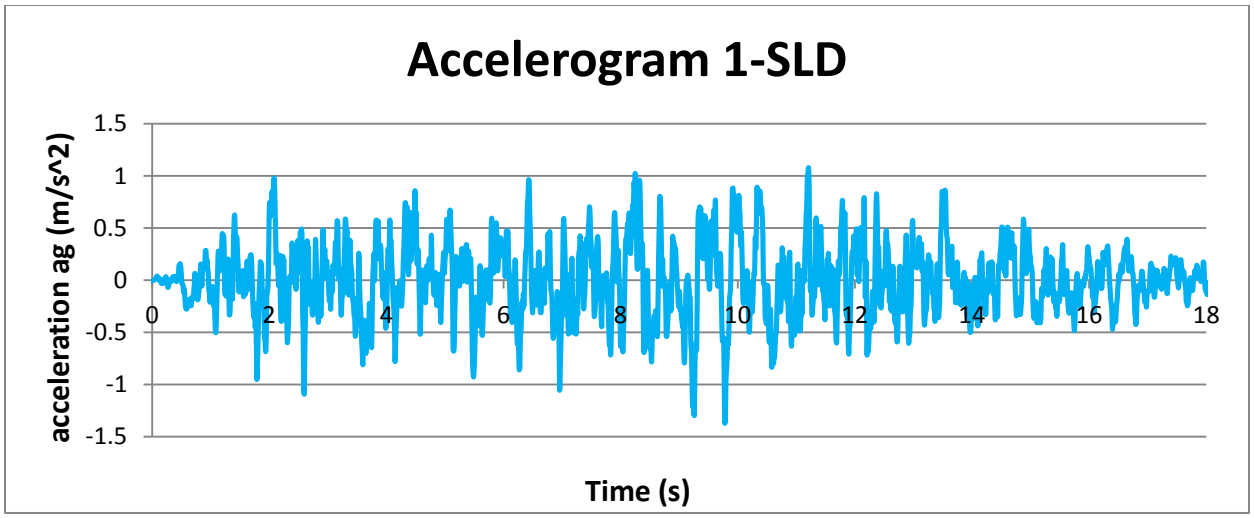

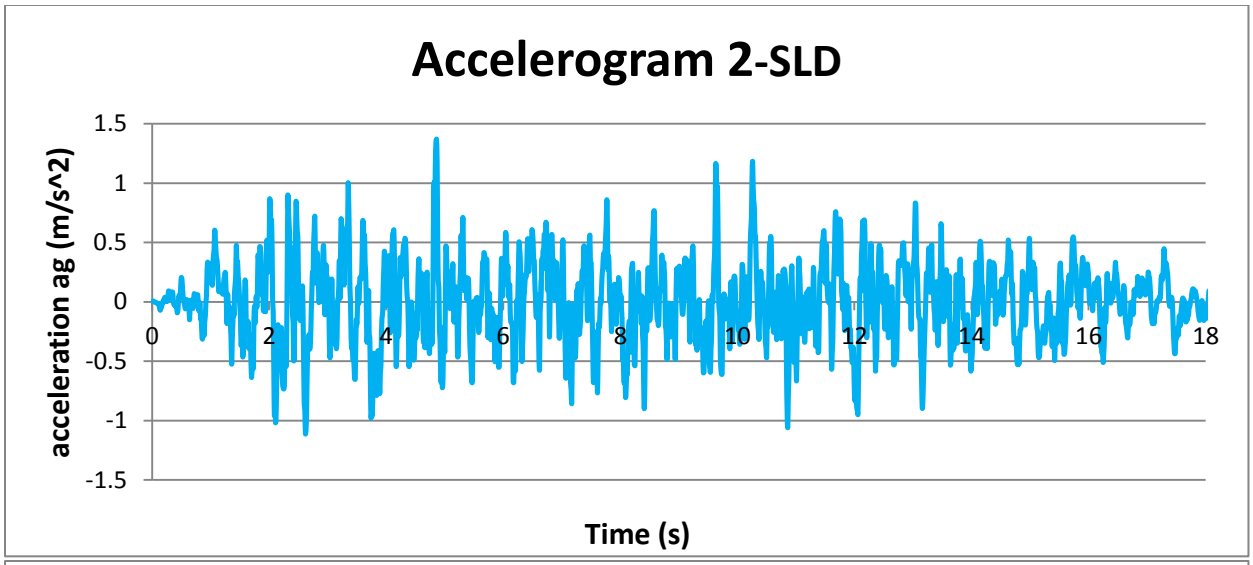
Accelerogram 2-SLD
acceleration ag (m/s^2)
1.5
1
0.5
0
-0.5
-1
-1.5
0
2
4
6
8
10
12
14
16
18
Time (s)

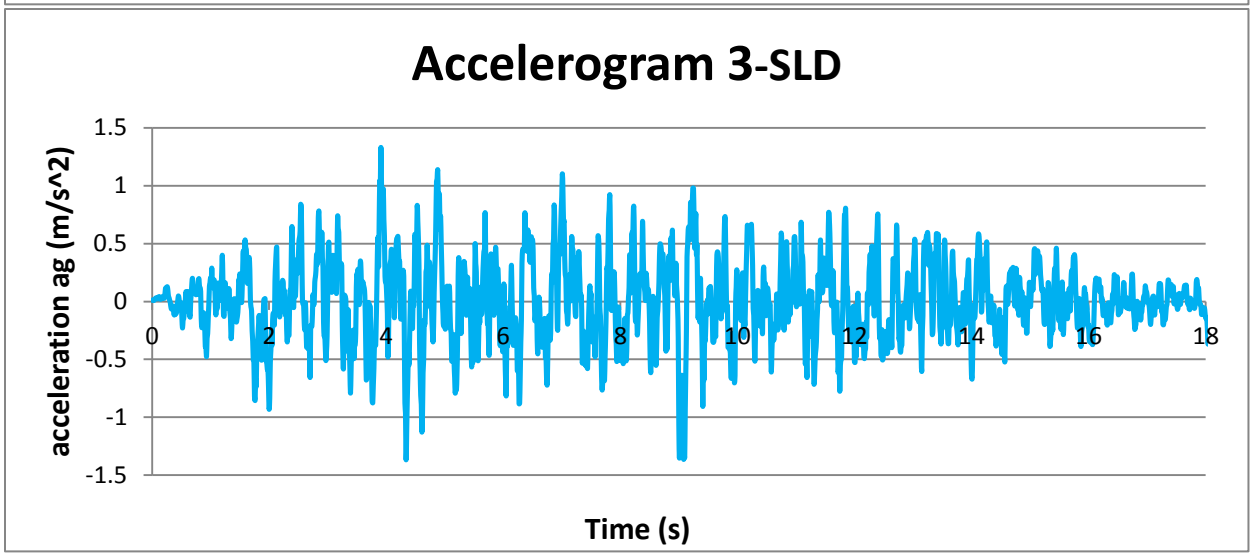
Accelerogram 3-SLD
acceleration ag (m/s^2)
1.5
1
0.5
0
-0.5
-1
-1.5
0
2
4
6
8
10
12
14
16
18
Time (s)

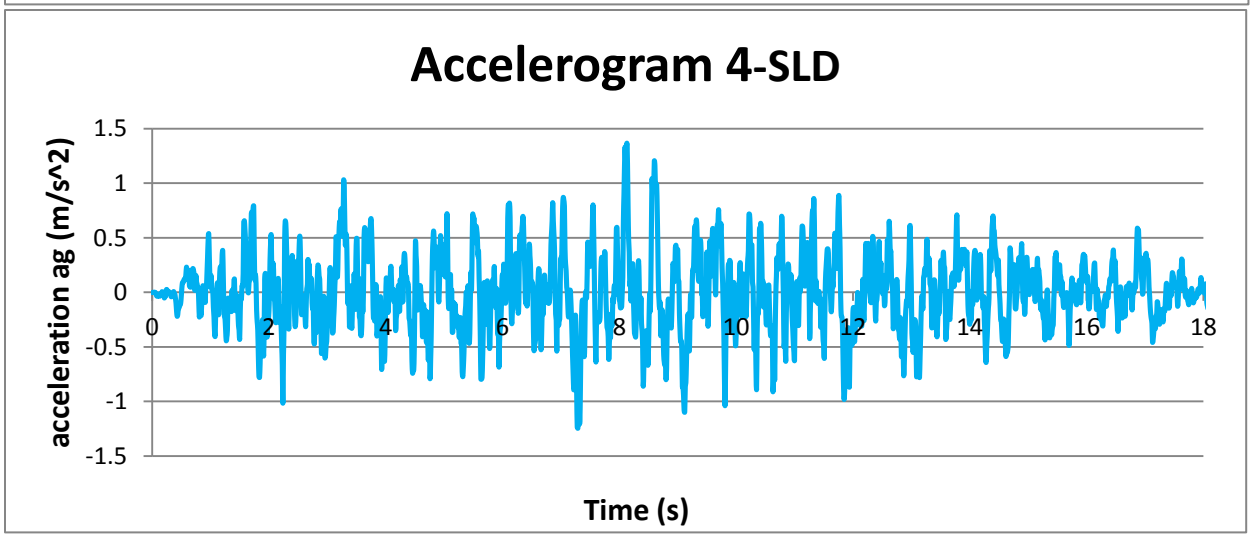
Accelerogram 4-SLD
acceleration ag (m/s^2)
1.5
1
0.5
0
-0.5
-1
-1.5
0
2
4
6
8
10
12
14
16
18
Time (s)

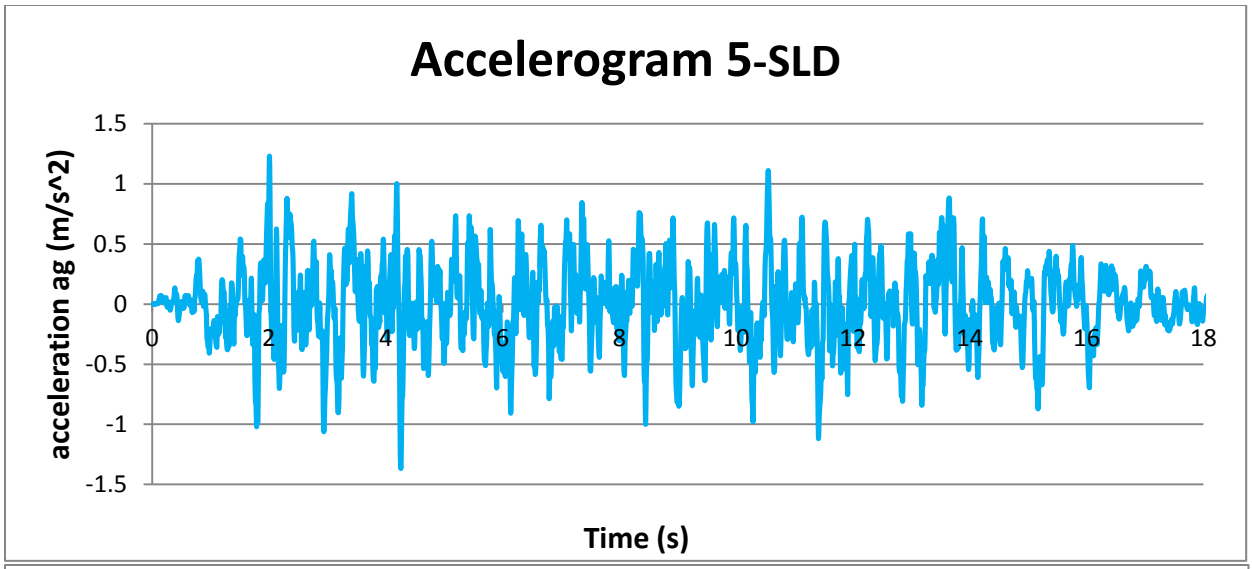
Accelerogram 5-SLD
acceleration ag (m/s^2)
1.5
1
0.5
0
-0.5
-1
-1.5
0
2
4
6
8
10
12
14
16
18
Time (s)

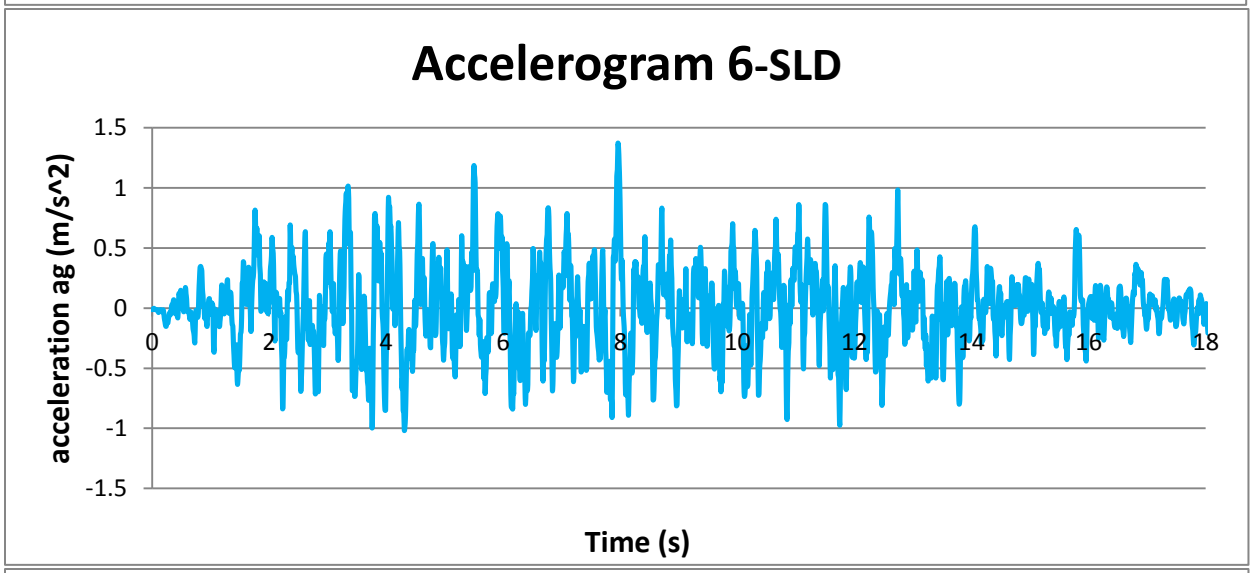
Accelerogram 6-SLD
acceleration ag (m/s^2)
1.5
1
0.5
0
-0.5
-1
-1.5
0
2
4
6
8
10
12
14
16
18
Time (s)

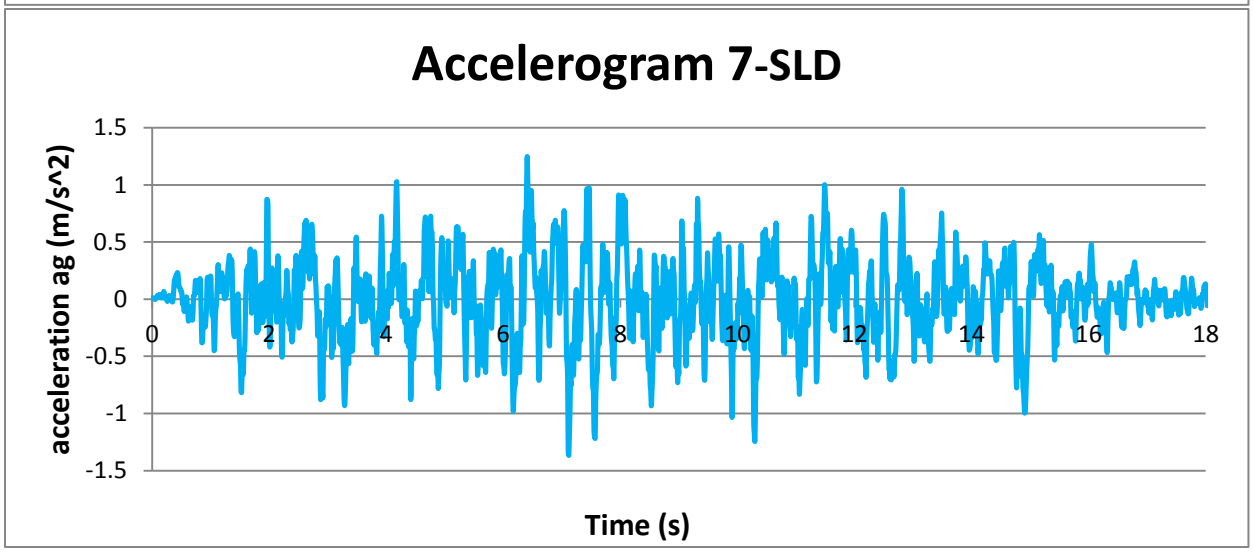
Accelerogram 7-SLD
acceleration ag (m/s^2)
1.5
1
0.5
0
-0.5
-1
-1.5
0
2
4
6
8
10
12
14
16
18
Time (s)

3.1.2.2 Response spectra and Accelerograms for SLV

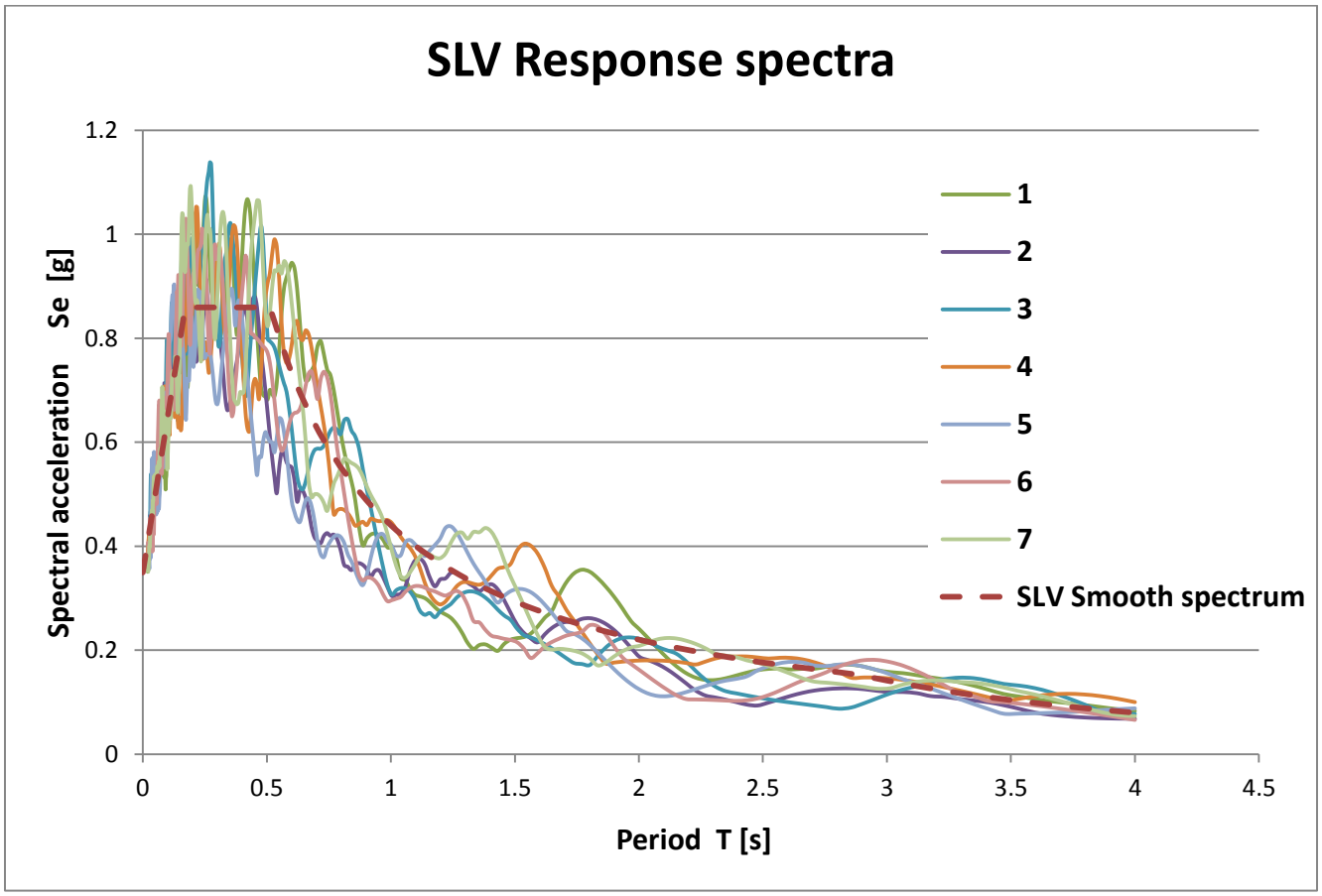

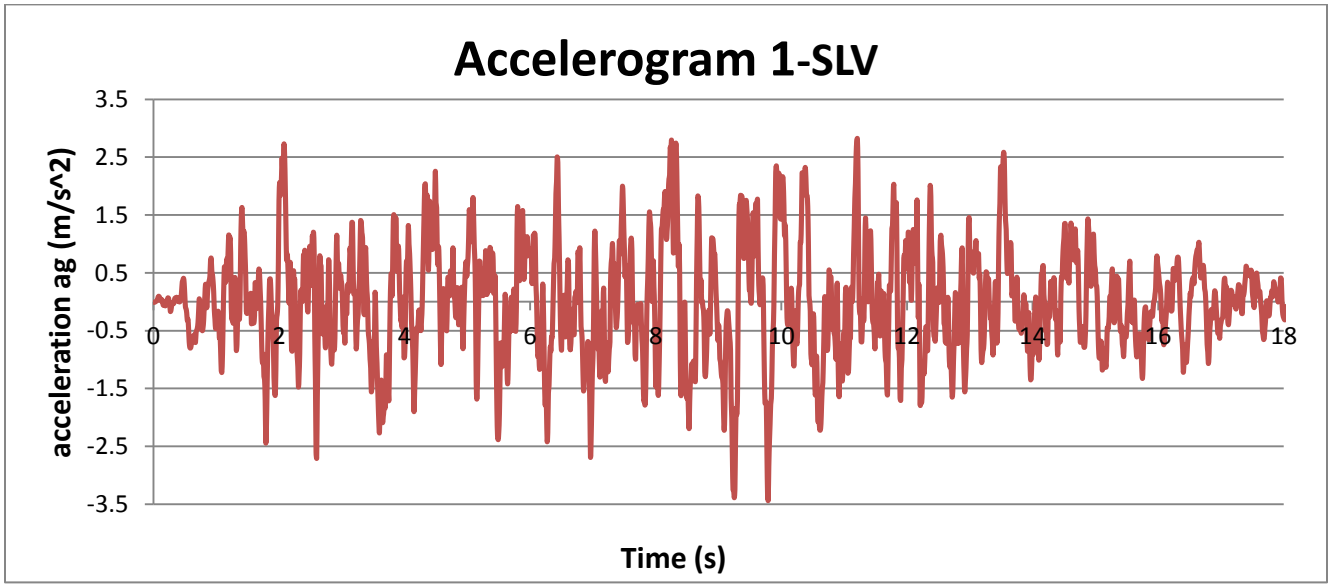

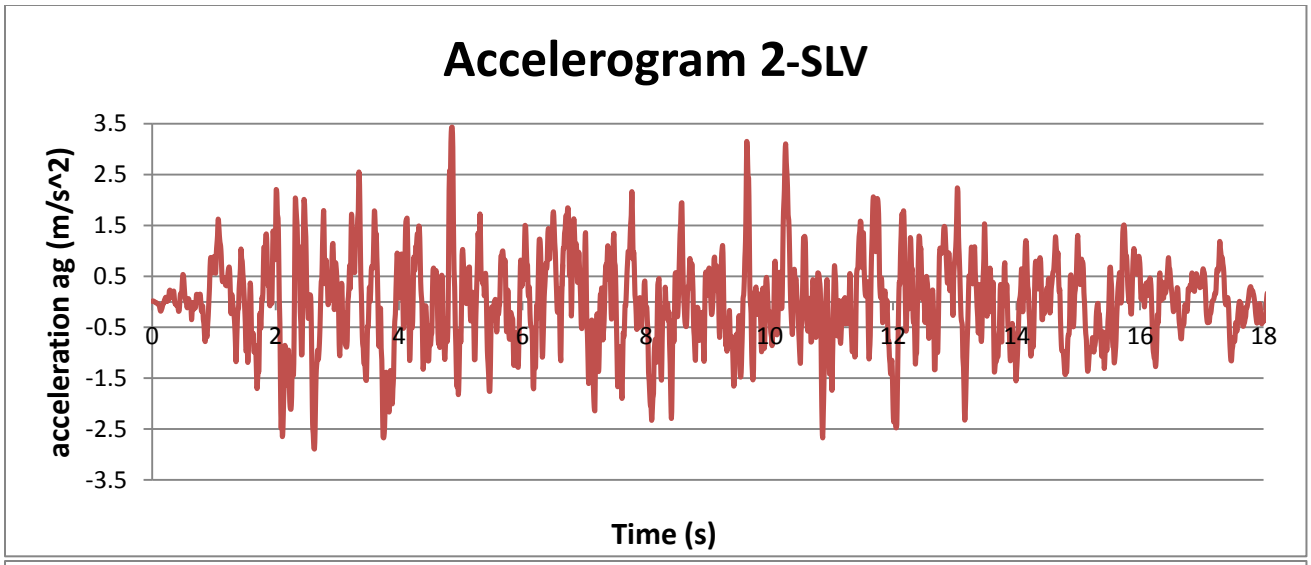
Accelerogram 2-SLV
acceleration ag (m/s^2)
3.5
2.5
1.5
0.5
-0.5
-1.5
-2.5
-3.5
0
2
4
6
8
10
12
14
16
18
Time (s)

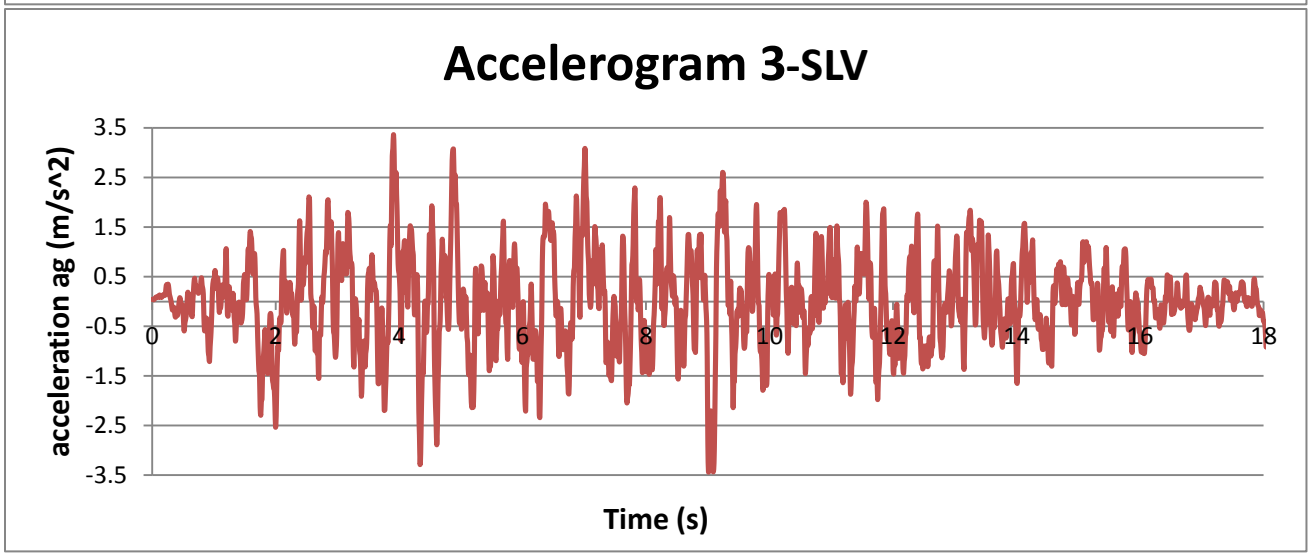
Accelerogram 3-SLV
acceleration ag (m/s^2)
3.5
2.5
1.5
0.5
-0.5
-1.5
-2.5
-3.5
0
2
4
6
8
10
12
14
16
18
Time (s)

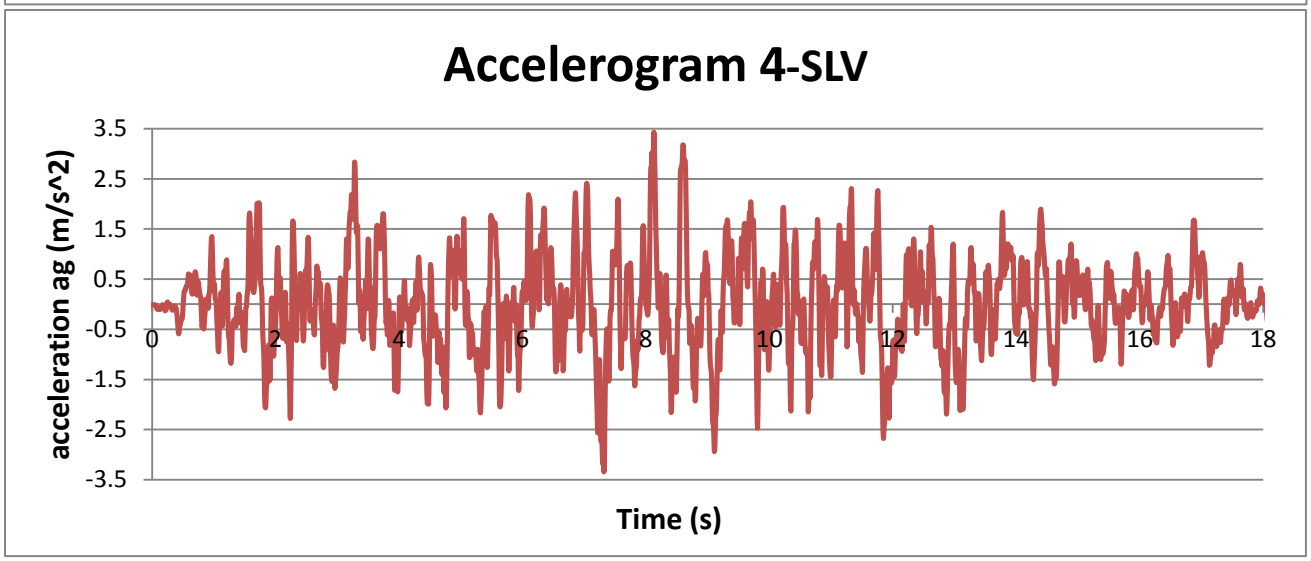
Accelerogram 4-SLV
acceleration ag (m/s^2)
3.5
2.5
1.5
0.5
-0.5
-1.5
-2.5
-3.5
0
2
4
6
8
10
12
14
16
18
Time (s)

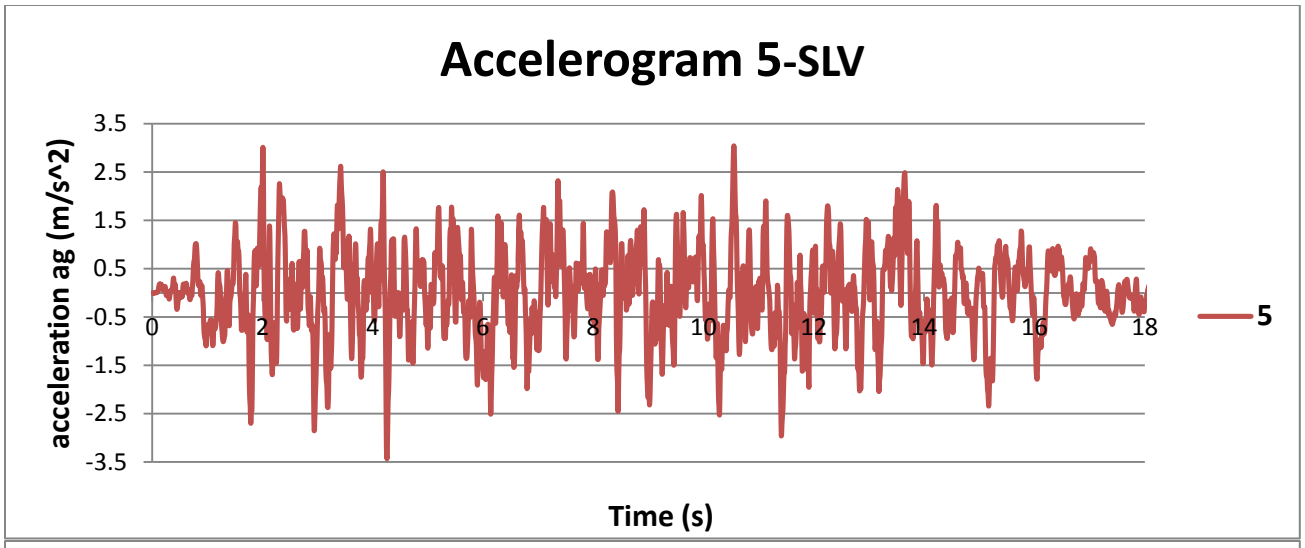
Accelerogram 5-SLV
acceleration ag (m/s^2)
3.5
2.5
1.5
0.5
-0.5
-1.5
-2.5
-3.5
0
2
4
6
8
10
12
14
16
18
Time (s)
5

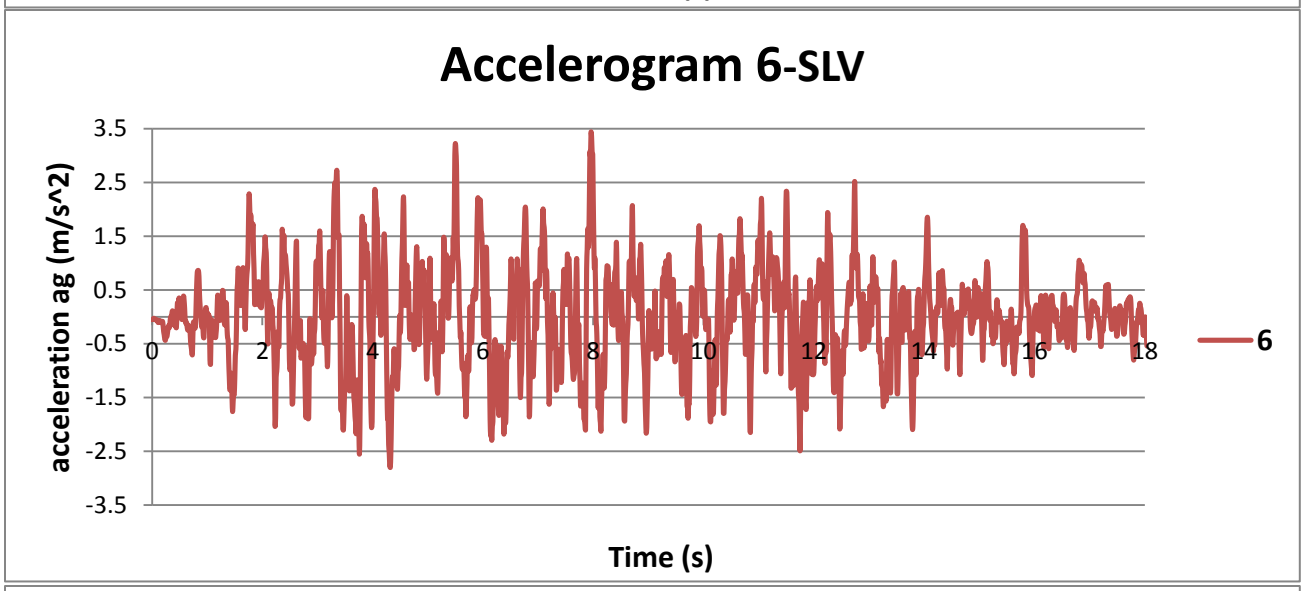
Accelerogram 6-SLV
acceleration ag (m/s^2)
3.5
2.5
1.5
0.5
-0.5
-1.5
-2.5
-3.5
0
2
4
6
8
10
12
14
16
18
Time (s)
6

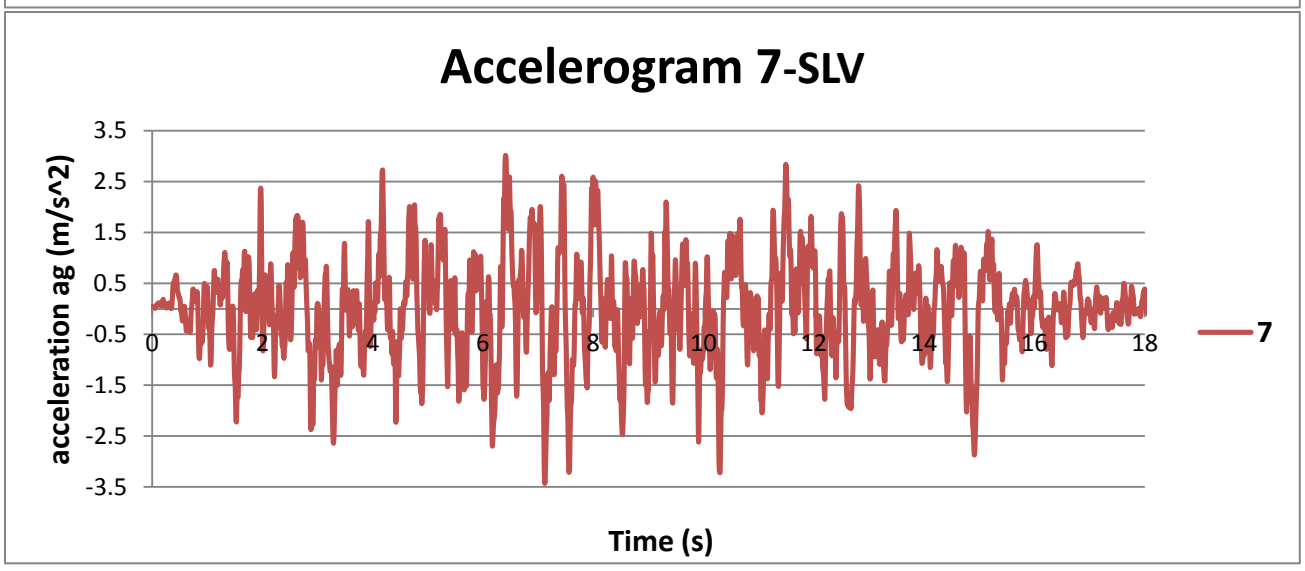
Accelerogram 7-SLV
acceleration ag (m/s^2)
3.5
2.5
1.5
0.5
-0.5
-1.5
-2.5
-3.5
0
2
4
6
8
10
12
14
16
18
Time (s)
7

3.2 Nonlinear Static (Pushover) analysis

Pushover analysis is popular in earthquake engineering, as is the response spectrum method of analysis. As the latter is a good equivalent static analysis (substitute) for the elastic dynamic analysis of structures to a given earthquake, likewise pushover analysis is a good equivalent non-linear static analysis (substitute) for the inelastic dynamic analysis of structures for the earthquake. Pushover analysis provides a load versus deflection curve of the structure starting from the state of rest to the ultimate failure of the structure.

The load is representative of the equivalent static load of a mode (generally taken as the fundamental mode) of the structure and may be conveniently taken as the total base shear of the structure. Similarly, the deflection may represent the deflection of any storey and may be conveniently selected as the top-storey deflection. [12]

The main idea is to apply a distribution of «increasing» forces in order to obtain something similar to an envelope of the maximum responses that we could get from nonlinear dynamic analysis with ground-motions of increasing intensities.

2D or 3D models of the structure may be used in this type of analysis. It is important to take into account the nonlinear behavior of materials as well as the nonlinear geometric effects. Particular distributions of lateral forces are applied and then are used to push the structure (**Figure 34**). The lateral forces are then scaled, proportionally to the initial distribution, in order to monotonically increment the displacement of a control point.

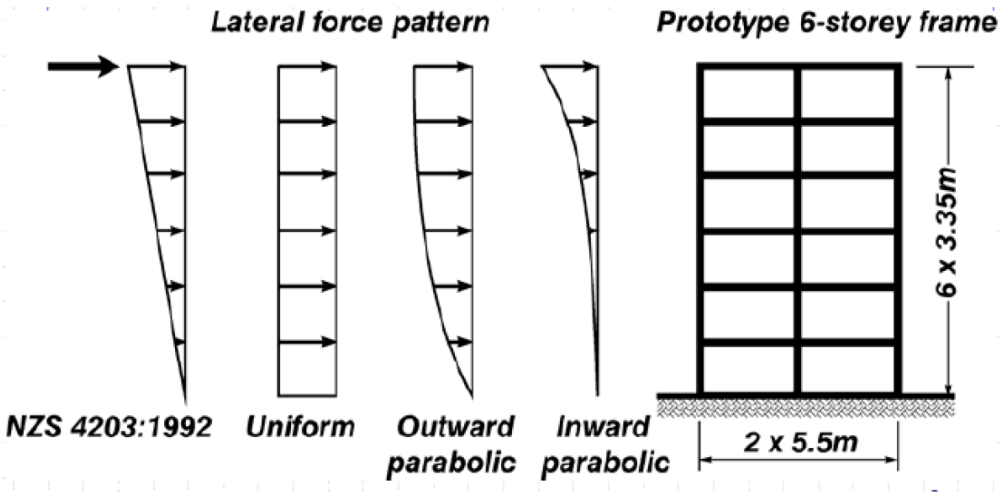

Figure 34- Example of different lateral force patterns

According to Euro code 8:

- At least two vertical distributions of the lateral loads should be applied:
  - A "uniform" pattern, based on lateral forces that are proportional to mass regardless of elevation (uniform response acceleration);
  - A "modal" pattern, proportional to lateral forces consistent with the lateral force distribution in the direction under consideration determined in elastic analysis.
- Lateral loads shall be applied at the location of the masses in the model. Accidental eccentricity shall be taken into account.
- The relation between base shear force and the control displacement (the "capacity curve") should be determined by pushover analysis for values of the control displacement ranging between zero and the value corresponding to 150% of the target displacement.
- The control displacement may be taken at the center of mass of the roof of the building. The top of a penthouse should not be considered as the roof. [10]

CHAPTER 4

4. BEHAVIOR OF THE NAKED STRUCTURE

4.1 Linear analysis

A linear analysis of the structure is firstly performed in order to check the actual effects (base shear) of the seismic actions. In this analysis, all structural elements are asked to behave in a full elastic way and thus plastic hinge definition is not needed

Results from both static pushover analysis and dynamic time-history analysis will be plotted. This can be a preliminary check of the finite element Model, and a confirmation of the actions produced by the seismic motion.

Figure 35-Figure 36 show the pushover capacity curve of the elastic un-equipped structure together with the results of the time history analysis of 14 accelerograms in both directions.

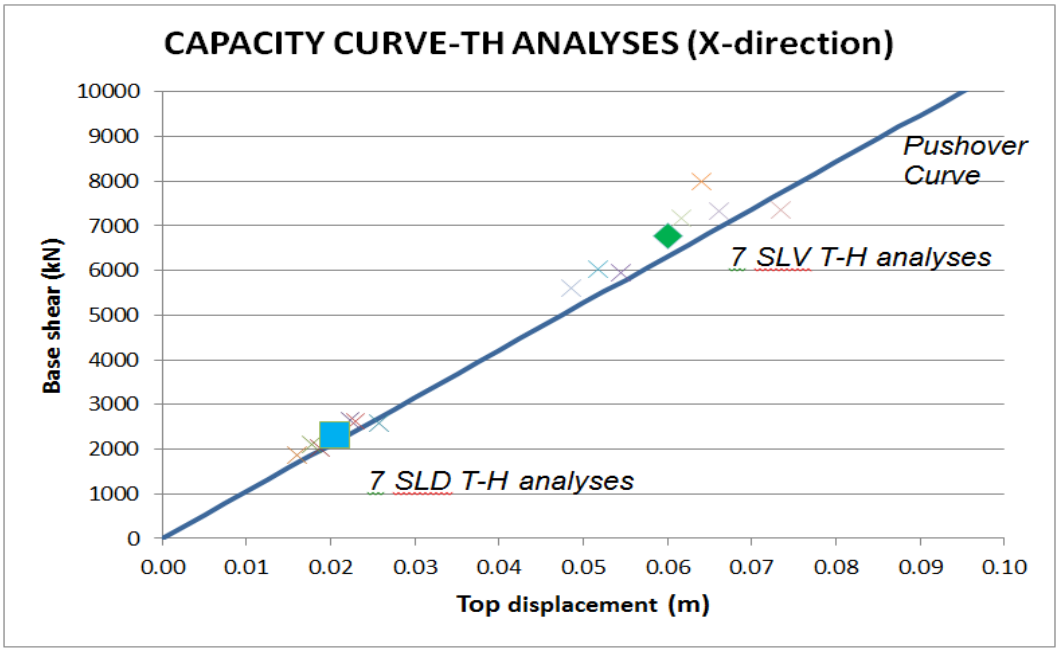

SLD:
$Vb = 2309\ kN$
$Dt = 2cm$

SLV:
$Vb = 6765\ kN$
$Dt = 6cm$

Figure 35- The results of Pushover and time-history analyses for the naked linear system in X-direction

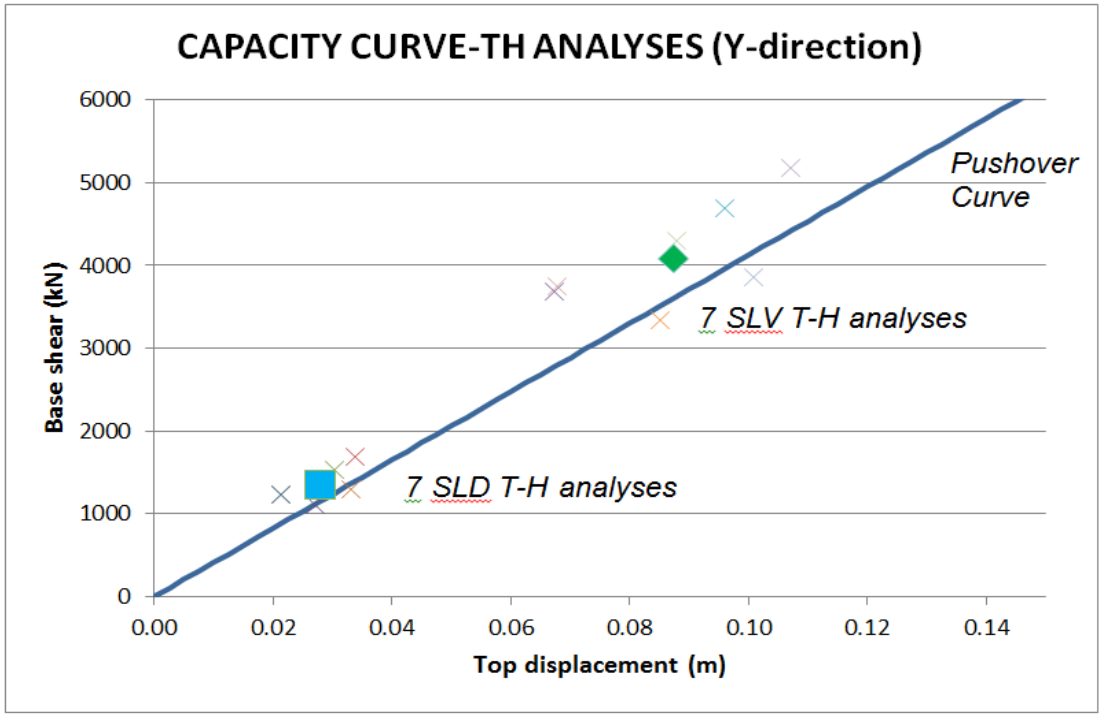

SLD:
$Vb = 1345.1\ kN$
$Dt = 2.7\ cm$

SLV:
$Vb = 4094.1\ kN$
$Dt = 8.7\ cm$

Figure 36- The results of Pushover and time-history analyses for the naked linear system in Y-direction

The capacity curve of the elastic structure shows a linear relationship between the base shear and the top displacement. The perfect elastic behavior of the structure gives a notion on the amount of base shear produced by the earthquakes. The 2 large points, the square and the diamond, correspond to the averages of the 7 SLV accelerograms and the 7 SLD accelerograms respectively. The 2 average points seem to be positioned on the capacity curve (line), and this gives a confirmation between the results of the static pushover and the time history analyses.

4.2 Non-Linear analysis (The Actual Capacity Curve)

4.2.1 General

High values of the deformations and stresses induced by earthquakes can cause the response of the structure exceeds the elastic limit. As a result, the materials will have the chance to dissipate energy by hysteresis through cycles of loading-unloading, thus not all of the energy transmitted by the earthquake translates into deformation of the structural elements. And this makes it possible to design the structural system for lower values of ground motion. The decrease in force is embedded in the behavior factor q.

On the other hand, it is necessary that the structure has a sufficient degree of ductility; to be able to withstand the inelastic displacements induced by shaking once crossed the linear limit. For this to happen, we must pay special attention to construction details (ex. beam-column joint).

Regarding the reinforced concrete elements, plastic hinges have been introduced at the ends of beams and columns, whose moment-curvature law depends on the geometrical and mechanical properties of the section as well as the level of the normal force. The normal force is usually assumed zero for the beams, while it is decisive when dealing with columns. The moment-curvature, shown in (**Figure 37**), presents an elastic branch until time yield strength, a plastic-hardening branch until the ultimate moment is reached, and finally a softening branch up to the null value of the moment (not shown in the figure).

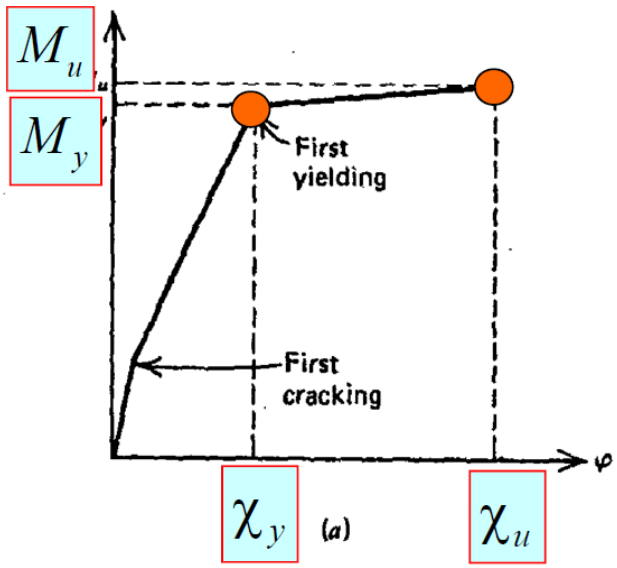

Figure 37- A typical Moment-Curvature relationship

4.2.2 Nonlinear analysis of reinforced concrete sections

The moment-curvature relationship for sections of reinforced concrete can be summarized using a Bilinear curve (**Figure 37**). The important points are given by the yield and the ultimate moments. It might be also necessary to define a slope for the softening branch, which is not shown in the picture.

The condition of yielding occurs when the profile of the steel in the section reaches a value equal to ε_{yd}, as represented in **Figure 38**. The couple moment-curvature peak is achieved by imposing the condition of concrete reaching its ultimate strength, as in **Figure 39**, where the concrete reaches the ultimate strain, equal to 3.5 ‰.

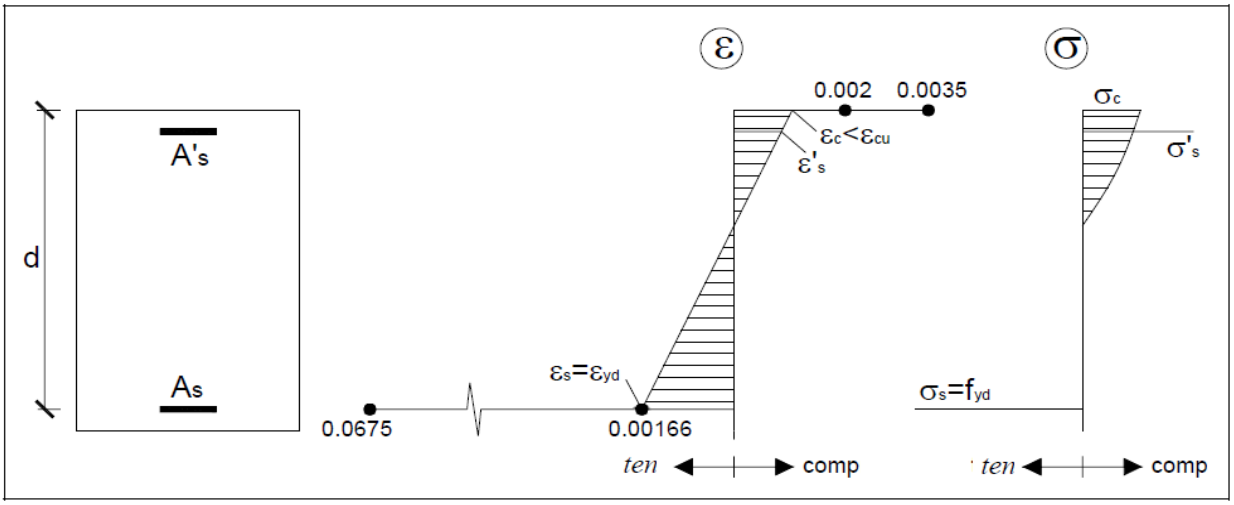

Figure 38- Stress of a generic concrete section at yielding state

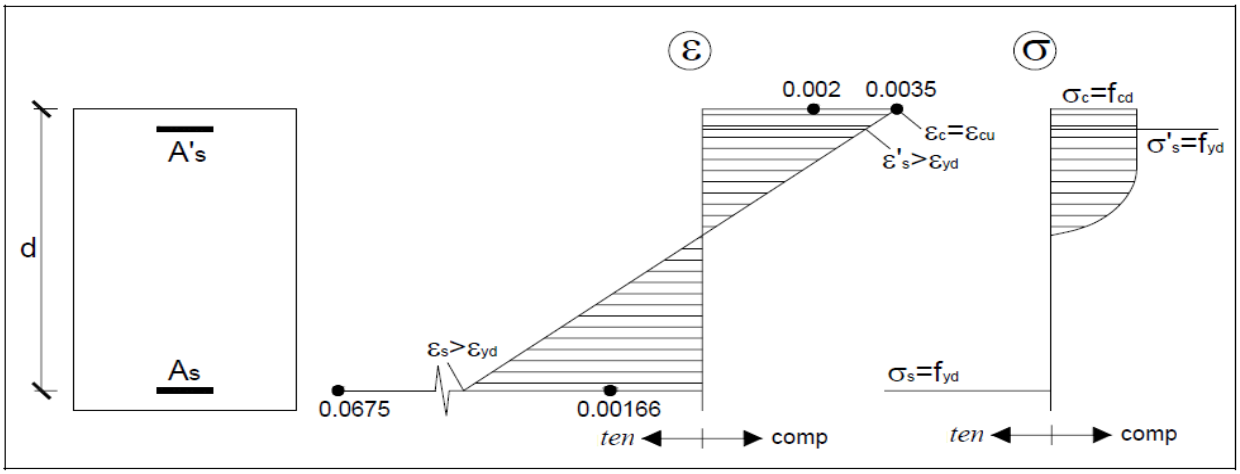

Figure 39- Stress and strain of a generic concrete section at ultimate state

For the calculation of the yielding moment My and the ultimate moment Mu, as well as their corresponding curvatures, these assumptions are taken into consideration:

- preservation of the section's plane
- perfect bonding between steel bars and concrete
- No tensile strength for concrete

- Parabola-rectangle constitutive law for concrete in compression, and elastic-perfectly plastic constitutive law for steel (**Figure 40**).

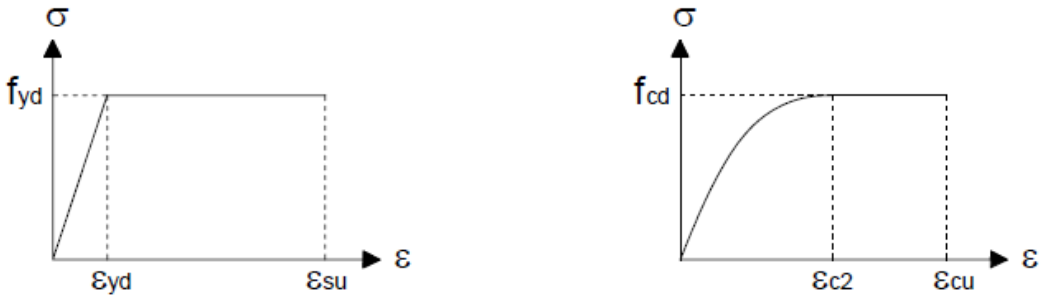

Figure 40- stress-strain Constitutive law for steel and concrete

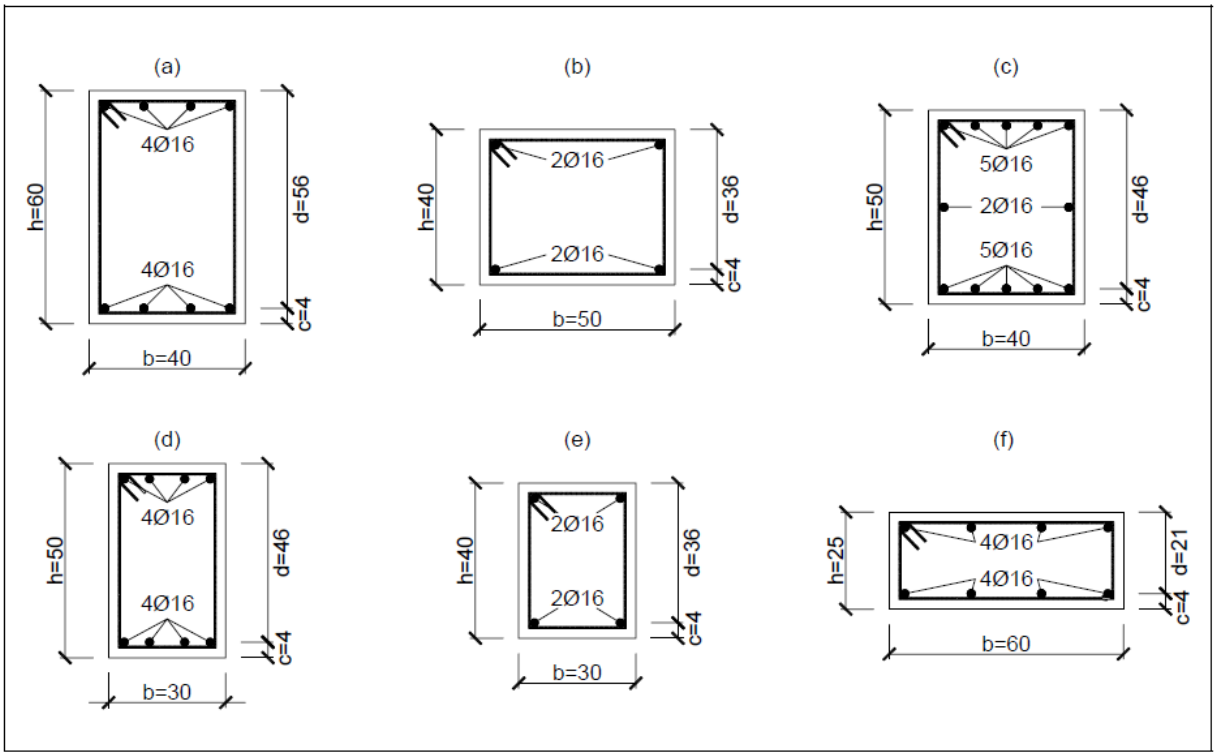

Figure 41- sections of RC elements: (a) Main beams, (b) Secondary beams, (c) Columns, (d) Beams of intermediate landings of the stairwell, (e) Side beams of the stairwell on the second and third levels, (f) One of the side beams of the stairwell on the first level.

Calculation for the four quantities $M_y, \chi_y, M_u, and\ \chi_u$ was carried out for all sections (**Figure 41**). Regarding the columns, different levels of normal force are used in the definition of the Moment-curvature law, because the moment capacity is sensitive to the level of axial force, and thus for each normal force level a different moment curvature relationship can be defined. For the sake of simplicity, we computed the four quantities for 12 normal force levels (**Table** 10).

Elements	**N [kN]**	**M_y [kN cm]**	**χ_y [1/cm]**	**M_u [kN cm]**	**X_u [1/cm]**
Beam 40x60	0	14871	3.291E-05	15026	9.072E-04
Beam 50x40	0	4860	4.941E-05	5169	1.263E-03
Beam 60x25	0	5428	9.682E-05	5702	1.043E-03
Beam 30x40	0	4775	5.162E-05	4913	1.043E-03
Beam 30x50	0	11968	4.261E-05	12111	8.276E-04
Column – M_3	100	18156	4.537E-05	19519	6.629E-04
Column – M_2	100	12360	5.857E-05	15337	5.848E-04
Column – M_3	150	19069	4.640E-05	20435	6.289E-04
Column – M_2	150	13035	5.995E-05	16011	5.523E-04
Column – M_3	200	19960	4.748E-05	21337	5.965E-04
Column – M_2	200	13692	6.137E-05	16669	5.222E-04
Column – M_3	250	20830	4.859E-05	22225	5.658E-04
Column – M_2	250	14330	6.285E-05	17311	4.944E-04
Column – M_3	300	21681	4.974E-05	23097	5.366E-04
Column – M_2	300	14950	6.439E-05	17936	4.687E-04
Column – M_3	350	22512	5.093E-05	23954	5.090E-04
Column – M_2	350	15553	6.598E-05	18543	4.407E-04
Column – M_3	400	23324	5.217E-05	24793	4.830E-04
Column – M_2	400	16139	6.763E-05	19046	4.191E-04
Column – M_3	450	24118	5.345E-05	25612	4.575E-04
Column – M_2	450	16709	6.935E-05	19491	4.024E-04
Column – M_3	500	24895	5.478E-05	26371	4.217E-04
Column – M_2	500	17262	7.112E-05	19929	3.865E-04
Column – M_3	550	25655	5.616E-05	27103	3.910E-04
Column – M_2	550	17801	7.297E-05	20359	3.715E-04
Column – M_3	600	26400	5.758E-05	27808	3.645E-04
Column – M_2	600	18325	7.488E-05	20781	3.574E-04
Column – M_3	700	27847	6.059E-05	29143	3.210E-04
Column – M_2	700	19331	7.891E-05	21601	3.313E-04

Table 10- Moments and curvatures at yielding and ultimate conditions for the various cross sections

4.2.3 Nonlinear analysis results

Non-linear pushover and time history analyses for the naked non-linear structure were performed. The nonlinearity of the structural elements has been introduced in SAP software, and the results have been checked with another software and they happened to match. **Figure 42Figure** 43 show the pushover capacity curve of the non-linear un-equipped structure together with the results of the time history analysis of 14 accelerograms, in both directions.

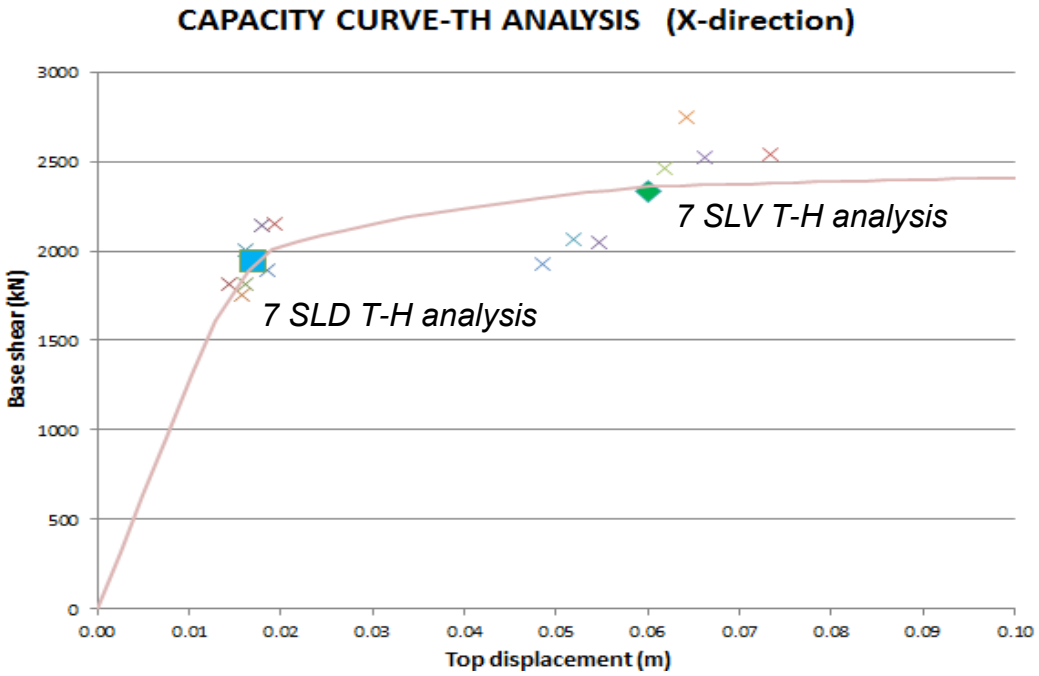

SLD:

$Vb = 1941 \ \ kN$

$Dt = 1.68cm$

SLV:

$Vb = 2332.9\ kN$

$Dt = 6$ cm

Figure 42- The results of Pushover and time-history analyses for the naked non-linear system in X-direction

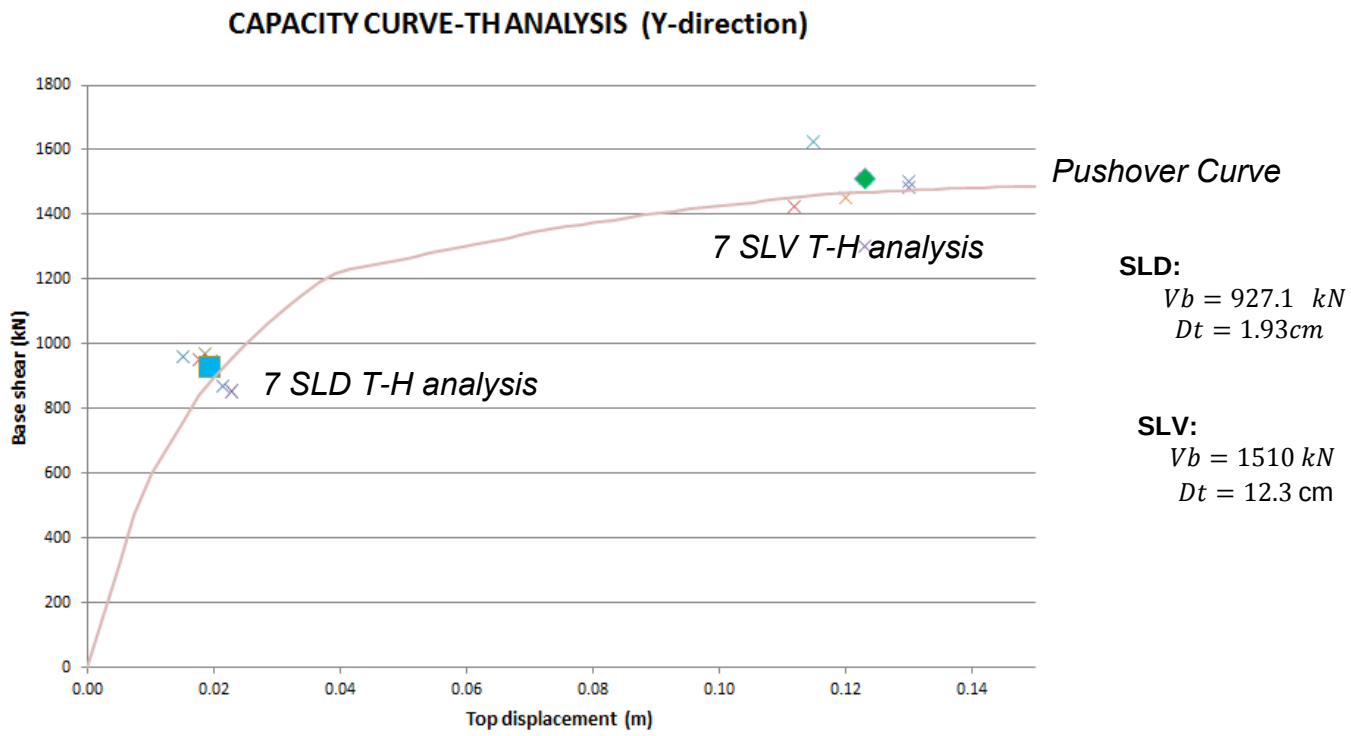

Figure 43- The results of Pushover and time-history analyses for the naked non-linear system in Y-direction

It is interesting to point out that the results of the SLD time history analysis for the linear system (**Figure 35-Figure** 36) are larger than of the non-linear system (**Figure 42Figure** 43). This means that our structure does not fully satisfy the yielding performance objective because it yielded before reaching the damage limit state. Therefore, this indicates the necessity of strengthening the structure.

X-direction:

SLD (Linear system): $Vb = 2309\ kN$ > SLD (non-linear system): $Vb = 1941\ kN$

Y-direction:

SLD (Linear system): $Vb = 1345\ kN$ > SLD (non-linear system): $Vb = 927.1\ kN$

CHAPTER 5

5. BEHAVIOR OF THE EQUIPPED STRUCTURE

5.1 Design of the CSB devices

In this Chapter, we will discuss the design procedure of the crescent shaped braces when installed in reinforced concrete or steel structures. Two methods for the preliminary design of CSB are proposed by the student, and will be explained in details. The first method can be used for designing/strengthening structures that do not satisfy a certain pre-defined performance objective (i.e. design inter-storey shear). Steel and precast reinforced concrete structures may be good examples of such structures. The second method will be devoted to stiff reinforced concrete structures that already satisfy the performance objectives but need to be strengthened for specific reasons. Finally, as an illustrative example, the second method will be applied to our case study.

5.1.1 Method I (flexible structures)

This is an iterative method, which is, like any approximated method, subject to several limitations. Only shear-type structures, where each floor can be assumed as a single degree of freedom, are applicable. In addition, the applications of this method are for the time being restricted to the planar analysis of structures. Thus, each direction will be dealt with independently, without coupling. This is a reasonable assumption for preliminary design. Nevertheless, this method can be extended beyond the planar analysis in order to be used for unsymmetrical structures, where the equations of motions are coupled by the torsional effect. However, this is beyond the scope of this research.

The main purpose of this method is to obtain the target lateral stiffness upon which we will design the crescent shaped braces. The stiffness distribution is assumed proportional to the storey shear, which is in turn assumed to be proportional to the mass and height of the corresponding floor. Once the stiffness is known, we will use the design formulas that we derived in chapter 1.1 to find the minimum moment of inertia of the cross section profile, which is to be chosen. In the following, we will list the procedure of the method and then we will describe each step in more details.

Procedure:

1. Assume a global stiffness matrix of the system.
2. Perform a modal analysis and find the shape, period, participation factor, and pseudo acceleration of each mode.
3. Find the displacements of the different modes, and get the inter-storey drifts. Inter-storey drifts of the different modes should be combined using SRSS rule.
4. Compare the actual inter-storey drifts with the design inter-storey drifts. If the actual and the design inter-storey drifts are different, adjust the global stiffness matrix and then go back to step 2.
5. Compute the stiffness of the braces at each floor by subtracting the stiffness of the naked structure from the global stiffness matrix that we reached in the final iteration.
6. At each level, calculate the target stiffness of a single CSB device.
7. Compute the moment of inertia and the arm of the CSB device. Then choose the section profile.

Step 1:

Assume a global stiffness matrix in such a way that the stiffness distribution along the building height is proportional to the storey shears. This matrix contains the stiffness of the structural element (known term) and the stiffness of the braces (unknown term). As an illustrative example, we will consider a 3 doffs system.

- Stiffness matrix of the un-equipped system (known):

$$[K] = \begin{bmatrix} k_1 + k_2 & -k_2 & 0 \\ -k_2 & k_2 + k_3 & -k_3 \\ 0 & -k_3 & k_3 \end{bmatrix}$$

Where:

$k_1, k_2, and\ k_3\ are\ the\ stiffnesses\ of\ the\ first, second, and\ third\ storeys\ respectively.$

- Stiffness matrix of the CSB system

$$[Kb] = \begin{bmatrix} k_{b1} + k_{b2} & -k_{b2} & 0 \\ -k_{b2} & k_{b2} + k_{b3} & -k_{b3} \\ 0 & -k_{b3} & k_{b3} \end{bmatrix}$$

Where:

$k_{b1}, k_{b2}, and\ k_{b3}$ are the stiffnesses of the lateral resisting system (CSB) at the first, second, and third storeys respectively.

- Global stiffness matrix of the system (naked structure+CSB)

$$[K^*] = [K] + [Kb] = \begin{bmatrix} k_1 + k_2 + k_{b1} + k_{b2} & -k_2 - k_{b2} & 0 \\ -k_2 - k_{b2} & k_2 + k_3 + k_{b2} + k_{b3} & -k_3 - k_{b3} \\ 0 & -k_3 - k_{b3} & k_3 + k_{b3} \end{bmatrix}$$

For simplification:

$$[K^*] = \begin{bmatrix} k_{b1}^* + k_{b2}^* & -k_{b2}^* & 0 \\ -k_{b2}^* & k_{b2}^* + k_{b3}^* & -k_{b3}^* \\ 0 & -k_{b3}^* & k_{b3}^* \end{bmatrix}$$

Where:

$$k_{b1}^{*} = k_1 + k_{b1}$$

$$k_{b2}^{*} = k_2 + k_{b2}$$

$$k_{b3}^{*} = k_3 + k_{b3}$$

In order to simplify the calculation we will assume that the stiffness distribution along the building height is proportional to the storey shears (**Table 11**) which is in turn proportional to the height and mass of each storey, and this will guarantee that the CSB devices will work effectively along the structure's height:

- Storey shear distribution:

Storey	zi [m]	mi [kg]	zi*mi [kg*m]	$\boldsymbol{Fi = Fb * (zi * mi)/(\sum zi * mi)}$	$\boldsymbol{F_{storey}}$(cumulative)
1	3.18	396738	1261626.84	$0.183 * Fb$	$1 * Fb$
2	6.5	363710	2364115	$0.342 * Fb$	$0.817 * Fb$
3	9.9	332008	3286879.2	$0.475 * Fb$	$0.475 * Fb$

Table 11- Storey shears distribution among the various storey levels

- Storey stiffness distribution:

$$k_{b2}^{*} = k_{b1}^{*} * 0.817$$

$$k_{b3}^{*} = k_{b1}^{*} * 0.475$$

This gives:

$$[K^{*}] = \begin{bmatrix} 1.817\ k_{b1}^{*} & -0.817\ k_{b1}^{*} & 0 \\ -0.817\ k_{b1}^{*} & 1.292\ k_{b1}^{*} & -0.475\ k_{b1}^{*} \\ 0 & -0.475\ k_{b1}^{*} & 0.475\ k_{b1}^{*} \end{bmatrix}$$

At this stage, it is enough to assume the global stiffness of the first storey k_{b1}^{*}, which is the sum of the first storey stiffness of the naked structure and the stiffness of the CSBs of the first storey, in order to get the global stiffness matrix.

Given that global matrix will be obtained by assuming k_{b1}^*, we can write the initial global matrix in cleaner way by setting the first term to be equal to k_{b1}^* and adjust all other terms accordingly:

$$[K^*] = \begin{bmatrix} k_{b1}^* & -0.449\, k_{b1}^* & 0 \\ -0.449\, k_{b1}^* & 0.711\, k_{b1}^* & -0.261\, k_{b1}^* \\ 0 & -0.261\, k_{b1}^* & 0.261\, k_{b1}^* \end{bmatrix}$$

Step 2:

Perform a modal analysis in order to find the shape, period, participation factor, and pseudo acceleration of each mode.

Free vibration equation of the 3 dof's:

$$[M] \cdot \ddot{u}(t) + [K^*] \cdot u(t) = 0$$

Where:

- $u(t) = \varphi_n * q_n(t)$
  - $\varphi_n \quad = mode\ shape$
  - $q(t) = A_n\, cos(w_n.t) + B_n \sin(w_n.t)$ (simple harmonic function)
- $\ddot{u}(t) = -w_n^2 * \varphi_n * q_n(t)$

-by substituting $u(t)\ and\ \ddot{u}(t)\ in\ the\ equation\ of\ motion\ we\ obtain$:

$[K.\varphi - w^2 \cdot M.\varphi] \cdot q(t) = 0$

-solution is different from trivial($q(t) = 0$), if and only if:

$[K - w^2 \cdot M] \cdot \varphi = 0$ (Matrix Eigen value problem)

-In order to get the solution of the Eigen value problem, the determinant of this matrix should be equal to zero:

$det([K] - w^2 \cdot [M]) = 0$ (Frequency equation)

By solving this equation, we obtain the spectral matrix and consequently the natural periods of the different modes.

- Spectral matrix: $[\Omega] = \begin{bmatrix} w_1^2 & 0 & 0 \\ 0 & w_2^2 & 0 \\ 0 & 0 & w_3^2 \end{bmatrix} \left[\frac{rad}{s}\right]^2$ = Spectral matrix
- Natural periods: $T_n = \frac{2\pi}{w_n}$ (sec) where n is the mode number

By substituting the Circular frequencies in the equation of motion, we can get the Modal matrix $[\emptyset]$ (3x3 matrix).

- Modal participation factor: $\Gamma_n = \frac{\{\varphi_n\}^T \cdot [M] \cdot \{1\}}{\{\varphi_n\}^T \cdot [M] \cdot \{\varphi_n\}}$
- Spectral acceleration:

In order to get the peak spectral acceleration of the system we can substitute the period of the first mode in the suitable equation of the elastic spectrum equations (SLD).

$0 \le T \le T_B \quad \rightarrow S_e(T) = a_g \cdot S \cdot \left[1 + \frac{T}{T_B} \cdot (\eta \cdot 2{,}5 - 1)\right]$

$T_B \le T \le T_C \quad \rightarrow S_e(T) = a_g \cdot S \cdot \eta \cdot 2{,}5$

$T_C \le T \le T_D \quad \rightarrow S_e(T) = a_g \cdot S \cdot \eta \cdot 2{,}5 \cdot \left[\frac{T_C}{T}\right]$

$T_D \le T \le 4\ s \quad \rightarrow S_e(T) = a_g \cdot S \cdot \eta \cdot 2{,}5 \cdot \left[\frac{T_C \cdot T_D}{T^2}\right]$

Step 3:

Having obtained the elastic spectral acceleration corresponding to the first mode period, it becomes possible to compute the elastic displacement induced by a ground motion of SLD level.

- $(u_{in})_{max} = \varphi_n \cdot \frac{\Gamma_n \cdot PSA(T_n)}{w_n^2} \quad [m]$

Consequently, we can obtain the inter-storey drifts between each 2 successive floors for the different modes:

- Inter-storey drift between storeys i and j: $\delta_{ij} = |u_j - u_i|$

The inter-storey drifts for the different modes should be combined using SRSS rule, which is accurate enough for a preliminary design.

- $r \cong \sqrt{\sum_{n=1}^{N}(r_n{}^2)}$

Step 4:

Compare the actual inter-storey drifts with the design inter-storey drifts. If any of the actual inter-storey drifts is larger than the maximum drift assigned by the code, i.e. $0.005h_s$, increase the assumed stiffnes matrix by a small increment (0.5 %) and repeat from step number 2. If, on the other hand, the actual drift was smaller than the maximum (conservative), the assumed stiffness matrix can be reduced iteratively by a small increment at a time until we get close enough to the performance objective (i.e. maximum storey drift). In case this method is performed numerically, we can introduce a tolerance between the actual and the design inter-storey drifts so the iterations can stop when the actual and the demand inter-storey drifts are close enough.

Step 5:

Compute the target stiffness of the CSB lateral resisting system at each floor by subtracting the stiffness of the naked structure from the global stiffness matrix that we reached in the final iteration.

$$[Kb] = [K^*] - [K] = \begin{bmatrix} k_{b1} + k_{b2} & -k_{b2} & 0 \\ -k_{b2} & k_{b2} + k_{b3} & -k_{b3} \\ 0 & -k_{b3} & k_{b3} \end{bmatrix}$$

Now we can obtain the stiffness of the CSB at different storey levels $k_{b1}, k_{b2}, and\ k_{b3}$

Step 6:

At each level, calculate the target stiffness of a single CSB. This can be done by dividing the target stiffness of the CSB system at a certain floor ($k_{b1}, k_{b2}, and\ k_{b3}$) over the number of braces at that floor.

$K_{CSB,i} = K_{b,i}/N_{CSB,i}$ Where i is the floor number

Step 7:

Use the design formulas derived in chapter 1.1 to get the minimum moment of inertia of the cross section profile as well as the arm of the CSB device. Once the inertia is known, we can choose among a number of sections that have equal or larger moment of inertia. Note that the section profile can control the post yielding behavior such as hardening and ductility (refer to section 1.2.2)

$$\xi = 0.75\frac{(\text{E.h.}\bar{F}_y)}{\bar{K}.L^2.f_y}.\left(\sqrt{1+5.33.\left(\frac{i}{h}\right)^2.\frac{\bar{K}.L}{E}.\frac{f_y}{\bar{F}_y}}\right)$$

$$J = \frac{L^3.K_{CSB,i}.\xi^2}{3E\ cos^2\alpha}$$

Where:

- E: $The\ elastic\ modulus$
- h: $Cross\ section\ height$
- i: $Radius\ of\ gyration\ of\ the\ cross\ section = \sqrt{J/A}$
- f_y: $The\ yield\ strength$
- L: $The\ diagonal\ length$
- $\bar{K}$: $Target\ initial\ lateral\ stiffness$
- $\bar{F}_y$: $The\ target\ yield\ strength$

- ξ: arm of the device (can be assumed 0.1 for preliminary design)
- α: $Diagonal\ inclination$

5.1.2 Method II (Stiff structures)

The first method cannot be entirely applied for structures that satisfy the pre-defined performance objective (i.e. design inter-storey drift) because in order to be valid, the vertical resisting system should have less stiffness than the target global stiffness. In this method, another approach is taken to define the target stiffness of the CSB devices. The CSB lateral resisting system will be assumed to contribute with a percentage of the lateral stiffness of the vertical resisting system. The first 5 steps of Method I will be replaced by only a single step in this method.

Procedure:

1. Define a contribution percentage for the CSB system and find the stiffness at the different stories.
2. At each level, calculate the target stiffness of a single CSB device.
3. Compute the moment of inertia and the arm of the CSB device. Then choose the section profile.

A detailed application of this method will be illustrated by the mean of a numerical example for our case study.

Step 1:

- **Define a contribution percentage for the CSB system and find the stiffness at the different stories.**

The level of contribution is imposed according to the designer's desire of reducing the storey shear that is absorbed by the vertical resisting system. In this example, we will assume a 25% contribution. For a better stiffness distribution, only the CSB system on the first storey will contribute in 25 % of the base shear while the stiffness of the CSB system on the other 2 storeys will follow the storey shear distribution.

$$K_{b,i} = 0.25 * K_{VRS,i}$$

Where:

- k_{b1} *is the target stiffness of the CSB system at floor i*
- $K_{VRS,i}$ *is the actual lateral stiffness of the vertical resisting system at floor i*

Storey shears distribution (recall):

Storey	zi [m]	mi [kg]	zi*mi [kg*m]	$\boldsymbol{Fi = Fb * (zi * mi)/(\sum zi * mi)}$	$\boldsymbol{F_{storey}}$**(cumulative)**
1	3.18	396738	1261626.84	$0.183 * Fb$	$1 * Fb$
2	6.5	363710	2364115	$0.342 * Fb$	$0.817 * Fb$
3	9.9	332008	3286879.2	$0.475 * Fb$	$0.475 * Fb$

In absence of more exact solution, the lateral stiffness of the vertical resisting system is assumed equal to $N * 9EI/h^3$ where E is the modulus of elasticity of concrete, I is the moment of inertia of the reinforced concrete section in the direction under consideration, h is the inter-storey height, and N is the number of reinforced concrete columns.

It is also necessary to assume a planar and an elevation distribution for the devices in the building. The distribution usually depends on the architectural limitations and therefore the

designer should keep in contact with the architecture when deciding the device positions. In our case study, the devices will be distributed as follow:

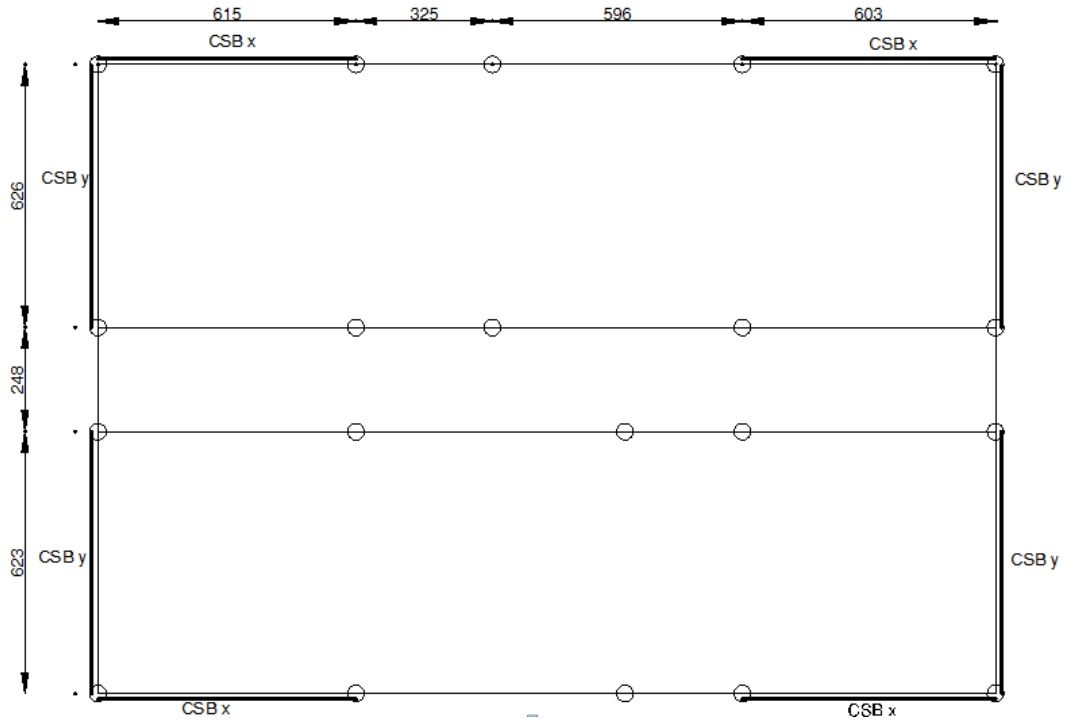

Figure 44- Planar distribution of the lateral resisting devices

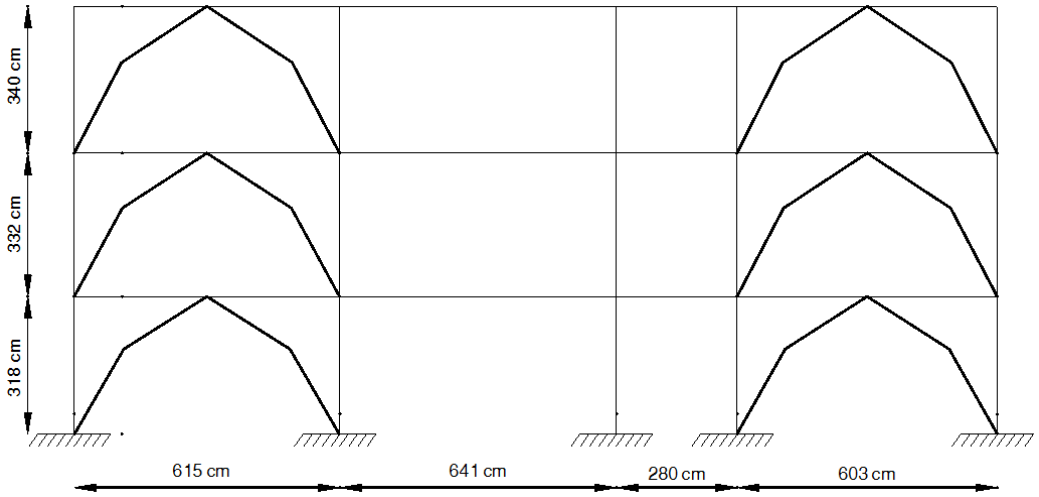

Figure 45- Distribution in X-direction

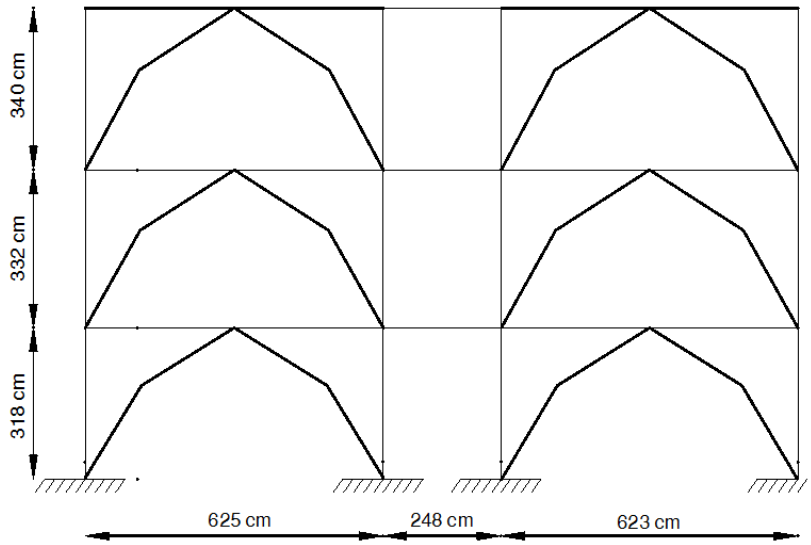

Figure 46- Distribution in Y-direction

Direction X:

- Storey 1: (25% of the Lateral stiffness in X-direction of the vertical resisting system)

$$K_{b,x,1} = 0.25 * 20 * 9 * 25 * 10^6 * \frac{(0.4 * 0.5^3)/12}{3.18^3} = 0.25 * 583068.9 = 145.76 * 10^3\ kN/m$$

- Storey 2: (storey shear distribution)

$$K_{b,x,2} = K_{b,x,1} * \frac{F_2}{F_1} = 145.76 * 10^3 * 0.817 = 119 * 10^3\ kN/m$$

- Storey 3: (storey shear distribution)

$$K_{b,x,3} = K_{b,x,1} * \frac{F_3}{F_1} = 145.76 * 10^3 * 0.475 = 69.39 * 10^3\ kN/m$$

Direction Y:

- Storey 1: (25% of the Lateral stiffness in Y-direction of the vertical resisting system)

$$K_{b,y,1} = 0.25 * 20 * 9 * 25 * 10^6 * \frac{(0.5 * 0.4^3)/12}{3.18^3} = 0.25 * 583068.9 = 93.3 * 10^3\ kN/m$$

- Storey 2: (storey shear distribution)

$$K_{b,y,2} = K_{b,y,1} * \frac{F_2}{F_1} = 93.3 * 10^3 * 0.817 = 76.22 * 10^3 kN/m$$

- Storey 3: (storey shear distribution)

$$K_{b,y,3} = K_{b,y,1} * \frac{F_3}{F_1} = 93.3 * 10^3 * 0.475 = 44.31 * 10^3\ kN/m$$

Step 2:

- **At each storey level, calculate the target stiffness of a single CSB device.**

For this specific case study we decided to install 8 CSB devices in each direction at all storey levels (**Figure 44-Figure** 46**).**

The stiffness of a single device is given by:

$K_{CSB,i} = K_{b,i}/N_{CSB,i}$ Where i is the floor number

Storey level	$K_{b,x,i}$ $(10^3\ kN/m)$	Number of devices $N_{csb,x}$	$K_{CSB,i}$ $(10^3\ kN/m)$
First	145.76	8	18.22
Second	119	8	14.87
Third	69.39	8	8.67

Table 12- Target stiffness of single CSBs at different levels in the X-direction

Storey level	$K_{b,y,i}$ $(10^3\ kN/m)$	Number of devices $N_{csb,y}$	$K_{CSB,i}$ $(10^3\ kN/m)$
First	93.3	8	11.66
Second	76.22	8	9.52
Third	44.31	8	5.53

Table 13- Target stiffness of single CSBs at different levels in the X-direction

Step 3:

- **Compute the moment of inertia and the arm of the CSB device. Then choose the section profile.**

Use the design formulas derived in chapter 1.1 to get the minimum moment of inertia of the cross-section profile, as well as the arm of the CSB device. Once the inertia is known, we can choose among a number of sections that have equal or larger moment of inertia. The design results can be found in **Table 14-Table** 15. Note that the section profile can control the post yielding behavior such as hardening and ductility (refer to section 1.2.2)

$$\xi = 0.75\frac{(\mathrm{E.h.}\overline{F}_y)}{\overline{K}.L^2.f_y}.\left(\sqrt{1+5.33.\left(\frac{i}{h}\right)^2.\frac{\overline{K}.L}{E}.\frac{f_y}{\overline{F}_y}}\right)$$

$$J = \frac{L^3.K_{CSB,i}.\xi^2}{3E\ cos^2\alpha}$$

Where:

- E: $The\ elastic\ modulus$
- h: $Cross\ section\ height$
- i: $Radius\ of\ gyration\ of\ the\ cross\ section = \sqrt{J/A}$
- f_y: $The\ yield\ strength$
- L: $The\ diagonal\ length$
- $\overline{K}$: $Target\ initial\ lateral\ stiffness$
- $\overline{F}_y$: $The\ target\ yield\ strength$
- ξ: arm of the device (can be assumed 0.1 for preliminary design)
- α: $Diagonal\ inclination$

J can be easily computed as all terms are known.

Storey level	$K_{CSB,i}\ (10^3\ kN/m)$	ξ	$L = \sqrt{(L_x/2)^2 + h_{s,i}^2}\ (m)$	$J\ (cm^4)$
First	18.22	0.1	4.45	5532.5
Second	14.87	0.1	4.52	4522.8
Third	8.67	0.1	4.58	2629

Table 14- Moments of inertia of single CSBs at different levels in the X-direction

Storey level	$K_{CSB,i}\ (10^3\ kN/m)$	ξ	$L = \sqrt{(L_y/2)^2 + h_{s,i}^2}\ (m)$	$J\ (cm^4)$
First	18.22	0.1	4.45	3823.3
Second	14.87	0.1	4.55	3125.6
Third	8.67	0.1	4.65	1817.8

Table 15- Moments of inertia of single CSBs at different levels in the Y-direction

Having obtained the minimum moment of inertia we can proceed and pick one of many available sections in the market. For this case study, 5 different profiles namely, HE, full rectangular, tubular rectangular, full circular, and tubular circular will be designed (**Table 16- Table** 21**)**. In order for the comparison to be valid, all section profiles will have the same inertia and the same section height. The HE section is chosen first. The other sections will be designed according to the actual inertia of the chosen HE profile. The pre-yielding behavior of all sections will be the same. However, it is not the case for post-yielding behavior where different profiles are characterized by different behaviors after the yielding point (refer to section 1.2.2).

Section Profile	**HE 200 B**	**Full rect.**	**Tubular rect.**	**Full circ.**	**Tubular circ.**
Inertia $\boldsymbol{J}\ (\boldsymbol{cm^4})$	5696	5696	5696	5696	5696
Height $\boldsymbol{h}\ (\boldsymbol{cm})$	20	20	20	-	-
Diameter $\boldsymbol{D}\ (\boldsymbol{cm})$	-	-	-	18.4	20
Width $\boldsymbol{b}\ (\boldsymbol{cm})$	20	8.54	10.55	-	-
Thickness $\boldsymbol{s}\ (\boldsymbol{cm})$	-	-	2.7	-	2.7

Table 16- Section profiles characteristics for $\boldsymbol{CSB_{x,1}}$

Section Profile	HE 160 M	Full rect.	Tubular rect.	Full circ.	Tubular circ.
Inertia J (cm^4)	5098	5098	5098	5098	5098
Height h (cm)	18	18	18	-	-
Diameter D (cm)	-	-	-	17.95	18
Width b (cm)	16.6	10.48	12.4	-	-
Thickness s (cm)	-	-	3	-	6

Table 17- Section profiles characteristics for $CSB_{x,2}$

Section Profile	HE 200 AA	Full rect.	Tubular rect.	Full circ.	Tubular circ.
Inertia J (cm^4)	2944	2944	2944	2944	2944
Height h (cm)	18.6	18.6	18.6	-	-
Diameter D (cm)	-	-	-	15.64	18.6
Width b (cm)	20	5.49	9.1	-	-
Thickness s (cm)	-	-	1.5	-	1.5

Table 18- Section profiles characteristics for $CSB_{x,3}$

Section Profile	HE 180 B	Full rect.	Tubular rect.	Full circ.	Tubular circ.
Inertia J (cm^4)	3831	3831	3831	3831	3831
Height h (cm)	18	18	18	-	-
Diameter D (cm)	-	-	-	16.7	18
Width b (cm)	18	7.88	9.4	-	-
Thickness s (cm)	-	-	2.6	-	2.6

Table 19- Section profiles characteristics for $CSB_{y,1}$

Section Profile	HE 140 M	Full rect.	Tubular rect.	Full circ.	Tubular circ.
Inertia J (cm^4)	3291	3291	3291	3291	3291
Height h (cm)	16	16	16	-	-
Diameter D (cm)	-	-	-	16.1	16
Width b (cm)	14.6	9.64	10.81	-	-
Thickness s (cm)	-	-	3	-	6

Table 20- Section profiles characteristics for $CSB_{y,1}$

Section Profile	HE 180 AA	Full rect.	Tubular rect.	Full circ.	Tubular circ.
Inertia J (cm^4)	1967	1967	1967	1967	1967
Height h (cm)	16.7	16.7	16.7	-	-
Diameter D (cm)	-	-	-	14.1	16.7
Width b (cm)	18	5.1	8.15	-	-
Thickness s (cm)	-	-	1.4	-	1.4

Table 21- Section profiles characteristics for $CSB_{y,3}$

5.2 Analysis of the linear structure equipped with the non-linear devices

Figure 47-Figure 48 show the pushover capacity curve of the elastic structure equipped with the inelastic devices, together with the results of the time history analysis of 14 accelerograms in both directions. It can be seen that the pushover line is no longer straight. This is due to the presence of the non-linear CSB devices. The effects of the devices are not recognizable because the structure here is assumed to behave in an elastic way with no limit. This is however not realistic because at a certain point the structure will yield and the forces will stop increasing. This analysis has been performed in order to determine the approximated actual forces produced by the earthquake. I mentioned "approximated" because the CSB devices are not linear and thus a portion of the forces are dissipated by hysteresis.

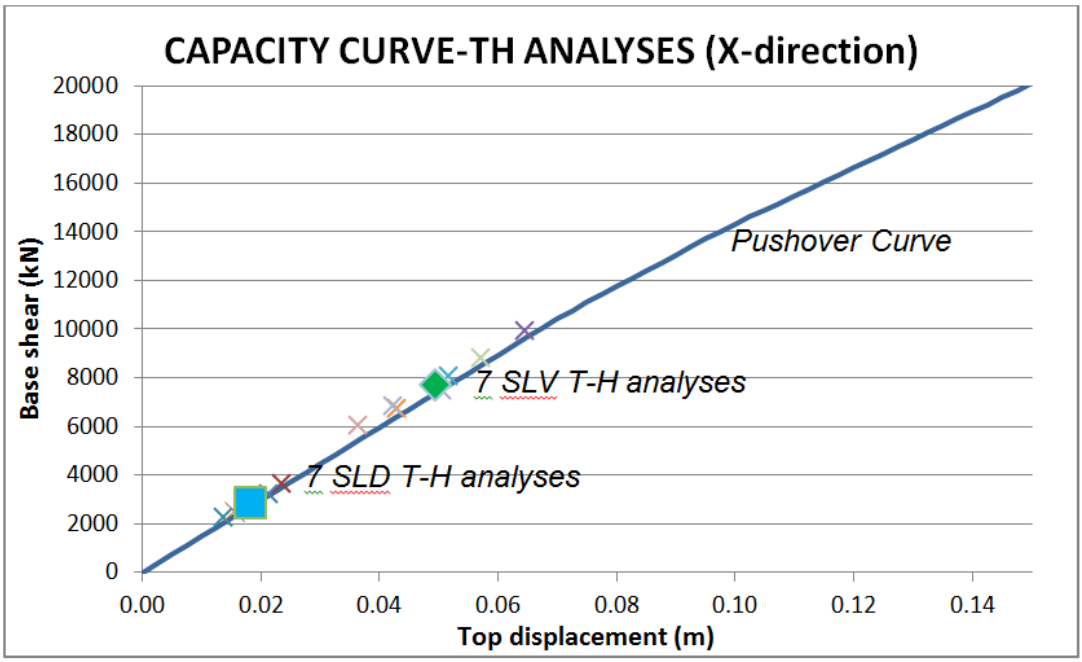

SLD:
$Vb = 2824.8\ \ kN$
$Dt = 1.82cm$

SLV:
$Vb = 7689.1\ kN$
$Dt = 4.9$ cm

Figure 47- The results of Pushover and time-history analyses for the equipped linear system in X-direction

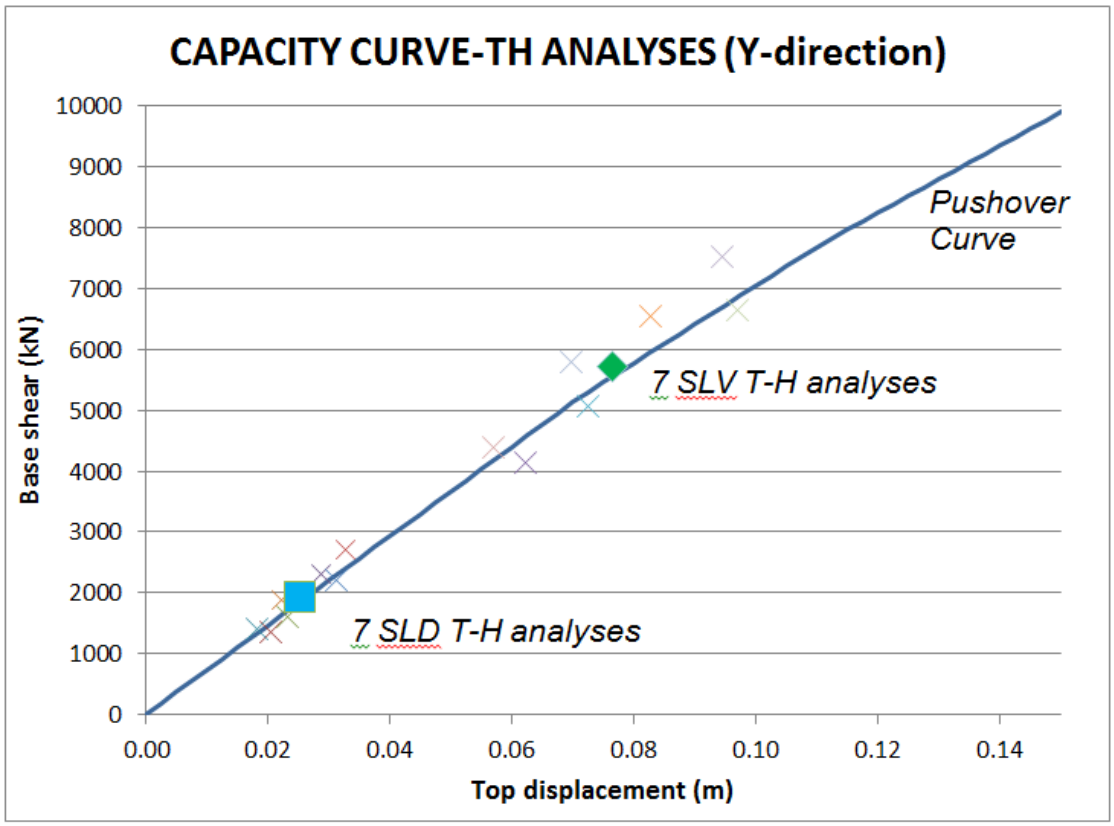

SLD:
$Vb = 1925.2 \ \ kN$
$Dt = 2.5 \ cm$

SLV:
$Vb = 5723.3 \ kN$
$Dt = 7.6$ cm

Figure 48- The results of Pushover and time-history analyses for the equipped linear system in Y-direction

5.3 Non-Linear analysis (The Actual Capacity Curve)

The non-linear results will be obtained from two different methods. The first method is the time history analysis while the second method is the N2 method. The N2 method is an approximated method that combines the pushover analysis of a multi-degree-of-freedom (MDOF) model with the response spectrum analysis of an equivalent single-degree-of-freedom (SDOF) system in order to get the global seismic demand. The purpose of performing this approximated method is to confirm the validity of the results we obtain from such a simple method. Non-linear time history analysis takes too long and thus it is not always feasible in terms of analysis time, so the need for such simple methods is getting high. For this reason, I decided

to spend some time on developing a full analysis for my case study using the N2 method. The results of both analyses will be compared at the end.

5.3.1 Method 1: Nonlinear Time-history analysis

Here we come to the non-linear analysis of the equipped structure. **Figure 49-Figure** 50 show the pushover capacity curve of the inelastic equipped structure, together with the results of the time history analysis of 14 accelerograms in both directions. The results of both EQ levels fall on the pushover curve. It is clear that the full behavior of the CSB devices is not utilized, because as shown in the graphs the results of time history analyses for both EQ levels belong to the first and second portions of the curve. Nevertheless, the structure might be exposed to higher (very rare) ground motion levels and so the 3rd portion could be reached.

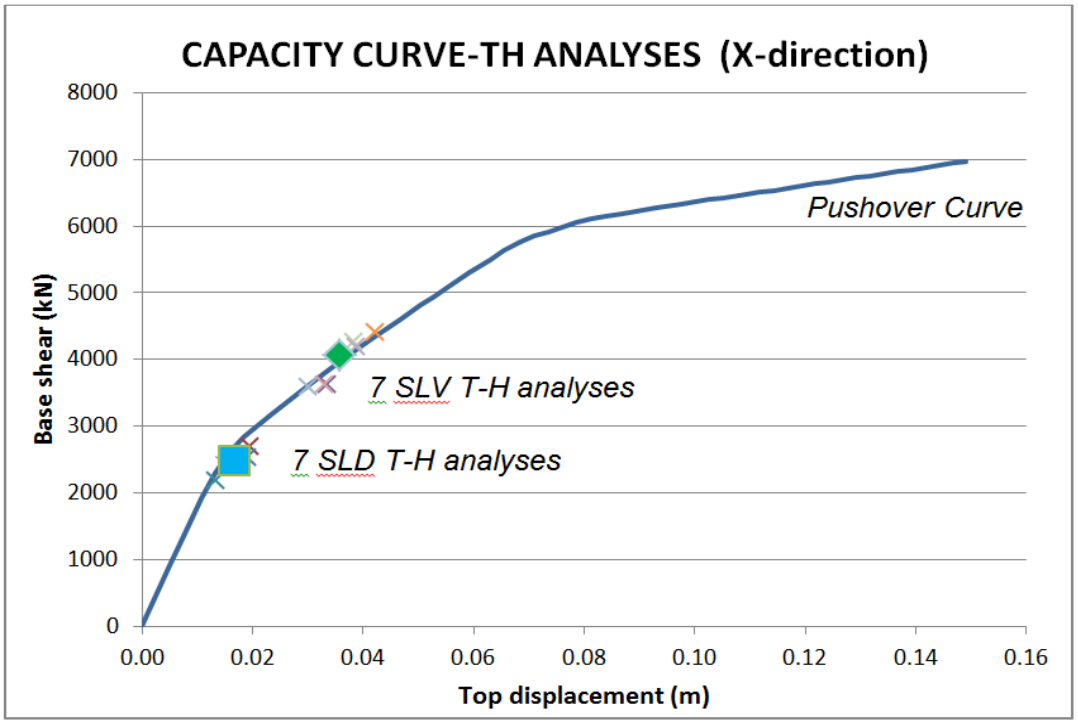

SLD:
$Vb = 2468.3\ kN$
$Dt = 1.6\ cm$

SLV:
$Vb = 4035\ kN$
$Dt = 3.6\ cm$

Figure 49- The results of Pushover and time-history analyses for the equipped non-linear system in X-direction

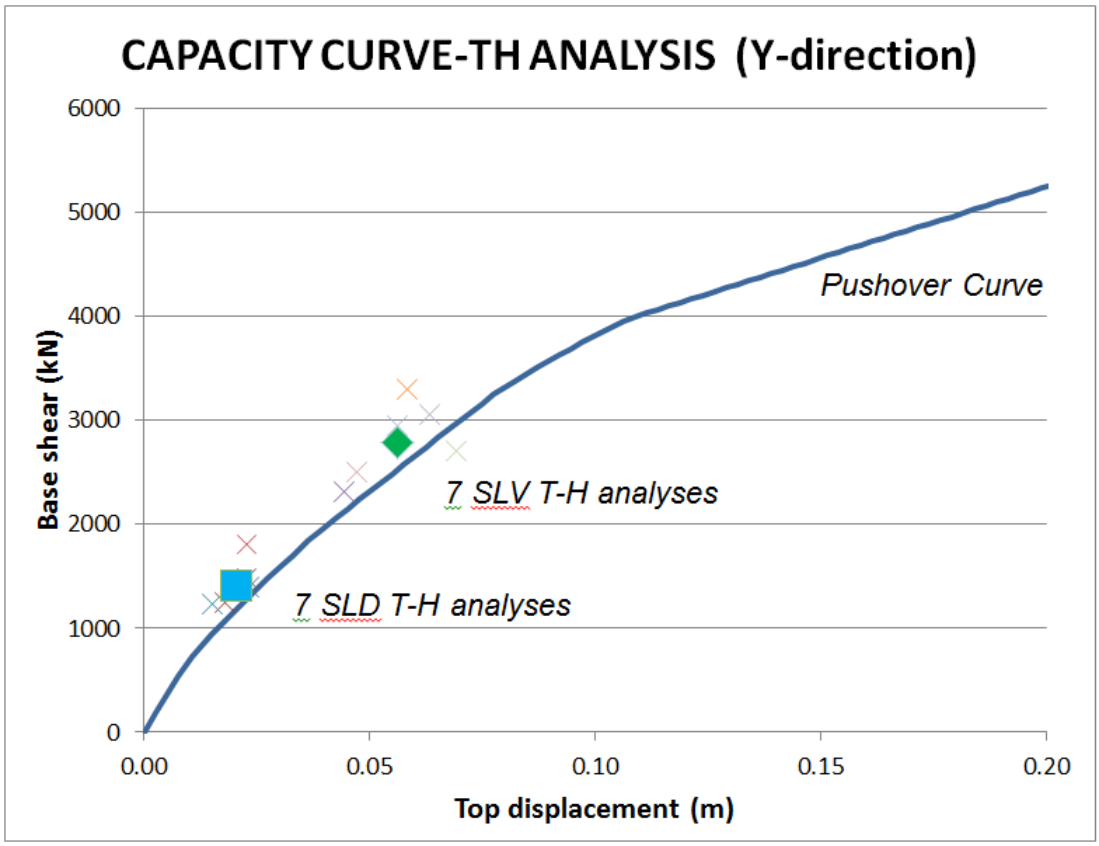

SLD:
$Vb = 1417.1\ kN$
$Dt = 2\ cm$

SLV:
$Vb = 2777.8\ kN$
$Dt = 5.6\ cm$

Figure 50- The results of Pushover and time-history analyses for the equipped non-linear system in Y-direction

5.3.2 Method 2: N2 method

In this section, we will present the N2-method that combines the pushover analysis of a multi-degree-of-freedom (MDOF) model with the response spectrum analysis of an equivalent single-degree-of-freedom (SDOF) system. The method is formulated in the acceleration - displacement format, which enables the visual interpretation of the procedure and of the relations between the basic quantities controlling the seismic response. Inelastic spectra, rather than elastic spectra with equivalent damping and period, are applied. This feature represents the major difference with respect to the capacity spectrum method. Moreover, demand quantities can be obtained without iteration. Generally, the results of the N2 method are reasonably accurate, provided that the structure oscillates predominantly in the first mode [13].

First, the steps of the N2-method will be listed. Then, as an illustrative example, this simple method will be applied to our case study. Detailed analysis will be performed for the X-direction only, and the results of the Y-direction will be plotted at the end as it follows exactly the same procedure.

5.3.2.1 Procedure of the N2-method

- STEP 1: **DATA**
  a) Structure
  b) Elastic acceleration spectrum Sae
- STEP 2: **DEMAND SPECTRA IN AD FORMAT**
  a) Determine elastic spectrum in AD format $S_{de} = \frac{T^2}{4\pi^2} S_{ae}$
- STEP 3: **PUSHOVER ANALYSIS**
  a) Assume displacement shape $\{\Phi\}$
  b) Determine vertical distribution of lateral forces $\{P\} = [M].\{\Phi\}$
  c) Determine base shear (V) – top displacement (Dt) relationship.
- STEP 4: **EQUIVALENT SDOF MODEL**
  a) Determine the equivalent mass of the SDOF system $m^* = \sum m_i.\emptyset_i$
  b) Transform MDOF quantities (Q) to SDOF quantities (Q*) $Q^* = Q/\tau$

  Where: $\tau = m^*/\sum m_i.\emptyset_i^2$ is a factor that controls the deformation from SDOF to MDOF
  c) Determine an approximate elasto-plastic force – displacement relationship
  d) Determine strength F_y^* , yield displacement D_y^* ,and period T^* where $T^* = 2\pi\sqrt{\frac{m^* D_y^*}{F_y^*}}$
  e) Determine capacity diagram (acceleration versus displacement) $S_a = F^*/m^*$

- STEP 5: **SEISMIC DEMAND FOR SDOF MODEL**
  a) Determine reduction factor $R_\mu = S_{ae}/S_{ay}$
  b) Determine displacement demand $S_d = D^*$
- STEP 6: **GLOBAL SEISMIC DEMAND FOR THE DOF MODEL**
  a) Transform SDOF displacement demand to the top displacement of the MDOF model

$$D_t = \text{r}.S_d$$

- STEP 7: **LOCAL SEISMIC DEMANDS**
  a) Perform pushover analysis of MDOF model up to the top displacement Dt (or to an amplified value of Dt)
  b) Determine local quantities (e.g. story drifts, rotations θ), corresponding to Dt
- STEP 8: **PERFORMANCE EVALUATION**
  a) Compare local and global seismic demands with the capacities for the relevant performance level.

5.3.2.2 Case study (x-direction)

STEP 1: **DATA**

The case study structure has already been described explicitly in chapter 2. However, in this analysis we used a planar MDOF structural model (**Figure 53**). Non-linear force-deformation relationships for structural elements are taken into consideration during the analysis. Seismic demand is initially defined in the form of the elastic (pseudo)-acceleration spectrum S_{ae}, which is a function of the natural period of the structure T (**Figure 51).**

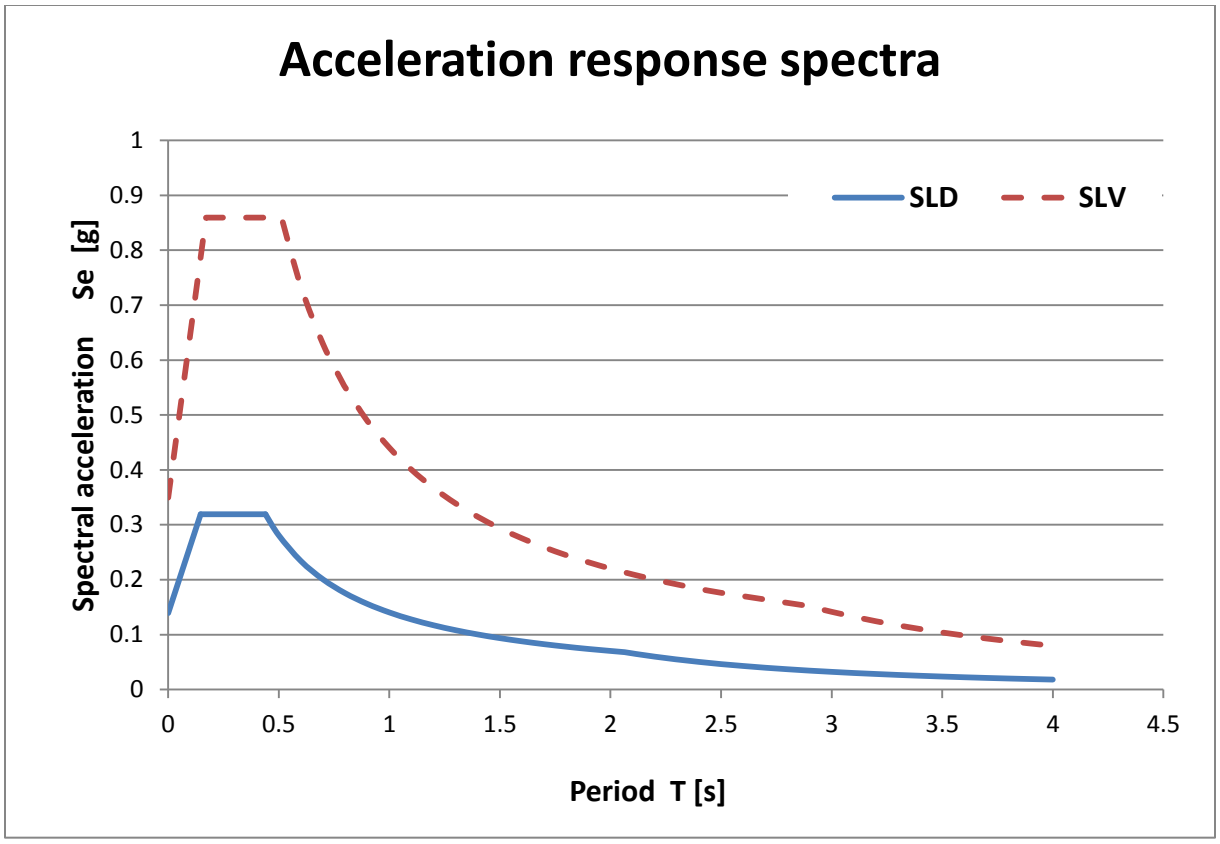

Figure 51- Elastic acceleration response spectra in the Se-T format

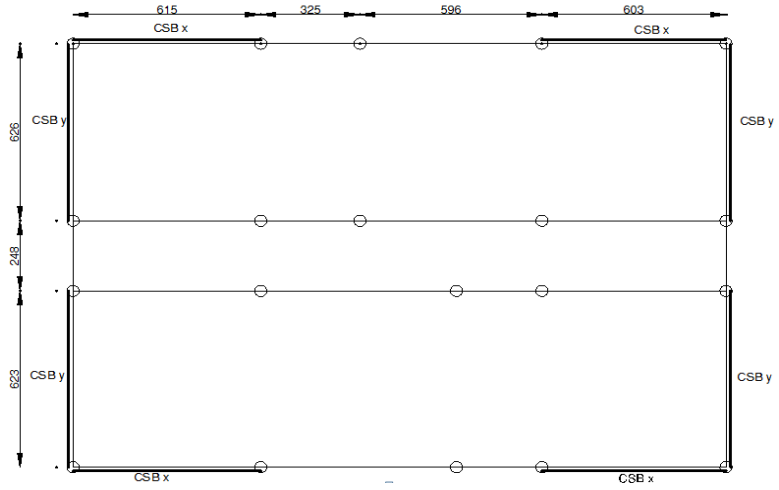

Figure 52- Plan view of the case study structure

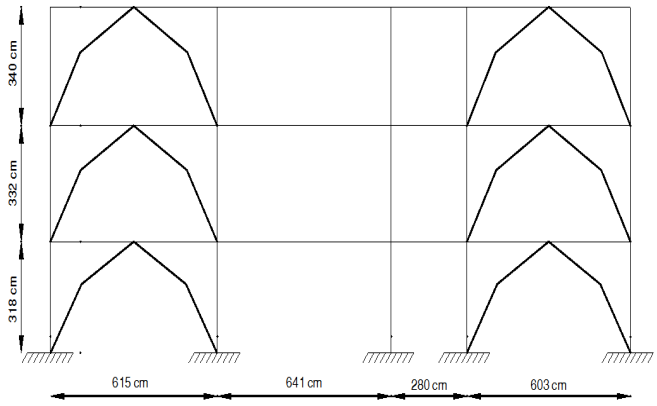

Figure 53- Elevation of the case study structure in the X-direction

- STEP 2: **DEMAND SPECTRA IN AD FORMAT**

a) Determine elastic spectrum in AD format

Starting from the acceleration spectrum, we will determine the inelastic spectra in acceleration – displacement (AD) format using this relationship: $S_{de} = \frac{T^2}{4\pi^2} S_{ae}$(**Figure 54**).

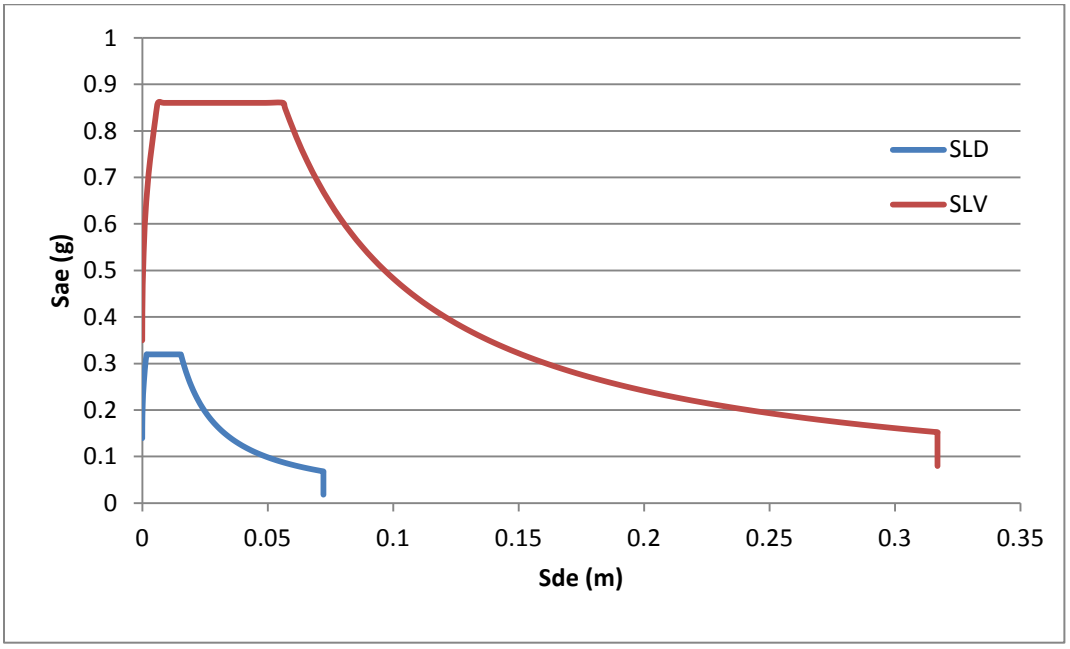

Figure 54- Elastic response spectra in AD format

Where S_{ae} and S_{de} are the values in the elastic acceleration and displacement spectrum, respectively, corresponding to the period T and a fixed viscous damping ratio.

- STEP 3: **PUSHOVER ANALYSIS**

a) Assume displacement shape $\{\Phi\}$

A linear displacement shape is assumed: $\{\Phi^T\} = [1,\ 0.65,\ 0.32]$

b) Determine vertical distribution of lateral forces $\{P\} = [M].\{\Phi\}$

The lateral force pattern is obtained from Equation 6 and normalized so that the force at the top is equal to 1.0

$$[M] = \begin{bmatrix} 332008 & 0 & 0 \\ 0 & 363710.5 & 0 \\ 0 & 0 & 396738 \end{bmatrix} [kg]$$

$$[\Phi] = \begin{bmatrix} 1 \\ 0.65 \\ 0.32 \end{bmatrix}$$

$$[P] = \begin{bmatrix} 1 \\ 0.718 \\ 0.383 \end{bmatrix}$$

a) Determine base shear (V) – top displacement (Dt) relationship.

With the force pattern [P], the software SAP 2000 yields the base shear V-top displacement Dt relationship shown in **Figure 55.**

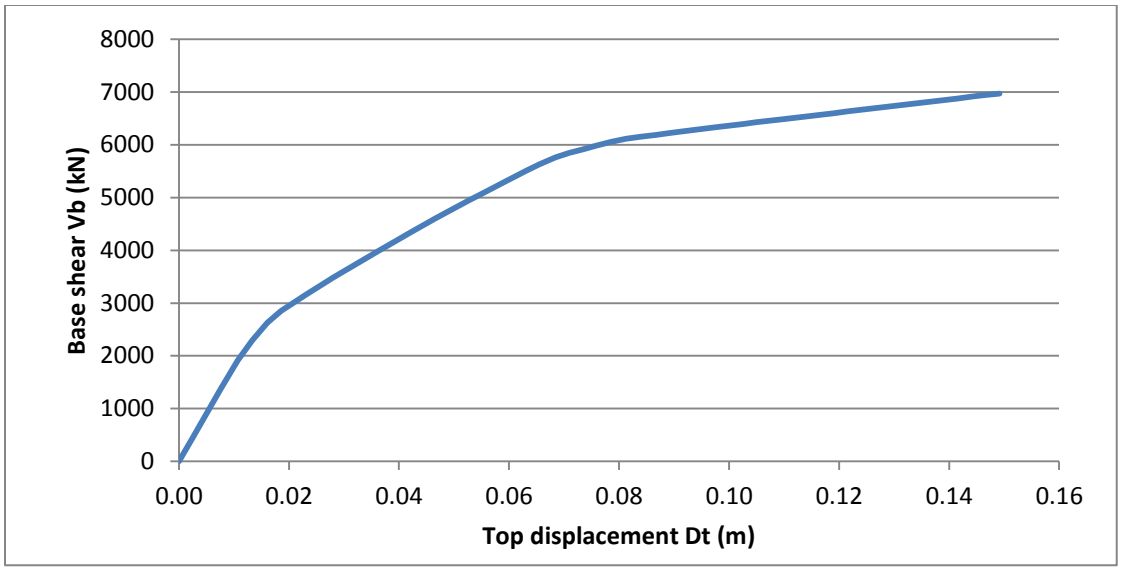

Figure 55- Base shear-Top displacement Pushover curve for the nonlinear system

- STEP 4: **EQUIVALENT SDOF MODEL**

a) Determine the equivalent mass of the SDOF system $m^* = \sum m_i . \emptyset_i = 697.95\ tons$

b) Transform MDOF quantities (Q) to SDOF quantities (Q*) $Q^* = Q/\tau$

Where: τ is a factor that controls the deformation from SDOF to MDOF

$$\tau = m^* / \sum m_i . \emptyset_i^2 = \ 1.318$$

The MDOF system is transformed to an equivalent SDOF system using:

$D^* = D/\tau \quad F^* = F/\tau$

The new pushover (force-displacement) curve is given in **Figure 56**.

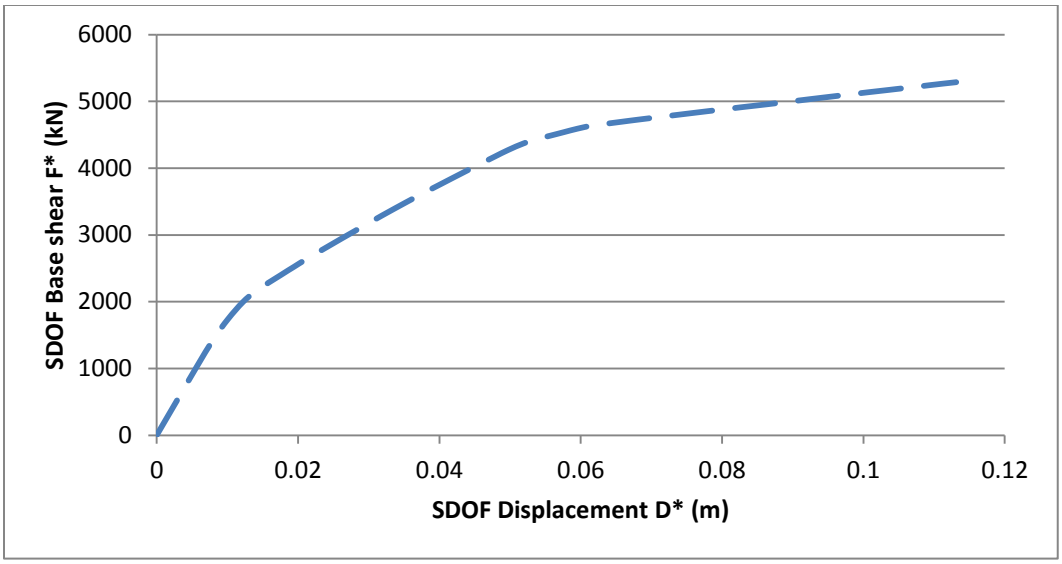

Figure 56- SDOF equivalent Pushover curve and the corresponding capacity diagram for the 3-storey RC frame

c) Determine an approximate elasto-plastic force – displacement relationship, and find the yield strength F_y^* , yield displacement D_y^* ,and period T^*

A bilinear idealization of the pushover curve is shown in **Figure 57**. The yield strength and displacement amount to $F_y^* = 4436\ kN\ \ and\ D_y^* = 3.85\ cm$. The elastic period is

$$T^* = 2\pi\sqrt{\frac{m^* D_y^*}{F_y^*}} = 0.489 \text{ s.}$$

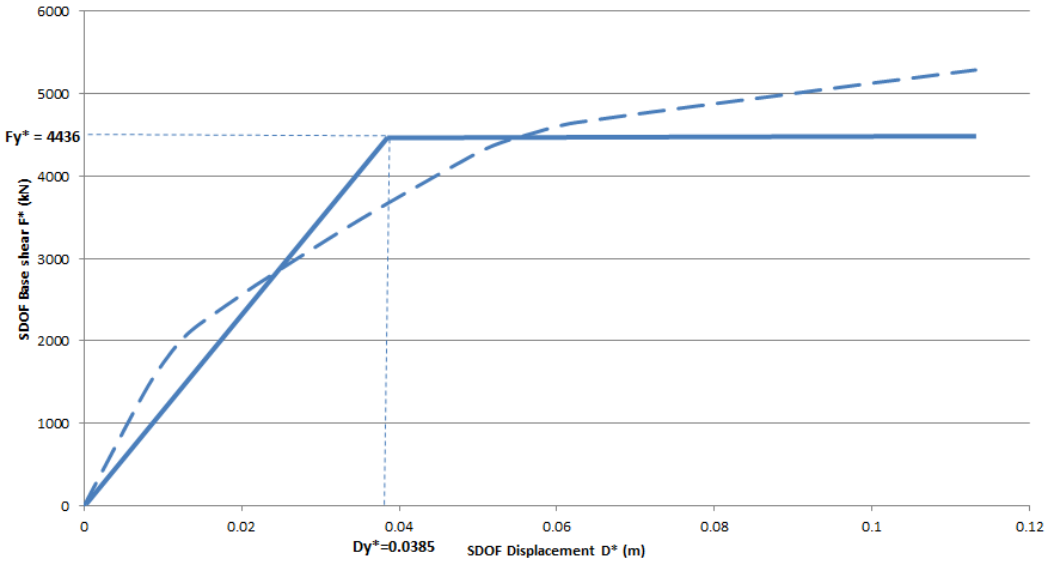

Figure 57- A bilinear idealization of the pushover curve

d) Determine capacity diagram (acceleration versus displacement)

The acceleration at the yield point amounts to $S_{ay} = \frac{F_y^*}{m^*} = \frac{4436\ kN}{697.95\ t} = 6.35\ m/s^2 = 0.647\ g$

➢ STEP 5: **SEISMIC DEMAND FOR SDOF MODEL**

a) Determine reduction factor R_μ

In the case of purely elastic behavior of the structure, seismic demand is represented by the intersection of the elastic demand spectrum and the line corresponding to the elastic period (T^*= 0.489 s) of the equivalent SDOF system. The values S_{ae} = 0.86 g and S_{de} = 4.13 cm are obtained in the case of the elastic SLV ground motion. The reduction factor $R_\mu$amounts to $R_\mu = S_{ae(T^*)}/S_{ay} = 0.86g/0.648g = 1.327$ (**Figure 58).**

Note that $R_\mu$is not the same as the reduction (behavior, response modification) factor *R* used in seismic codes. The code reduction factor *R* takes into account both energy dissipation and the so-called over-strength.

b) Determine displacement demand $S_d = D^*$

If the elastic period T^* is larger than or equal to Tc, the inelastic displacement demand S_d is equal to the elastic displacement demand S_{de}. The ductility demand then, defined as $\mu = S_d/D_y^*$, is equal to R_μ. If, on the other hand, the elastic period of the system is smaller than T_C, the ductility demand can be calculated from: $\mu = \left(R_\mu - 1\right)\frac{Tc}{T^*} + 1$

The period of the system $T^* = 0.489$ s is smaller than $Tc = 0.51$ s. Thus, the equal energy rule applies: $\mu = \left(R_\mu - 1\right)\frac{Tc}{T^*} + 1 = (1.327 - 1) * \frac{0.51}{0.489} + 1 = 1.34$

The inelastic Demand curve of the SLV earthquake level (**Figure 58**) can be built by applying the following relationships for all possible periods:

$S_d = \mu . D_y^* = \mu . \frac{S_{de}}{R_\mu}$

$S_a = S_{ae}/R_\mu$

Where:

$$R_\mu = \mu \quad for \;\; T^* \geq Tc$$

$$R_\mu = (\mu - 1) * \frac{T^*}{Tc} + 1 \;\; for \; T^* < Tc$$

Note that the ductility μ for the system is constant($\mu = 1.34$) regardless the period

From **Figure 58** the displacement demand of the equivalent SDOF is slightly different from the elastic displacement ($S_d = 5.2$ and $S_{de} = 5.11\, cm$), this is because they do not fall within the Equal Displacement region.

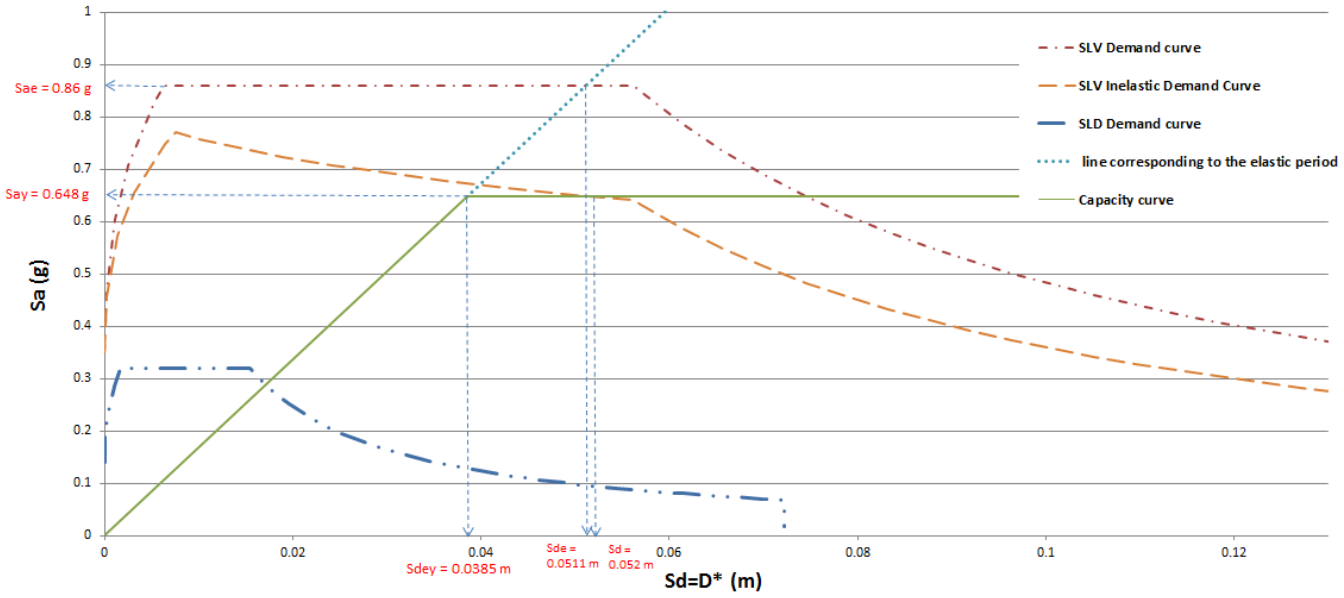

Figure 58- Demand spectra for two levels of ground motion and capacity diagram for the case study

➢ STEP 6: **GLOBAL SEISMIC DEMAND FOR THE MDOF MODEL**

a) Transform SDOF displacement demand to the top displacement of the MDOF model

The displacement demand of the equivalent SDOF system is transformed back to the top displacement of the MDOF system using the already introduced relation:

$$D_t = \text{r}.S_d = 1.318 * 0.052 = 0.0685\ m$$

$$D_t = 6.85\ cm$$

➢ STEP 7: **LOCAL SEISMIC DEMANDS (BEYOND THE SCOPE OF THE WORK)**

a) Perform pushover analysis of MDOF model up to the top displacement Dt (or to an amplified value of Dt)

b) Determine local quantities (e.g. story drifts, rotations θ), corresponding to Dt

➢ STEP 8: **PERFORMANCE EVALUATION (BEYOND THE SCOPE OF THE WORK)**

a) Compare local and global seismic demands with the capacities for the relevant performance level.

5.3.3 Comparison of the 2 methods

Two non-linear methods for the analysis of the non-linear system have been performed in the previous section. The first method is the time history analysis, while the second method is the N2-method. Time-history analysis was performed with the "Direct Integration" function, which is very accurate as it solves the equation of motion at each instance of time. However, the drawback we pay is the time. The analysis of the 14 accelerograms (7 SLD and 7SLV) took 110 hours to complete. Obviously, this is not always feasible in terms of time. The other method "N2-method" is very simple because it combines the pushover analysis of the MDOF system with the response spectrum of the SDOF, and It is not time consuming to obtain the pushover curve, thanks to the available finite element programs.

From each method, we could obtain the force and displacement at the two ground motion levels SLD and SLV. The N2-method yielded larger values than the time history analysis, which is expected because the N2-method is a non-linear equivalent linear analysis method, and it is meant to be conservative.

Since this work is not direction towards comparing non-linear analysis methods, I will avoid comparing the numbers I obtained from both methods. This could be a future research undertaken by another student. Besides, not much effort has been put in the N2-method, and thus I will leave this comparison open for others to judge.

CHAPTER 6

6. COMPARISON

Finally, we will compare the equipped and the unequipped systems in terms of performance under the two ground motion levels SLD and SLV. The results of the pushover and the time history analyses for both systems will be plotted together in one graph so the comparison will be possible **Figure 59-Figure** 60.

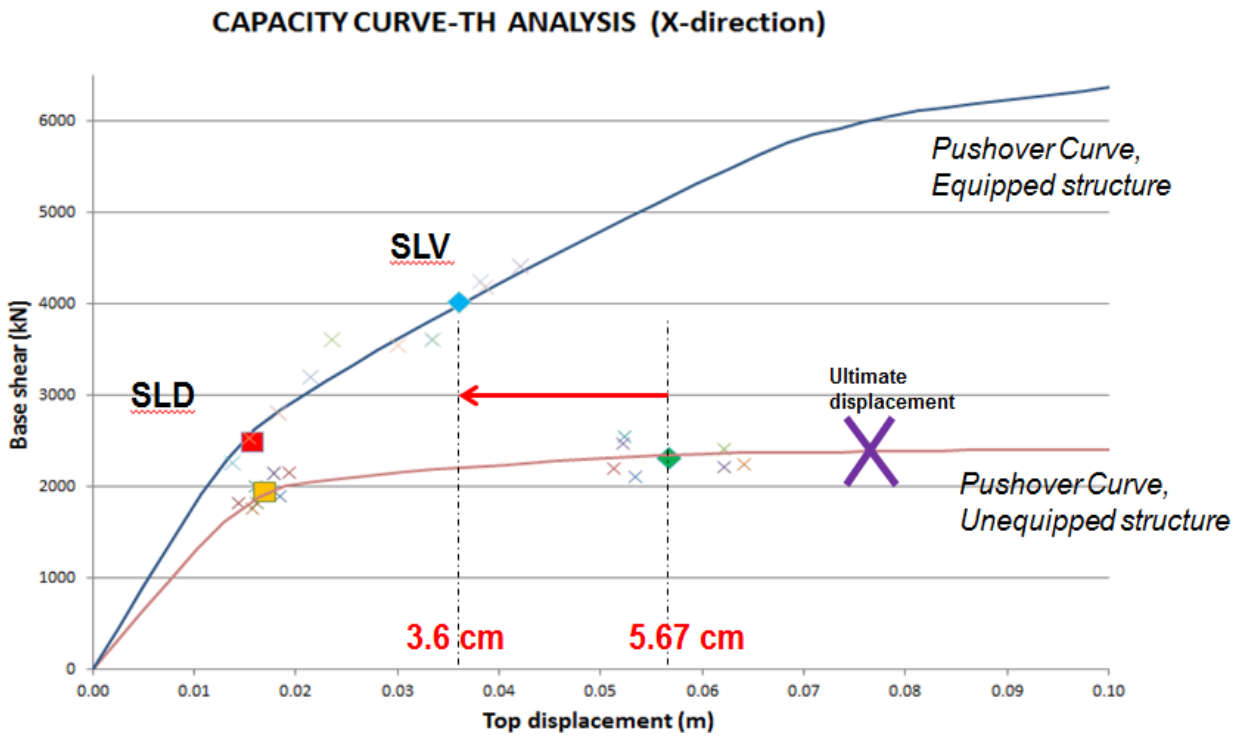

Figure 59- Pushover and time history analyses results for the equipped and the naked structures in the X-direction

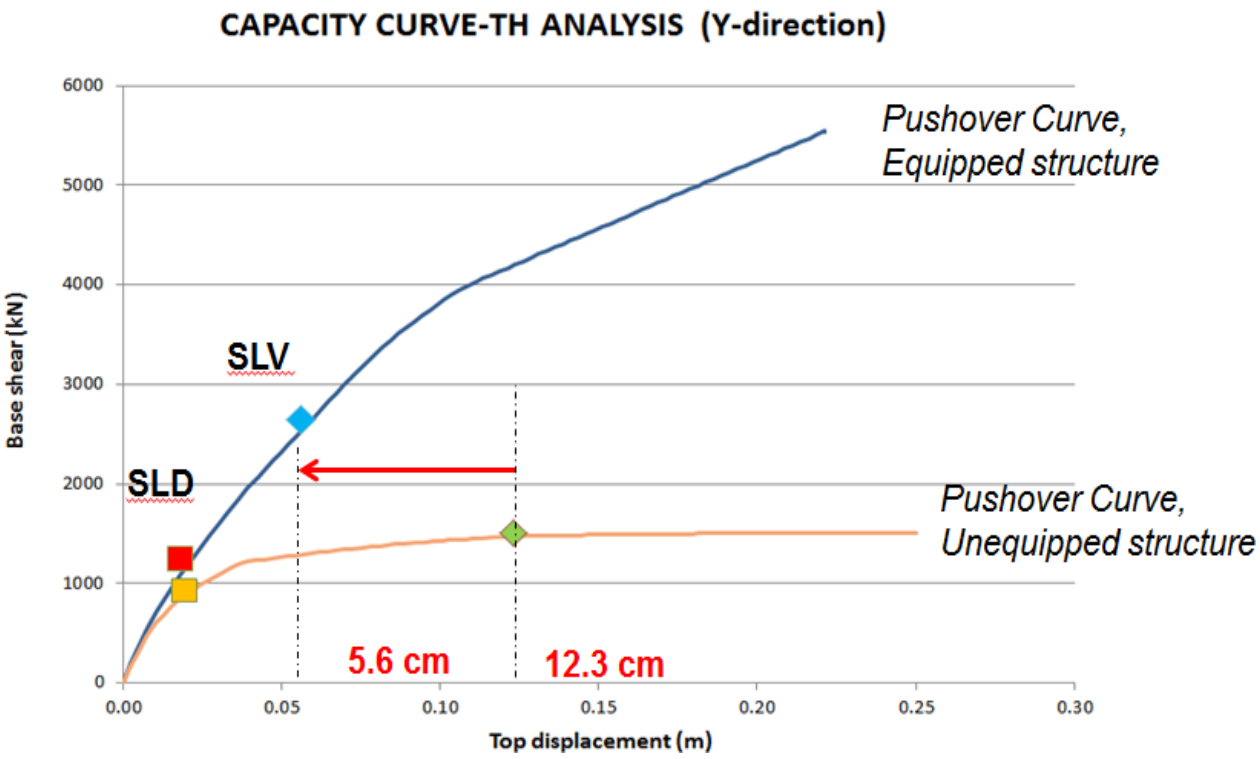

Figure 60- Pushover and time history analyses results for the equipped and the naked structures in the Y-direction

It is clear that we have improvements in the elastic and plastic regions. Our structure is now able to stand the same force with less displacement. In the x-direction, the displacement is reduced from 5.67 cm to 3.6 cm (36 % improvement). Similarly, in the y-direction the displacement has reduced from 12.3 cm to 5.6 cm (54 % improvement).

The results indicate how efficient the devices were, especially in the y-direction. Now after this significant reduction in displacement, the safety margin between the actual displacement and the ultimate displacement became larger.

CHAPTER 7

7. CONCLUSION AND FURTHER DEVELOPMENT

The main objective of the work was to improve the global behavior of RC structures by adding pre-designed CSB devices. Those devices were designed in such a way that the actual curve of the building matches the pre-defined objective curve. In order to achieve this goal, an understanding study of the local behavior of the bracing element was carried out.

Out of this research project we can conclude the follow:

1. The local study of the CSB device indicates that:
    - Different configurations shows different axial force distribution is columns and foundations.
    - Using an approximated constitutive law for the device might lead to different results.
2. Two effective methods for sizing the CSB devices have been proposed, where one of them has been illustrated using a case study example in which it showed effectiveness.
3. The comparison between the non-linear analysis results of the equipped and unequipped systems showed improvement in terms of displacement (damage).

To sum up, The Crescent-Shaped Braces can be a good solution for strengthening existing structures or even designing new structures to match certain predefined performance objectives.

Working on this subject can be further developed in the future. Regarding the CSB device, more effort can be put in the design of the crescent-shaped braces to meet other performance objectives which are not studied in this work, such as ductility. In addition, the problem of buckling can be an issue since we are dealing with slender elements.

Furthermore, different types of structures equipped with the CSB devices can be of a concern. For instance, the precast reinforced concrete structure might be interesting to study since they are characterized by large displacement, so our devices might show effectiveness in reducing the displacement and thus increasing the performance.

Acknowledgements

I wish to express my most sincere gratitude and appreciation to Prof. Stefano Silvestri for his guidance, patience, and encouragement throughout the development of the project.

I would like also to thank Dr. Michele Palermo, who was instrumental in getting me started with the research and without whose help, guidance, and patience the thesis would not have been successful.

BIBLIOGRAPHY

[1] M. Palermo, I. Ricci, S. Gagliardi, S. Silvestri, T. Trombetti and G. Gasparini, "Multi-performance seismic design through an enhanced first-storey isolation system," *Eng Struct,* vol. 59, pp. 495-506, 2014.

[2] M. Palermo, S. Silvestri, G. Gasparini and T. Trombetti, "Crescent shaped braces for the seismic design of building structures," *Materials and Structures,* vol. 48, no. 5, pp. 1485-1502, 2014.

[3] T. Trombetti, S. Silvestri, Gasparini G and I. Ricci, "Stiffness-strength-ductility design approaches for crescent-shaped braces," *Open Constr Build Technol J,* vol. 3, pp. 127-140, 2009.

[4] I. Ricci, S. Gagliardi, G. Gasparini, S. Silvestri, T. Trombetti and M. Palermo, "First-storey isolation concept for multi-performance seismic design of steel buildings," in *Proceedings of the 15th world conference on earthquake engineering*, Lisbon, 2012.

[5] C. Christopoulos and A. Filiatrault, "Principles of passive supplemental damping and seismic isolation," in *IUSS Press*, Pavia, 2006.

[6] F. Ponzo, D. Cesare, D. Nigro, A. Vulcano, F. Mazza, M. Dolce and C. Moroni, "JETPACS project: dynamic experimental tests and numerical results obtained for a steel frame equipped with hysteretic damped chevron braces," *J Earthq Eng,* vol. 16, pp. 662-685, 2012.

[7] SeismoStruct, "Seismosoft Earthquake Engineering Software Solutions," [Online].

Available: http://www.seismosoft.com/en/HomePage.aspx.

[8] Eurocode 2:Design of concrete structures-Part 1-1:General rules and rules for buildings, Brussels: CEN national Members, 2004.

[9] E. Wilson and R. Clough, "Seismic analysis," [Online]. Available: https://en.wikipedia.org/wiki/Seismic_analysis#endnote_IDA.

[10] Eurocode 8: Design of structures for earthquake resistance -Part 1: General rules, seismic actions and rules for buildings, Brussels: CEN national Members, 2004.

[11] Vanmarcke, H. Erik, Cornell, C. Allin, Gasparini, A. Dario, Hou and Shou-nien, "The Earthquake Engineering Online Archive," Department of Civil Engineering, Massachusetts Institute of Technology, Cambridge, Massachusetts, 2011. [Online]. Available: http://nisee.berkeley.edu/elibrary/Software/SIMQKE1ZIP.

[12] T. Datta, SEISMIC ANALYSIS OF STRUCTURES, Delhi,India: John Wiley&Sons (Asia) Pte Ltd, 2010.

[13] P. Fajfar and M. EERI, "A Nonlinear Analysis Method for Performance Based Seismic Design," *Earthquake Spectra*, vol. 16, no. 3, pp. 573-592, 2000.